

Diagnostic Imaging and the Structure- Function Relationship in Glaucoma

A thesis submitted to the University of Manchester for the degree
of Doctor of Philosophy in the Faculty of Life Sciences

2010

Jonathan Denniss

Contents

List of Tables	8
List of Figures	10
Abbreviations	12
Abstract	13
Declaration	14
Thesis Format	14
Copyright Statement	15
Acknowledgements	16
1. Glaucoma	17
1.1 Types of Glaucoma	17
1.1.1 Aetiology	17
1.1.2 Structural	18
1.1.3 Age of onset	18
1.2 Ocular Hypertension	19
1.3 Primary Open-Angle Glaucoma	19
1.4 Epidemiology	20
1.4.1 Prevalence	20
1.4.2 Incidence	21
1.5 POAG Risk factors	22
1.5.1 Age	23
1.5.2 State of the Individual	23
1.5.3 Ocular Risk Factors	24
1.5.4 Systemic Risk Factors	25
1.6 Treatment of POAG	26
1.6.1 Medical Treatment	27
1.6.2 Laser Treatment	28

1.6.3 Surgical Treatment.....	29
1.7 Recent Major Glaucoma Related Trials.....	30
1.7.1 The Ocular Hypertension Treatment Study (OHTS)	30
1.7.2 Collaborative Initial Glaucoma Treatment Study (CIGTS)	30
1.7.3 Collaborative Normal Tension Glaucoma Study (CNTGS)	31
1.7.4 Advanced Glaucoma Intervention Study (AGIS)	31
1.7.5 Early Manifest Glaucoma Trial (EMGT)	31
2. The Optic Nerve Head	33
2.1 The Healthy Optic Nerve Head	33
2.2 Blood Supply to the Optic Nerve Head	34
2.2.1 Surface Nerve Fibre Layer	35
2.2.2 Prelaminar Region	35
2.2.3 Lamina Cribrosa Region	35
2.2.4 Retrolaminar Region	36
2.3 The Optic Nerve Head in Glaucoma 1 –Mechanisms of Damage	36
2.3.1 Mechanical Theory of Damage	36
2.3.2 Vascular Theory of Damage	37
2.4 The Optic Nerve Head in Glaucoma 2 –Signs of Damage.....	38
2.4.1 Cup/Disc (C/D) Ratio.....	38
2.4.2 Neuroretinal Rim	39
2.4.3 Blood Vessels.....	40
2.4.4 Lamina Cribrosa.....	41
2.4.5 Peripapillary Atrophy.....	42
2.4.6 Retinal Nerve Fibre Layer.....	42
2.5 The Optic Nerve Head in Glaucoma 3 -Types of Damage	43

2.5.1 Focal Glaucomatous Optic Disc (Type 1)	43
2.5.2 Myopic Glaucomatous Optic Disc (Type 2)	44
2.5.3 Senile Sclerotic (Atrophic Glaucomatous) Optic Discs (Type 3)	44
2.5.4 Generalised Enlargement of the Optic Cup (Type 4)	45
3. Current Optic Nerve Head Imaging Methods in Glaucoma	46
3.1 Traditional Methods	46
3.1.1 Direct and Binocular Indirect Ophthalmoscopy	46
3.1.2 Fundus Photography	46
3.2 Newer Technologies	47
3.2.1 Optical Coherence Tomography	47
3.2.2 Scanning Laser Polarimetry	48
3.2.3 Confocal Scanning Laser Ophthalmoscopy	49
3.3 Techniques for measurement of optic nerve head blood flow and oxygenation	50
3.3.1 Angiography	51
3.3.2 Laser Doppler Velocimetry and Flowmetry	51
3.3.3 Multispectral Imaging	52
4. The Visual Field in Glaucoma	54
4.1 The Normal Visual Field	54
4.2 Perimetry	55
4.3 Patterns of Glaucomatous Damage	55
4.3.4 Paracentral defects	56
4.3.5 Arcuate defects	56
4.3.6 Nasal step	56
4.3.7 Overall depression in sensitivity	57

4.4 Statistical Indices of Visual Field Damage.....	57
4.4.1 Total and Pattern Deviation Probability Maps	57
4.4.2 Global Visual Field Indices	58
4.4.3 Glaucoma Hemifield Test.....	59
4.4.4 Reliability Indices.....	59
5. The Structure-Function Relationship in Glaucoma	61
5.1 Early Work	61
5.2 Behavioural Experiments	62
5.3 The Topographic Structure-Function Relationship	65
5.4 In-vivo measurements.....	67
5.6 Future Direction in Structure-Function Relationships	69
5.7 Structure-function summary.....	70
6. Discus – Investigating subjective judgement of glaucomatous damage in optic disc photographs.	71
Contribution.....	71
Publications.....	71
Conference Presentations	71
6.1 Abstract.....	72
6.2 Introduction	73
6.3 Methods.....	74
6.3.1. Selection of Images.....	74
6.3.2 Expert Observers	76
6.3.3. Experiments.....	76
6.3.4 Analysis	77
6.4 Results	79
6.5 Discussion	83

6.6 Acknowledgements..... 87

7. Evaluating the strength of the topographic structure-function relationship in glaucoma..... 88

Contribution..... 88

Publications..... 88

Conference Presentations 88

7.1 Abstract..... 89

7.2 Introduction 90

7.3 Methods..... 93

7.3.1 Study population..... 93

7.3.2 Grading and grouping of visual field points 95

7.3.3 Optic disc sectors 98

7.3.4 Discordance measure 99

7.3.5 Generation of random structure-function maps 101

7.4 Results 101

7.5 Discussion 103

7.6 Acknowledgements..... 107

8. Testing of a high-resolution multispectral fundus imaging system for measurement of optic disc tissue oxygenation 108

8.6 Contribution 108

8.1 Abstract..... 109

8.2 Introduction 110

8.3 Methods..... 111

8.3.1 The Multispectral System	111
8.3.2 Subjects	113
8.3.3 Image Capture	114
8.3.4 Production of Spatial Oxygenation Maps	114
8.3.5 Data Analysis	116
8.4 Results	117
8.5 Discussion	123
9.0 The relationship between optic disc oxygenation and visual field sensitivity in glaucoma.....	127
Contribution.....	127
Publications.....	127
Conference Presentations	127
9.1 Abstract.....	128
9.2 Introduction	129
9.3 Methods.....	130
9.3.1 Patients.....	130
9.3.2 Multispectral Imaging.....	131
9.3.3 Data analysis	133
9.4 Results	134
9.4.1 Altitudinal relationships.....	136
9.4.2 Global relationships.....	138
9.5 Discussion	139

10. The relationship between neuroretinal rim oxygenation and visual field sensitivity in glaucoma	143
Contribution.....	143
Publications (in preparation)	143
10.1 Abstract	144
10.2 Introduction	145
10.3 Methods	146
10.3.1 Patients.....	146
10.3.2 Multispectral Imaging.....	147
10.3.3 Data analysis.....	147
10.4 Results.....	149
10.4.1 Altitudinal relationships	149
10.4.2 Global relationships	153
10.5 Discussion.....	154
11. Conclusions.....	157
Appendix I: Beer-Lambert Law determination of chromophore concentrations.....	162
Appendix II: Complete List of Publications.....	165
Appendix III: Complete List of Conference Presentations.....	166
References	167

Final word count 49,326

List of Tables

Table	Description	Page
1.1	Estimated prevalence of POAG according to age and race	21
1.2	The incidence of definite open-angle glaucoma in those aged over 40 years in four major studies	22
6.1	Inclusion criteria for VF-positive and VF-negative groups	75
6.2	Characteristics of VF-positive and VF-negative groups	76
7.1	Age and visual field global characteristics of subjects	94
7.2	Distribution of assigned MRA grades to individual optic disc sectors from the HRT	95
7.3	Differences in optic disc sectors between those described by Garway-Heath et al (2000) and those used in the HRT Moorfields Regression Analysis	98
7.4	Comparison of chosen visual field grade boundaries with those suggested by Hodapp et al (1993)	106
8.1	Estimated within-subject standard deviations of optic disc sector oxygenation for all 12 images, within sets of 3 consecutively captured images, and between average values from sets (all patients).	120
9.1	Pearson correlation coefficients and associated p-values for differences in optic disc oxygenation and NRR area compared to differences in visual field sensitivity in corresponding areas	138
10.1	Pearson correlation coefficients and associated p-values for differences in oxygenation between whole optic disc sectors and the NRR within optic disc sectors compared to differences in visual field sensitivity in corresponding areas	152
10.2	Pearson correlation coefficient, adjusted r^2 and contribution of individual variables to multiple regression of superior-inferior differences in NRR area and oxygenation vs. superior-inferior differences in visual field sensitivity in corresponding areas	153

List of Figures

Figure	Description	Page
1.1	Screening IOP vs. Relative Risk of POAG in the Baltimore Eye Survey	19
1.2	Increasing prevalence of POAG with age	23
1.3	Nine-year relative risk of open-angle glaucoma by baseline IOP	24
2.1	Schematic representation of the optic nerve blood supply	34
2.2	Schematic representation of the ONH blood supply	35
2.3	Vertical C/D ratio vs. vertical ONH diameter in glaucoma patients and controls	39
2.4	Illustration of four common progressions of glaucomatous ONH damage	40
2.5	Illustration of an inferior ONH splinter haemorrhage	41
2.6	Illustration of α - and β - PPA	42
2.7	Focal Glaucomatous ONH showing inferior focal NRR loss	44
2.8	Myopic glaucomatous ONH with polar notching, tilted appearance and temporal PPA	44
2.9	Senile sclerotic glaucomatous ONH with diffuse thinning of NRR and complete ring of PPA	45
2.10	Glaucomatous ONH with generalised cup enlargement	45
3.1	Absorption spectra of oxyhaemoglobin, deoxyhaemoglobin, water and tissue scattering components of blood	52
4.1	Illustration of the hill of vision (sensitivity profile) and corresponding seen visual fields	55
4.2	The anatomical distribution of retinal nerve fibres as traced from a silver-stained retina and a schematic diagram of the same	56
4.3	Illustration of typical progression of visual field damage patterns in glaucoma	57
5.1	Primate RGC loss vs. visual sensitivity loss plotted on log-linear axis	64
5.2	Primate RGC loss correlated with visual sensitivity plotted on log-log axes and with retinal eccentricity taken into account	64
5.3	Visual field divisions and corresponding optic nerve head sectors	66
5.4	Visual sensitivity vs. RNFL thickness for superior and inferior arcuate areas of the visual field, plotted on both log-linear and linear axes	68
6.1	Screenshot of Discus software	77
6.2	ROC curves for the classification of optic disc photographs by the 12 expert observers	80-82
6.3	Performance (area under ROC curve) of combined expert panel as a function of number of included observers	83
7.1	Representation of the 24-2 visual field sectors as defined by Garway-Heath (2000) with colour and numerically-coded corresponding optic disc sectors for a right eye	92

Figure	Description	Page
7.2	Example of how visual field points were graded and grouped	97
7.3	Distribution of grades assigned to sectors of optic discs and corresponding visual field sectors according to the Garway-Heath map for all subjects	99
7.4	Number of individual optic disc sectors and corresponding visual field groups (according to the Garway-Heath map) given each grade for all subjects	100
7.5	The computer-generated map which produced minimum discordance from a sample of 10,000	102
8.1	The multispectral imaging system	112
8.2	Flow chart describing the images captured for each patient	113
8.3	Flow chart showing how each monochromatic image series was converted to a single oxygenation map	115
8.4	The eight 45° sectors into which the optic disc was divided	116
8.5	Monochromatic images of one subject's optic disc taken at 8 different wavelengths	117
8.6	Oxygenation map derived from the images in figure 8.5	118
8.7	Six masked oxygenation maps of the same optic disc taken on the same day	118
8.8	Coefficients of variation in optic disc sector oxygenation across all 12 images for all subjects	119
8.9	Example Bland-Altman analysis of between-session test-retest variability for sector B (superior-temporal sector)	121
8.10	Mean and 95% range of optic disc sector oxygenation values across all images of all subjects with mean test-retest difference and limits of repeatability	122
9.1	The multispectral imaging system	132
9.2	Diagram of optic disc and visual field sectors for a right eye, adapted from Garway-Heath <i>et al</i> (2002)	134
9.3	Spatial oxygenation maps of the optic discs of 2 patients with corresponding visual field greyscale plots	135
9.4	Inferior-superior differences in optic disc oxygenation and NRR area vs. superior-inferior difference in visual field sensitivity	136
9.5	Differences in oxygenation and NRR rim area between vertically opposing optic disc sectors vs. differences between sensitivity of corresponding visual field areas	137
10.1	Diagram of optic disc and visual field sectors for a right eye, adapted from Garway-Heath <i>et al</i> (2002)	148
10.2	Example of a spatial oxygenation map, re-sampled and aligned HRT3 topography image, and masked oxygenation map leaving only NRR tissue	149
10.3	Inferior-superior differences in NRR oxygenation vs. superior-inferior difference in visual field sensitivity	150
10.4	Differences in NRR oxygenation between vertically opposing optic disc sectors vs. differences between sensitivity of corresponding visual field areas	151

Abbreviations

AGIS	-Advanced Glaucoma Intervention Study
ANSI	-American National Standards Institute
AUROC	-Area Under Receiver Operating Characteristic (Curve)
CCD	-Charge-Coupled Device
CCT	-Central Corneal Thickness
C/D	-Cup/Disc Ratio
CIGTS	-Collaborative Initial Glaucoma Treatment Study
CNTGS	-Collaborative Normal Tension Glaucoma Study
CPSD	-Corrected Pattern Standard Deviation
CSLO	-Confocal Scanning Laser Ophthalmoscopy
dB	-Decibel
DC	-Direct Current
EMGT	-Early Manifest Glaucoma Trial
FN	-False Negative
FP	-False Positive
GHT	-Glaucoma Hemifield Test
GPS	-Glaucoma Probability Score
HFA	-Humphrey Field Analyzer®
HRT	-Heidelberg Retina Tomograph®
IOP	-Intraocular Pressure
ISNT	-Inferior>Superior>Nasal>Temporal (neuroretinal rim configuration)
MD	-Mean Deviation
MRA	-Moorfields Regression Analysis
MWU	-Mann-Whitney U Test
NHS	-National Health Service
NRR	-Neuroretinal Rim
OCT	-Optical Coherence Tomography
OHTS	-Ocular Hypertension Treatment Study
OLGA	-Optometrist-Led Glaucoma Assessment
ONH	-Optic Nerve Head
PD	-Pattern Deviation
POAG	-Primary Open-Angle Glaucoma
PPA	-Peripapillary (Chorioretinal) Atrophy
PSD	-Pattern Standard Deviation
RGC	-Retinal Ganglion Cell
RNFL	-Retinal Nerve Fibre Layer
ROC	-Receiver Operating Characteristic
RPE	-Retinal Pigment Epithelium
SBM	-Structure-Based Map
SF	-Short-term Fluctuation
SITA	-Swedish Interactive Thresholding Algorithm
sMRA	-Sectoral Moorfields Regression Analysis
SVP	-Spontaneous Venous Pulsation
TD	-Total Deviation
UV	-Ultraviolet
VFI	-Visual Field Index

Abstract

This thesis describes a series of investigations into the use of optic nerve head (ONH) imaging in primary open-angle glaucoma (POAG), and its relation to visual function. Accurate diagnosis is a key issue in POAG, particularly the difficult task of separating those with early disease from those healthy individuals who display signs of POAG. The purpose of this work is to improve diagnostic methods in glaucoma through use of ONH imaging and its relationship with visual field (VF) loss.

First, the performance of a group of expert clinicians evaluating ONH photographs for glaucomatous damage was investigated. The results showed that even when their assessments are combined discrimination between eyes with and without POAG (based on VF loss) is far from perfect, highlighting the need for improvements in diagnosis.

The possibility of combining structural and functional data to aid diagnosis was then considered. This requires VF loss and ONH damage to be strongly topographically related. The strength of this relationship was evaluated in 185 patients with POAG. 10,000 computer-generated maps between the ONH and VF were tested and the topographic relationship measured with each of these was compared to that using a published structure-based map. The weak topographic relationships found suggest that the application of these maps to individual patients is limited with current measures.

The next chapter describes how a multispectral imaging (MSI, also called *hyperspectral* imaging) system was set-up for spatial evaluation of ONH oxygenation using a Beer-Lambert law model. Test-retest repeatability was tested and found to be acceptable for the purposes of the following studies.

The MSI system was then used for an investigation of the relationship between ONH oxygenation and VF loss. 33 eyes of 18 patients underwent VF testing, MSI and HRT3 imaging. Superior-inferior asymmetries in VF sensitivity were compared to superior-inferior asymmetries in ONH oxygenation measured by MSI and in neuroretinal rim (NRR) area measured by HRT3. This way we take advantage of the typical progression of POAG and each eye acts as its own reference, negating the effect of a wide normal range and overlap between health and disease. This study found, for the first time, a strong association between ONH oxygenation and VF sensitivity.

A re-analysis of the 33 ONH oxygenation maps was then performed to assess oxygenation only in the area of the NRR as defined by the HRT. Superior-inferior asymmetries in NRR oxygenation were then compared to superior-inferior asymmetries in VF loss, and the associations found were similarly strong. This study shows that MSI is capable of detecting areas of NRR deemed healthy tissue by structural imaging techniques, which are in fact poorly oxygenated and associated with VF defects.

These findings show that NRR oxygenation measured by MSI is strongly related to VF loss. This important information complements existing technologies and may aid in the future diagnosis and management of patients with POAG.

Declaration

No portion of the work referred to in this thesis has been submitted in support of an application for another degree or qualification of this or any other university or other institute of learning.

Thesis Format

This thesis is presented in 'Alternative Format'. The decision to present the thesis this way was taken as several of the chapters featured here had already been prepared for submission to refereed journals. The thesis constitutes a review of the literature on the subject matter (chapters 1-5) followed by reports of 5 projects (chapters 6-10). Where manuscripts based on these chapters have been published, or submitted for publication in a refereed journal it is indicated on the first page of the chapter. The author's contribution to the work presented in each chapter is also identified on the first page of each chapter. Chapter 11 draws together the conclusions of the thesis with a view to how this work relates both scientifically and clinically to the 'bigger picture' in glaucoma. Suggestions for further work are also made in this chapter. Finally in Appendices II and III are complete lists of all publications and conference presentations made in relation to this work.

Copyright Statement

- i. The author of this thesis (including any appendices and/or schedules to this thesis) owns certain copyright or related rights in it (the “Copyright”) and he has given The University of Manchester certain rights to use such Copyright, including for administrative purposes.

- ii. Copies of this thesis, either in full or in extracts and whether hard or electronic copy, may be made **only** in accordance with the Copyright, Designs and Patents Act 1998 (as amended) and regulations issued under it or, where appropriate, in accordance with licensing agreements which the University has from time to time. This page must form part of any such copies made.

- iii. The ownership of certain Copyright, patents, designs, trade marks and other intellectual property (the “Intellectual Property”) and any reproductions of copyright works in the thesis, for example graphs and tables (“Reproductions”), which may be described in this thesis, may not be owned by the author and may be owned by third parties. Such Intellectual Property and Reproductions cannot and must not be made available for use without the prior written permission of the owner(s) of the relevant Intellectual Property and/or Reproductions.

- iv. Further information on the conditions under which disclosure, publication and commercialisation of this thesis, the Copyright and any Intellectual Property and/or Reproductions described in it may take place is available in the University IP Policy (see <http://www.campus.manchester.ac.uk/medialibrary/policies/intellectual-property.pdf>), in any relevant Thesis restriction declarations deposited in the University Library, The University Library’s regulations (see <http://www.manchester.ac.uk/library/aboutus/regulations>) and in The University’s policy on presentation of Theses.

Acknowledgements

Firstly I would like to thank Professor David Henson who has been an excellent supervisor, providing extremely valuable insight into all my work. In addition, his day-to-day support, kindness and understanding has made my time as a PhD student thoroughly enjoyable. Our regular discussions on all manner of topics will be sorely missed when I leave the department.

My thanks also go to Dr Ingo Schiessl and Dr Paul Artes who have each co-supervised much of this work. Without Dr Schiessl's scientific perspective, critical eye and clear thinking much of this work might not have been completed. Dr Artes' influence and encouragement from across the Atlantic extends throughout this work, and I would like to particularly thank him for his help and support during his last weeks in Manchester, when I'm sure he had enough to do! Drs Schiessl and Artes both also took much time to introduce me to the initially highly frustrating business of computer programming, allowing me to develop skills which will be invaluable throughout my career.

I also thank Dr Vincent Nourrit for all the time spent helping me to understand the optical and image processing aspects of the multispectral imaging work, and Ms Cecilia Fenerty for her valuable clinical perspective on my work and aid in patient recruitment. I am grateful to all the Doctors and Optometrists in the glaucoma service at Manchester Royal Eye Hospital who helped me recruit patients and collect data, and to the patients themselves for giving up their time.

I gratefully acknowledge the College of Optometrists for the PhD studentship which funded this work. The College of Optometrists and the Imaging and Perimetry Society provided travel bursaries which aided me in presenting my work at international conferences. This work was also supported by the NIHR Manchester Biomedical Research Centre and the Manchester Academic Health Sciences Centre (MAHSC).

Finally I would like to thank my family for their continuing support in all I do.

1. Glaucoma

The term 'glaucoma' describes a group of progressive optic neuropathies characterised by changes in the appearance of the optic nerve head (ONH, also called the optic disc in some instances) and which give rise to specific patterns of visual field loss. Glaucoma is the world's second leading cause of blindness (Quigley, 1996) and accounts for over one million outpatient appointments annually in the UK National Health Service (NHS) alone (NICE, 2009). Many aspects of glaucoma, such as its biological basis and the factors influencing disease progression, are not yet fully understood (Weinreb and Khaw, 2004). Treatment of glaucoma reduces the rate of visual loss in many patients, though some types are asymptomatic until late on in the progression of the disease when significant visual field loss has already occurred. Early detection and treatment of glaucoma is the subject of much research due to the widespread belief that the risk of progression to significant visual loss is reduced when treatment is initiated at the early stages of the disease. Detection of glaucoma relies upon examination of the ONH, retinal nerve fibre layer (RNFL), and visual field. Raised intraocular pressure (IOP) is also a risk factor for glaucoma and currently the only treatable one, so IOP measurement is also important (Coleman, 1999, Boland and Quigley, 2007). It has been estimated from population-based surveys that in developed countries around 50% of open-angle glaucoma cases are currently undetected, and this rate is likely to be much higher in developing countries (Quigley, 1996).

1.1 Types of Glaucoma

Glaucoma may be classified based on aetiology, ocular structures, and age of onset.

1.1.1 Aetiology

Glaucoma may be primary or secondary. Glaucoma is said to be primary if there are no other known ocular or systemic causes for glaucomatous damage; examples include primary open-angle glaucoma (POAG), normal tension glaucoma, and primary angle-closure glaucoma.

Secondary glaucoma is usually associated with raised IOP as a result of some form of obstruction to aqueous outflow such as in pigment dispersion syndrome, exfoliation syndrome, some forms of uveitis, or following trauma. Secondary glaucoma may also be lens related, for example a hypermature cataract may release proteins into the aqueous humour which can build

up in the trabecular meshwork, obstructing aqueous outflow (phacolytic glaucoma). Secondary glaucoma may also be drug induced, for example by steroid use.

1.1.2 Structural

Glaucoma may also be classified on the basis of the gonioscopic appearance of the anterior chamber drainage angle. In POAG the drainage angle is open and aqueous outflow unobstructed. It is also possible to have secondary open-angle glaucoma, in which, whilst the drainage angle is open, there is still obstruction to aqueous outflow such as the build-up of exfoliative material in the trabecular meshwork (exfoliation glaucoma). In closed-angle glaucoma the anterior chamber drainage angle, and therefore aqueous outflow, is blocked by peripheral iris tissue. This may happen by several mechanisms; commonly, a 'pupil block' prevents the flow of aqueous from the posterior chamber, into which it is secreted by the ciliary body, into the anterior chamber. This is often caused by lens-iris adhesions and results in a pressure gradient between the posterior and anterior chambers which causes a bowing forward of the iris, blocking the drainage channel (Coleman, 1999). Alternatively, in an anatomically predisposed eye with a narrow anterior chamber angle, dilation of the pupil, either in dark adaptation or by pharmaceutical means, can cause peripheral iris to block the anterior chamber angle preventing aqueous outflow. In certain inflammatory conditions such as anterior uveitis, peripheral anterior synechiae may also form, blocking the anterior chamber angle (Coleman, 1999). This would be a form of secondary closed-angle glaucoma.

1.1.3 Age of onset

Whilst glaucoma is generally a disease of old-age, there are certain types of glaucoma which occur at a much earlier age. Congenital glaucoma or buphthalmos occurs when a child is born with a developmental abnormality such as a malformation of the trabecular meshwork which hinders aqueous outflow. Juvenile glaucoma has onset in early childhood and is more commonly open-angle, but often arises secondary to intraocular surgery such as following extraction of a congenital cataract.

1.2 Ocular Hypertension

Ocular hypertension is diagnosed when a person has IOP raised consistently above the normal range in the absence of detectable glaucomatous damage to the ONH or visual field. Raised IOP is commonly defined as being 22mmHg or more, however, the exact cut-off level used to define ocular hypertension has been inconsistent in previous studies, where cut-off levels from 18 to 26mmHg have been used (Tavares et al., 2006). Patients with ocular hypertension are at increased risk of developing glaucoma and so may be regularly reviewed by clinicians for signs of progression to glaucoma. Figure 1.1 below shows data from the Baltimore Eye Survey, which indicates the relative risk of POAG with increasing IOP at screening.

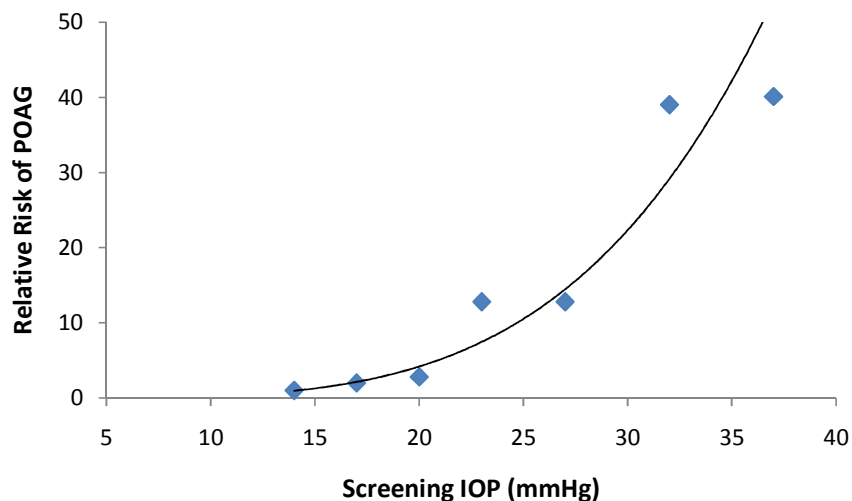


Figure 1.1: Screening IOP vs. Relative Risk of POAG in the Baltimore Eye Survey (data from Sommer et al., 1991b)

1.3 Primary Open-Angle Glaucoma

POAG is the most common type of glaucoma in the UK (Kroese and Burton, 2003). It is a chronic, progressive, generally bilateral, but often asymmetric disease affecting adults, and is usually asymptomatic until in advanced stages (Kroese and Burton, 2003, Coleman, 1999). It is a diagnostic feature of POAG that IOP is raised above 21mmHg at some point, however it should be noted that up to 40% of people with otherwise characteristic POAG have IOP consistently within the normal range (Kroese and Burton, 2003). These people are historically defined as having normal tension glaucoma. This type of glaucoma is otherwise indistinguishable from

POAG and it should be noted that the cut-off value between 'normal' and 'high' IOP is based on the statistically derived 97.5% probability level and the incorrect assumption that IOP in the general population is normally distributed (Hollows and Graham, 1966). It is now accepted that the distribution of IOP in the general population is non-Gaussian, being skewed towards higher IOPs. The division of POAG into normal- and high-tension is therefore outdated, and IOP is now considered to be a risk-factor rather than a diagnostic factor.

The remainder of this chapter will be centred on POAG (as this is the subject of the research in the later chapters).

1.4 Epidemiology

In the UK, the vast majority (80-90%) of patients with glaucoma are detected by optometrists during routine eye examination of patients attending for other ophthalmic needs such as correction of refractive error (Laidlaw et al., 1994). Glaucoma is the second most common cause of blindness certification in the UK (Kroese and Burton, 2003), and accounts for around 25% of ophthalmology outpatients appointments, amounting to over one-million appointments per year in the NHS alone (Spry et al., 1999, NICE, 2009).

1.4.1 Prevalence

The prevalence of a disease is the proportion of the population with the disease at a given time. In 1996 it was estimated that there totalled over 66 million sufferers of all types of glaucoma worldwide, with at least 6.8 million bilaterally blind (Quigley, 1996). This figure is likely to continually increase as a result of demographic changes and increasing life expectancy (Tuck and Crick, 2003). A common finding amongst many epidemiological trials is that as many as 50% of people with POAG remain undetected for various reasons, though this figure may reduce as glaucoma detection methods are improved and newer technologies are utilised more regularly on the general population (Rudnicka et al., 2006). The variability of the definition of glaucoma in prevalence surveys makes it difficult to compare the data between studies, especially between studies from different parts of the world, where the distribution of the various forms of glaucoma vary, for example in Japan where 92% of open-angle glaucoma

patients have IOP within the 'normal' range (Kroese and Burton, 2003, Foster et al., 2002, Rudnicka and Owen, 2007).

For POAG, reported prevalence ranges from 0.03% in China to 8.76% in St. Lucia (Rudnicka and Owen, 2007). In white people aged over 40 years from Europe, Australia, and America, prevalence is 1-3% (depending on subject age groups), whilst higher prevalence is reported in black populations such as in Africa (3-4%), and especially the Caribbean (7-9%) (Rudnicka and Owen, 2007, Rudnicka et al., 2006). The Baltimore Eye Study directly compared the prevalence of POAG in whites and blacks from the same geographical area, and concluded that prevalence was 4.3 times higher in blacks than in whites after age-adjustment (Tielsch et al., 1991). In 2006 a systematic review and meta-analysis of 46 cross-sectional studies including 2509 cases of primary open-angle glaucoma was carried out (Rudnicka et al., 2006). The results are summarised in Table 1.1.

Table 1.1: Estimated prevalence of POAG according to age and race (after Rudnicka et al., 2006)

Age Range (y)	Predicted Prevalence of OAG (95% CrI)		
	White	Black	Asian
30-39	—	1.8 (1.2-2.7)	0.4 (0.3-0.6)
40-49	0.4 (0.3-0.6)	2.9 (1.9-4.4)	0.6 (0.4-1.0)
50-59	0.8 (0.5-1.2)	4.6 (3.1-6.8)	1.0 (0.6-1.6)
60-69	1.6 (1.1-2.5)	7.2 (4.9-10.6)	1.6 (1.0-2.4)
70-79	3.3 (2.2-4.9)	11.2 (7.6-16.1)	2.5 (1.6-3.8)
80-89	6.6 (4.4-9.7)	16.9 (11.7-23.8)	3.8 (2.3-5.9)
90-95	10.8 (7.2-15.8)	22.5 (15.7-31.2)	—

1.4.2 Incidence

The incidence of a disease describes the number of new cases occurring within a given time period. Incidence of POAG is much more difficult to measure than prevalence, as whilst measuring prevalence requires only a cross sectional survey, measurement of incidence requires a cohort of subjects to be followed over a period of time. This is a particular problem in POAG as the disease is slowly progressive and so subjects must be followed for many years if an accurate measure of incidence is to be obtained. In general, it is not possible to simply

estimate incidence from age-specific prevalence because prevalence is a function of both incidence and disease duration, between which there is no simple relationship. However it has been suggested that irreversible but non-fatal diseases such as POAG, may be an exception to this, and it may be possible to estimate incidence from age-specific prevalence in these cases (Leske et al., 1981). This method has been used in several epidemiological studies since and gives us a reasonable estimate of incidence in different age-groups and geographical regions.

In white populations at age 55 years estimates of incidence range from 4 to 24 per 10,000 per year, and at age 75 years 20 to 28 per 10,000 per year. In black populations where prevalence of POAG is higher, incidence is of course also greater, with rates of 30 per 10,000 per year in those aged 40-49 years and 105 per 10,000 per year in those aged over 70 years (Leske et al., 2001). Table 1.2 below summarises some of the main studies into the incidence of open-angle glaucoma:

Table 1.2: The incidence of definite open-angle glaucoma in those aged over 40 years in four major studies (after Leske, 2007)

Study, year, follow-up	n*	Population	Average %/year
Dalby, Sweden, 1989, 10yrs	26	1511	0.24
Melbourne, Australia, 2002, 5yrs	12	3271	0.10
Rotterdam, The Netherlands, 2005, 6yrs	29	6780	0.12
Barbados, West Indies, 2007, 9yrs	124	3222	0.50

*number of incident cases identified by each study

1.5 POAG Risk factors

The underlying cause and mechanisms of glaucomatous damage are currently not fully understood, although many risk factors have been identified in epidemiological studies.

1.5.1 Age

Older age is consistently associated with POAG (Boland and Quigley, 2007). People over 70 years old are 3-4 times more likely to develop POAG than 40-50 year olds (Mitchell et al., 1996, Schoff et al., 2001, Mukesh et al., 2002). Older age may account for ganglion cell death by temporal deterioration of supporting tissues, or it may simply be a measure of the length of time a person is exposed to other risk factors (Boland and Quigley, 2007). Figure 1.2 below shows the prevalence of POAG with age as found in two studies in the UK.

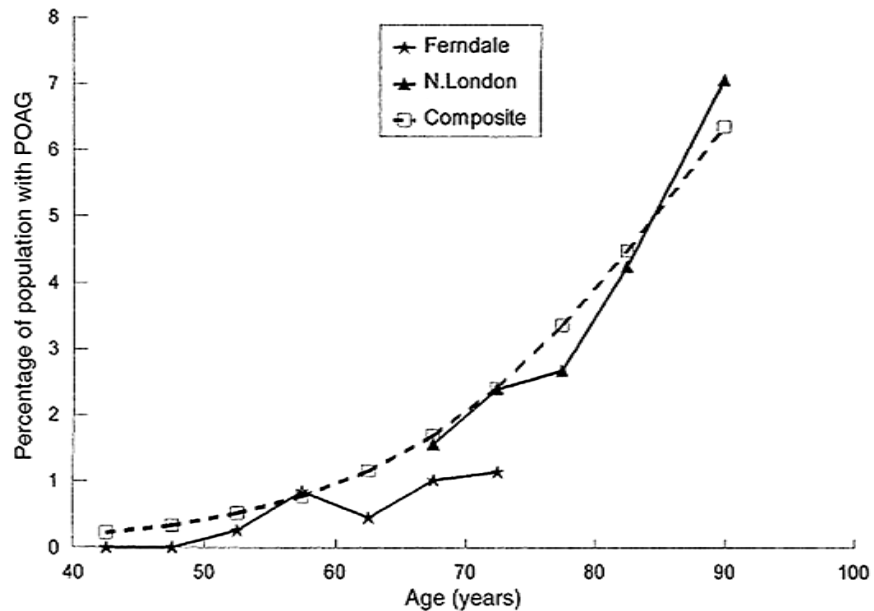


Figure 1.2: Increasing prevalence of POAG with age (after Tuck and Crick, 2003)

1.5.2 Profile of the Individual

Whilst gender as a risk factor for POAG has previously been a controversial issue, a recent meta-analysis of gender differences in POAG prevalence in whites found that men were 1.23 times more likely to have POAG than women (Rudnicka et al., 2006). Ethnicity is difficult to define as a risk factor due to the difficulty in specifying ethnic derivation in surveys. However, in general POAG is significantly more prevalent in black (particularly Afro-Caribbean) populations than any other, and prevalence in Asian and European populations seems similar (Boland and Quigley, 2007, Leske, 2007). Family history of POAG amongst first-degree relatives is another well-known risk factor, although this may be affected by increased awareness and therefore likelihood of being detected amongst first-degree relatives of POAG sufferers (Boland and

Quigley, 2007, Leske, 2007). The lifetime risk of glaucoma has been reported to be nine times higher in first-degree relatives of glaucoma sufferers than in controls (Wolfs et al., 1998) and incidence of glaucoma is doubled in this population (Le et al., 2003). Risk of developing glaucoma has been shown to be higher with sibling family history than with parental family history, especially in twins (Nemesure et al., 1996, Gottfredsdottir et al., 1999).

1.5.3 Ocular Risk Factors

Raised IOP is consistently reported as a major risk factor for POAG, and as the only known modifiable risk factor, it is the subject of many studies. It may be the case that both increased IOP and increased fluctuations in IOP are independent risk factors for POAG, and IOP during sleep has also been suggested as a risk factor (Boland and Quigley, 2007). IOP is, however, limited as a predictor as up to half of patients with open-angle glaucoma have IOPs consistently within the normal range (Kroese and Burton, 2003, Leske, 2007). Figure 1.3 below shows the nine-year relative risk of open-angle glaucoma by baseline IOP.

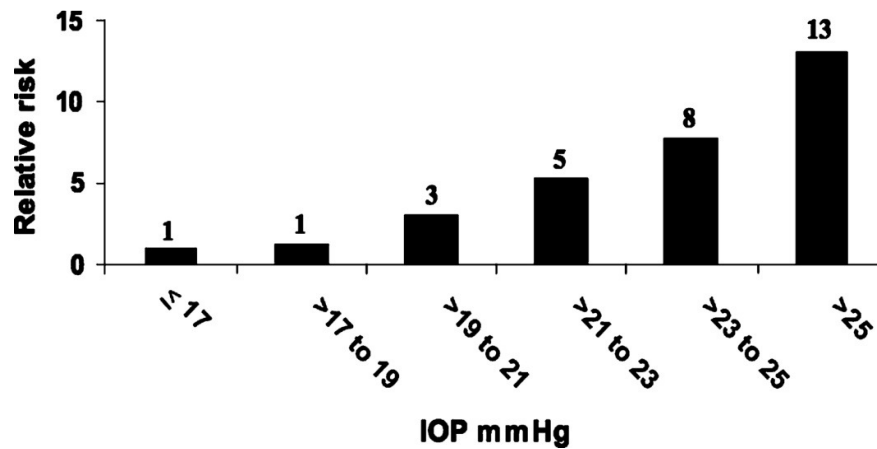


Figure 1.3: Nine-year relative risk of open-angle glaucoma by baseline IOP (after Nemesure et al., 2007)

ONH size has also been investigated as a risk factor for POAG, with larger discs being slightly more at risk (Quigley et al., 1999). This is possibly due to a biomechanical disadvantage of having a larger scleral opening and lamina cribrosa, but morphological studies have shown that larger discs have more nerve fibres and so a potentially greater structural reserve which may delay functional loss (Jonas et al., 1992). One exception to this is in black patients where the

risk factor of commonly large ONH size is compounded by having proportionally less neuro-retinal rim area for a given ONH area than other ethnic groups (Varma et al., 1994).

Refractive error is also a risk factor for POAG, with low myopia (<3.00D) doubling the risk, and higher myopia tripling the risk (Mitchell et al., 1999). The association between myopia and POAG was originally thought to be due to selection bias, with myopes more likely to attend for eye examination, but the association has since been proved, and appears to be independent of IOP (Rudnicka and Owen, 2007, Boland and Quigley, 2007, Mitchell et al., 1999).

Central corneal thickness (CCT) has been proposed as a risk factor for POAG (Gordon et al., 2002). It has been found that patients with thinner CCT are more likely to first present to an ophthalmologist with a greater level of glaucomatous damage than those with thicker CCT (Herndon et al., 2004). There are several possible reasons for this, for example, thin CCT artefactually reduces conventionally measured IOP so a person is likely to be referred later for ocular hypertension (Boland and Quigley, 2007), also a thin CCT may be indicative of a thinner and more elastic lamina cribrosa which increases the vulnerability of the optic nerve to damage (Leske, 2007, Leske et al., 2008). This last theory is supported by the evidence that ocular hypertensive patients (after IOP has been corrected for CCT) without glaucomatous damage generally have thicker than average corneas, suggesting a possible protective mechanism (Herndon et al., 2004).

1.5.4 Systemic Risk Factors

Both low and high blood pressure have previously been reported as risk factors for POAG (Boland and Quigley, 2007). Whilst in theory a high systemic blood pressure may result in greater capillary perfusion to retinal ganglion cells thus helping to prevent POAG, the complications associated with systemic hypertension such as atherosclerosis probably reduce blood flow enough to balance this out and so systemic hypertension bears no significant relationship with POAG (Leske, 2007). However, low ocular perfusion pressure (blood pressure minus IOP) has been associated with POAG in various studies, suggesting that systemic

hypotension in combination with ocular hypertension bears a significant relationship with POAG (Tielsch et al., 1995b, Bonomi et al., 2000).

Previously diabetes mellitus has been quoted as a risk factor for POAG, and it is true that diabetics tend to have higher IOP (Tielsch et al., 1995a). However, epidemiological studies have found no significant association between diabetes and POAG, despite the raised IOP which would normally predispose to POAG (Gordon et al., 2002, Tielsch et al., 1995a). Because of this some now believe that diabetes somehow protects against POAG, although the relationship remains unclear.

Migraine and other vasospastic phenomena such as Raynaud's disease have also been associated with increased risk of POAG (Wang et al., 1997, Broadway and Drance, 1998). The risk of POAG in patients with a history of migraine or severe headache has been reported as increased by several times, particularly for POAG with lower IOP (Phelps and Corbett, 1985). This increased risk has however been disputed, other studies finding no association between headache and POAG (Klein et al., 1993). Any effect of migraine on POAG is thought to be due to a vasospasm as migraine sufferers have been found to have reduced cerebral blood flow (Phelps and Corbett, 1985). There is a logical link between vasospasm and decreased blood flow to the ONH resulting in ganglion cell death, and it has been shown that a history of cold-induced vasospasm or simply cold extremities is more common in certain sub-groups of POAG (those with focal ischaemic ONH damage –discussed in chapter 2.5) (Broadway and Drance, 1998).

1.6 Treatment of POAG

POAG treatment aims to preserve visual function and thereby maintain a certain quality of life, without causing untoward side-effects. At the present time, most treatments are directed solely at the reduction of IOP as this is the only modifiable risk factor for the disease. A 'target pressure' is set at a level below which progression is estimated to be unlikely and treatment aims to keep IOP below this level. Of course, there is no single IOP below which progression does not occur and so the target pressure must be regularly revised for every patient. In some

patients it may not be possible to halt progression by lowering IOP, or it may not be possible to achieve sufficient lowering of IOP to halt disease progression (Weinreb and Khaw, 2004).

There are three main treatment modalities in POAG: medical, laser surgery and incisional surgery. Medical treatment is usually the primary treatment for POAG, with laser or surgical treatment being considered when medical treatment fails to lower IOP sufficiently, the patient experiences severe side-effects of drops, or the patient fails to comply with medical treatment regimens (Wilkins et al., 2007).

1.6.1 Medical Treatment

Medical treatment is usually in the form of topical hypotensive agents which reduce IOP either by increasing aqueous outflow or by reducing aqueous secretion. Prostaglandin analogues increase aqueous outflow by the uveoscleral route and are a common first line of POAG treatment in Europe and the USA due to their effective lowering of IOP, once-daily application, and comparative lack of systemic side-effects (Weinreb and Khaw, 2004). Common side-effects of prostaglandin analogues include increased iris pigmentation, darkening and thickening of the eyelashes, and rarely cystoid macular oedema (Weinreb and Khaw, 2004). Examples of prostaglandin analogues include Latanoprost (Xalatan™) and Travoprost (Travatan™).

Probably the second most widely used form of topical ocular hypotensive medication are β -blockers. These are effective at lowering IOP by reducing aqueous secretion but have more serious systemic side-effects such as bradycardia, increased asthma and bronchospasm. As such β -blockers must be used with care, especially in elderly patients. Examples of topical β -blockers are Timolol (Timoptol™) and Betaxolol (Betoptic™).

Less commonly used as first-line therapy (due to less efficient reduction of IOP) are carbonic anhydrase inhibitors (Dorzolamide, Brinzolamide) which reduce aqueous secretion and have few systemic side-effects (Weinreb and Khaw, 2004). Also less effective than prostaglandin analogues and β -blockers are α 2-agonists (Brimonidine, Apraclonidine) which both decrease aqueous secretion and increase aqueous outflow, albeit with several side-effects including

sedation, and respiratory arrest in children (Weinreb and Khaw, 2004). Miotics (Pilocarpine), which increase aqueous outflow, have historically been used frequently in POAG treatment but are now less common due to the blurring of vision caused by the miosis and the greater efficacy of other medications in lowering IOP.

Other medications currently being trialled for use in POAG include neuroprotective agents. These are drugs already used in Parkinson's disease and stroke which have theoretical benefits in reducing ganglion cell death and therefore preventing progression of POAG. However, there is no clinical evidence as yet that these drugs have any benefit in POAG and so they remain a prospect for the future (Weinreb and Khaw, 2004).

1.6.2 Laser Treatment

Like medical treatment, laser treatment for POAG aims to reduce IOP either by means of increasing aqueous outflow, or by decreasing aqueous secretion. There are two main types of laser treatment for POAG: laser trabeculoplasty, and laser diode cyclophotocoagulation (cyclodiode).

Laser trabeculoplasty (selective or argon) is the most widely used laser treatment in POAG. The procedure involves laser light being directed at the trabecular meshwork inducing a biological change to facilitate aqueous outflow (Weinreb and Khaw, 2004). A high proportion of patients respond to this treatment within the first few months, but most will gradually lose this effect (Weinreb and Khaw, 2004).

Cyclodiode laser tends to be used in advanced POAG when other medical and surgical treatments have failed (Weinreb and Khaw, 2004). Laser light is directed through the sclera and is preferentially absorbed by the ciliary processes which are damaged, reducing aqueous secretion (Weinreb and Khaw, 2004). Cyclodiode laser treatment is somewhat unpredictable, usually has a temporary effect, and often needs to be repeated (Weinreb and Khaw, 2004).

1.6.3 Surgical Treatment

Surgical treatment for POAG aims to reduce IOP by increasing aqueous outflow. The most common surgical procedure is trabeculectomy, which involves the creation of a drainage channel through the full thickness of the sclera into the sub-conjunctival space. The outer sclera is loosely replaced over the channel to create a 'guarded sclerostomy' which allows aqueous to drain from the anterior chamber, collecting under the conjunctiva, whilst providing resistance to prevent hypotony.

Whilst trabeculectomy is rarely performed as a primary treatment for POAG, studies have shown that the risk of failure of trabeculectomy is increased with prolonged hypotensive medication, so surgery, if it is necessary, is normally considered within 1-2 years of starting medical treatment (Wilkins et al., 2007). The main reason for failure of trabeculectomy is fibrosis or healing of the conjunctiva over the scleral flap, preventing aqueous flow out of the flap (Wilkins et al., 2007). In recent years the use of antimetabolites such as 5-Fluorouracil and Mitomycin C which were originally developed as anti-cancer drugs to prevent this fibrosis has halved the failure rate of trabeculectomy in patients considered at risk of this complication (Wilkins et al., 2007, Weinreb and Khaw, 2004).

Following trabeculectomy failure other forms of surgery, most commonly the Molteno Tube, may be considered (Wilkins et al., 2007). In this form of surgery aqueous is allowed to flow out through a tube into the subconjunctival space, though hypotony can be a problem if too much aqueous is allowed to flow out (Wilkins et al., 2007). As an alternative to trabeculectomy, non-penetrating glaucoma surgery may be considered. These procedures (the most common being deep sclerectomy) are similar to a trabeculectomy except no sclerostomy is created. This technique has been reported to lower IOP (though not as efficiently as trabeculectomy) with fewer post-operative complications (Wilkins et al., 2007).

1.7 Recent Major Glaucoma Related Trials

1.7.1 The Ocular Hypertension Treatment Study (OHTS)

This multicentre prospective study compared rate of conversion to POAG in ocular hypertensives with and without topical hypotensive medication. Patients were followed up biannually for at least five years, with the primary outcome measure being reproducible visual field or ONH damage. Treated patients had a mean IOP reduction of 22.5%, compared to 4% reduction in non-treated controls (Kass et al., 2002). With this treatment a 50% reduction in risk of progression to POAG was found, however, over 90% of untreated patients did not convert to POAG during the study period (Kass et al., 2002). The study had a large number of participants and careful follow-up but has since been criticised for its relatively small number of POAG end-points, a number of which had questionable 'normal' status at baseline. Also some of the participants were found to have corneas thick enough to explain their high tonometry readings, which when corrected were actually below the study inclusion criteria. The study highlights the fact that it is not necessary to treat most ocular hypertensives, and that it is necessary to look at the whole risk profile of the patient rather than just IOP when considering treating ocular hypertension.

1.7.2 Collaborative Initial Glaucoma Treatment Study (CIGTS)

This was a randomised clinical trial on 607 newly-diagnosed POAG patients who were treated to obtain a pre-determined reduction of IOP, either by topical medication or trabeculectomy. The main outcome variables investigated were visual field loss and quality of life. After follow-up of 4-5 years no significant difference was found in visual field loss or quality of life between the two treatments, although IOP was further reduced by trabeculectomy (Lichter et al., 2001). Although this study proves the efficacy of medical treatment, it has been widely criticised as follow-up was too short and disease too mild to show significant differences in progression between the two groups. It has also been criticised for a lack of standardisation in the treatments given.

1.7.3 Collaborative Normal Tension Glaucoma Study (CNTGS)

Treatment versus no treatment in normal tension glaucoma was compared in this multi-centre randomised trial, with disease progression being monitored over 5-7 years as the primary outcome measure. Progression occurred in 12% of treated eyes and 35% of controls, which may be because progression was IOP related in a proportion of the treated eyes (Schulzer et al., 1998). What proportion of the untreated eyes would not have progressed if treated is not known. The study had a wide range of patients (excluding only very advanced glaucoma) and good baseline measurements were obtained (at least three consistent visual field plots). However, IOP measurements were not corrected for central corneal thickness, patients were included with IOP up to 24mmHg which is higher than the standard definition of normal tension glaucoma, and whilst disc haemorrhage was used as an inclusion criteria for progression it was not used as an outcome measure. There may also be an issue that patients with severe visual field defects may have reached the limit of their measurable progression and may not progress further (Traverso et al., 2003).

1.7.4 Advanced Glaucoma Intervention Study (AGIS)

Another multi-centre, prospective, randomised study, this time of patients with advanced POAG which cannot be controlled with medical therapy alone. Patients were randomised to two laser/surgical treatment sequences and followed-up at six-monthly intervals for 4-7 years. The study found that eyes which had IOP <18mmHg at every follow-up visit showed no significant visual field progression, whilst eyes with IOP >18mmHg at any point during follow up all showed evidence of visual field progression (Van Veldhuisen et al., 2000). This suggests that both low IOP and low fluctuation of IOP can prevent progression of visual field loss in advanced glaucoma. However, the study used only one visual field test as a baseline, and the spread of visual field progression was very small, achieving statistical significance only by the large number of participants.

1.7.5 Early Manifest Glaucoma Trial (EMGT)

This randomised trial was the first study of treatment vs. no treatment in Caucasian patients with early, previously untreated, POAG; outcome measures being clear visual field progression or glaucomatous ONH damage. The study found that a 25% decrease in IOP and a maximum

absolute IOP of 25mmHg reduced risk of disease progression by 50%, and that risk of progression decreased by 10% with every mmHg of IOP reduction from baseline to initial follow-up (Heijl et al., 2002, Leske et al., 2003). Some untreated patients, however, had not progressed at all after several years of follow-up, supporting the idea that patients with lower risk of progression may be monitored untreated (Traverso et al., 2003).

2. The Optic Nerve Head

2.1 The Healthy Optic Nerve Head

Axons of retinal ganglion cells (RGCs) form the innermost layer of the retina, the RNFL. These axons converge on the ONH to form the approximately one million nerve fibres of the optic nerve. These fibres then leave the eye after traversing the lamina cribrosa, a series of perforated sheets of connective tissue, and synapse in the lateral geniculate nucleus of the brain. (Weinreb and Khaw, 2004)

The circumferential convergence of RGC axons on the ONH leaves a physiological central depression called the cup which is usually visible ophthalmoscopically. The area surrounding the physiological cup is the neuroretinal rim (NRR), made up primarily of ganglion cell axons. (Weinreb and Khaw, 2004)

Healthy ONHs vary widely in area, with a mean of $2.69 \pm 0.70 \text{mm}^2$ (Jonas et al., 1988). It has a vertically oval shape with mean vertical diameter $1.92 \pm 0.29 \text{mm}$ and mean horizontal diameter $1.76 \pm 0.31 \text{mm}$ (Jonas et al., 1988).

The normal optic cup is generally round or horizontally oval. The NRR follows the 'ISNT' configuration, whereby it is thickest inferiorly, followed by superiorly, nasally, and thinnest temporally (Jonas et al., 1988). Three main types of optic cup have historically been reported: a small central 'dimple' cup, usually seen in smaller discs, a larger round 'punched-out' cup which has steep borders and is usually seen in larger discs, and cups with a gradually sloping temporal wall which tend to be in average sized discs (Jonas et al., 1988). The cup/disc (C/D) ratio in healthy optic discs ranges enormously from 0.00 to 0.85 (mean 0.34 ± 0.25) vertically, and from 0.00 to 0.87 (mean 0.39 ± 0.28) horizontally, with larger optic discs and 'punched-out' cups tending to have larger C/D ratios which may be outside this range (Jonas et al., 1988).

2.2 Blood Supply to the Optic Nerve Head

Accurately describing the blood supply to the ONH is not a trivial task, not least because of the necessary complexity of a system which must supply nutrients to a variety of ocular structures without compromising the visual pathway. Many authors have used different techniques both *in-vivo* and *post-mortem* to evaluate the vasculature and the limitations of these techniques make direct comparison between studies difficult. Also, there exists a huge variation in patterns of ONH blood supply between individuals. In a study of 100 human eyes, for example, no two eyes were found to have identical patterns of ONH blood supply (Singh and Dass, 1960). Nevertheless, the ONH can be broadly thought of, in terms of blood supply, as consisting of four distinct regions, described in the anterior-posterior direction below (Flammer et al., 2002, Hayreh, 2001). Figure 2.1 below is a schematic diagram of the blood supply to the optic nerve, and figure 2.2 gives a more detailed view of the ONH blood supply.

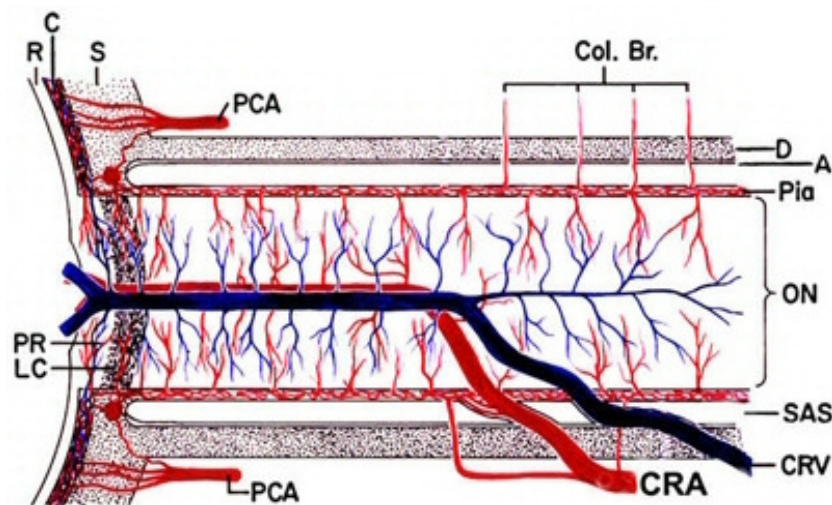


Figure 2.1: Schematic representation of the optic nerve blood supply (after Hayreh, 1974). Abbreviations (clockwise from top left): R=retina, C=choroid, S=sclera, PCA=posterior ciliary artery, Col.Br.=collateral branches, D=dura, A=arachnoid, ON=optic nerve, SAS=subarachnoid space, CRV=central retinal vein, CRA=central retinal artery, LC=lamina cribrosa, PR=prelaminar region

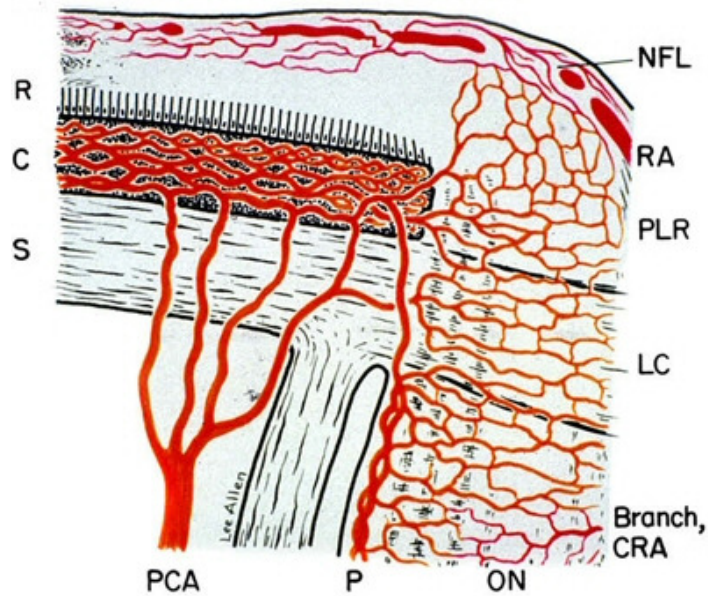


Figure 2.2: Schematic representation of the ONH blood supply (after Hayreh, 1978).

Abbreviations (clockwise from top right): NFL=nerve fibre layer, RA=retinal arteriole, PLR=prelaminar region, LC=lamina cribrosa, CRA=central retinal artery, ON=optic nerve, P=pia, PCA=posterior ciliary artery, S=sclera, C=choroid, R=retina.

2.2.1 Surface Nerve Fibre Layer

This most anteriorly superficial region of the ONH is supplied mainly (or often solely) by small branches of the central retinal artery which become retinal arterioles as they leave this area. In some cases the temporal part of this region is supplied by the posterior ciliary artery circulation from deeper regions.

2.2.2 Prelaminar Region

The region between the surface layer and the lamina cribrosa is supplied by small branches from the peripapillary choroid and short posterior ciliary arteries.

2.2.3 Lamina Cribrosa Region

This region is supplied by branches from the short posterior ciliary arteries, either directly or from the Circle of Haller and Zinn which, when present, is formed by the short posterior ciliary arteries.

2.2.4 Retrolaminar Region

The region immediately posterior to the lamina cribrosa often receives blood from two sources. The first source is from the pial vascular plexus and is present in all cases. The second source is more inconsistent; in some cases the axial centrifugal vascular supply, which is derived from branches of the central retinal artery may also contribute blood to this area.

Drainage of the ONH is solely via the central retinal vein except in the prelaminar region where there is also some drainage into the peripapillary choroidal veins.

2.3 The Optic Nerve Head in Glaucoma 1 –Mechanisms of Damage

POAG is a neurodegenerative disease characterised by the slow, progressive degeneration of RGCs with increasing excavation of the optic cup (Weinreb and Khaw, 2004). The exact mechanisms by which this occurs are poorly understood, and it is thought that POAG is a multifactorial disease. The level of IOP is without doubt related to death of RGCs in at least some POAG patients, but this alone cannot account for all cases of POAG, as up to half have normal IOPs and some continue to progress despite well controlled IOP (Weinreb and Khaw, 2004, Fechtner and Weinreb, 1994). There are several theories of how glaucomatous damage occurs, the main ones being broadly described as the mechanical theory and the vascular theory (although it should be remembered that these two theories are not mutually exclusive).

2.3.1 Mechanical Theory of Damage

Congenital, angle closure and secondary glaucomas show that in many patients raised IOP alone is sufficient to lead to glaucomatous optic neuropathy. The mechanical theory relates to the direct effect of raised IOP on the ONH and RNFL.

The role of IOP as a risk factor may be due to mechanical compression of RGC axons disrupting axoplasmic transport, or altered support of RGC axons due to pressure induced distortion of the lamina cribrosa (Fechtner and Weinreb, 1994, Flammer et al., 2002). Although risk of glaucoma increases with IOP some eyes seem more resistant to high IOP than others. This may be due to

differences in lamina cribrosa structure between individuals (Fechtner and Weinreb, 1994). Pressure-induced changes in extracellular matrix and glial tissue have also been reported in glaucoma, but it is currently unclear whether this is a cause or effect of glaucomatous damage (Fechtner and Weinreb, 1994).

The role of IOP is supported by the beneficial effect of IOP lowering treatment, even in normal-tension glaucoma patients (Collaborative Normal-Tension Glaucoma Study Group, 1998).

2.3.2 Vascular Theory of Damage

The ocular circulation is highly regulated in order to meet the changing metabolic needs of ocular structures under changing visual stimulation, and with varying perfusion pressure. Under normal conditions reduced perfusion pressure or increased metabolic demand is compensated for by a reduction in resistance to flow by alterations in blood vessel diameter (autoregulation).

Comparing studies of ocular circulation in glaucoma is difficult due to the inclusion of patients at different stages of different types of glaucoma in various studies, however generally studies agree that there is reduced ocular perfusion in glaucoma patients (Flammer et al., 2002). It is also the case that there is a generalised reduction in blood flow (involving the ONH, choroidal and retinal circulation) in glaucoma patients (Michelson et al., 1998a, Michelson et al., 1998b), which is more marked both in those with lower IOP (Drance et al., 2001) and those with more rapidly worsening visual field loss (Yamazaki and Drance, 1997). This reduction in blood flow is unlikely to be purely a secondary effect of mechanical factors in glaucoma as it is not confined to the eye; retrobulbar and even peripheral blood flow is also reduced in many patients with glaucoma (Gasser and Flammer, 1991). A study of low-tension glaucoma patients using magnetic resonance imaging found that there was an increased rate of diffuse cerebral small-vessel ischaemic changes in these patients compared to controls, further suggesting a vascular cause for glaucoma, at least in a subgroup of patients (Stroman et al., 1995).

There is some evidence in support of a failure of autoregulation mechanisms in glaucoma. For example, glaucoma patients more often suffer from vasospastic conditions than controls

(Gasser and Flammer, 1991), and vasospasm is associated with progressive glaucoma (Ghergel et al., 2000). Indeed, it has been suggested that in some patients glaucoma is an ocular manifestation of primary vasospastic syndrome (Ghergel et al., 2000). Vasospasm may be considered an independent risk factor for glaucoma, but it should also be regarded as potentially making the eye more susceptible to IOP-related damage.

Another possible factor in glaucomatous damage is reperfusion injury (Flammer et al., 2001), caused by the production of free radicals during reperfusion of temporarily ischaemic tissue leading to a significant increase in oxidative stress. This is consistent with evidence showing that IOP fluctuation is more strongly correlated to progression of visual field damage than mean IOP.

2.4 The Optic Nerve Head in Glaucoma 2 –Signs of Damage

2.4.1 Cup/Disc (C/D) Ratio

Classically, the measurement or estimation of C/D ratio has been a mainstay of glaucoma assessment, with a large C/D ratio being a common sign of POAG. When assessing C/D ratio a major consideration is the size of the ONH itself. As shown in figure 2.3, physiological cup size increases with disc size, meaning that whilst a C/D ratio of 0.55 may be perfectly normal in a large disc, it could also be pathological in a small disc. In population based studies it has been found that less than 2.5% of healthy eyes have C/D ratio greater than 0.7 (assuming a Gaussian distribution), but it is important to note that this alone is not particularly useful in glaucoma assessment (Garway-Heath et al., 1998) and that using a cut off of 0.5 still only yields a 52% sensitivity and 89% specificity for detection of POAG in the general population (Garway-Heath et al., 1998). It should also be noted that this is a difficult area to study as there is considerable inter-racial variability in ONH size so results are highly dependent on the population studied. As glaucomatous damage has been shown to preferentially affect the superior and inferior NRR, it is usual to assess the C/D ratio in the vertical meridian as this is logically more sensitive to glaucomatous damage. Another problem with using C/D ratio in glaucoma assessment is inter-observer variability, which can be reduced by using a stereo method to view the ONH (Garway-

Heath et al., 1998). There is also a small but significant non-pathological increase in cup size with age (Garway-Heath et al., 1998).

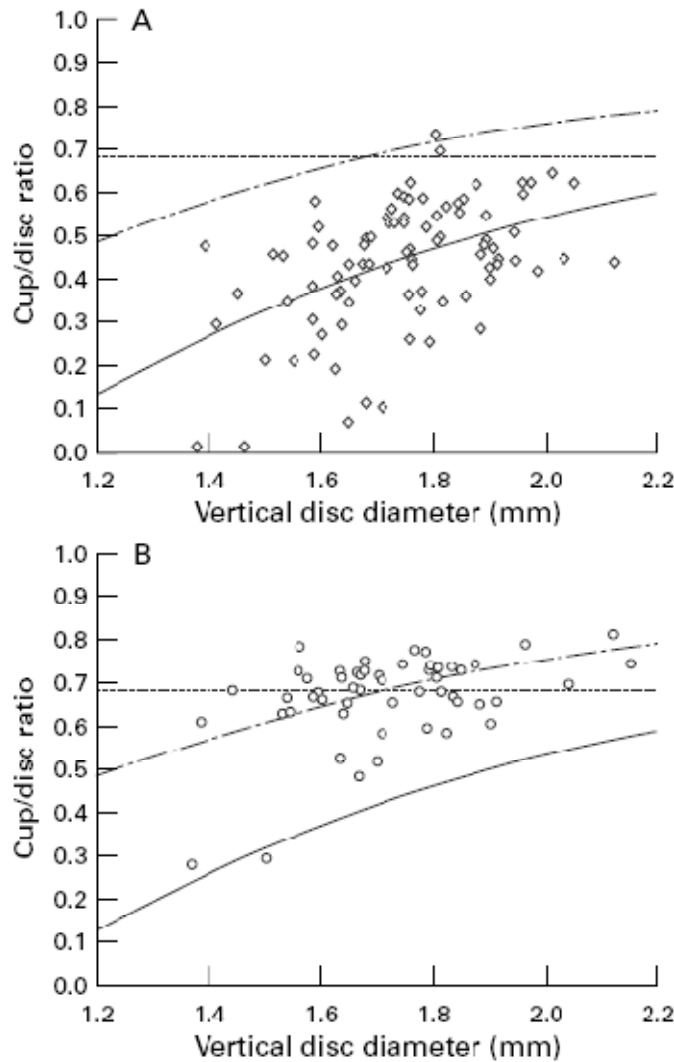


Figure 2.3: Plot of vertical C/D ratio against vertical ONH diameter in (A) control subjects and (B) glaucoma patients.

Solid curve: ONH size dependent mean

Broken curve: ONH size dependent upper limit of normal

Dotted line: ONH size independent upper limit of normal

(after Garway-Heath et al.,1998)

2.4.2 Neuroretinal Rim

In assessing an ONH for POAG it is important to consider the appearance of the NRR; indeed, due to the wide variation of C/D ratios in normals, changes in NRR width and shape may provide more useful information in diagnosis of POAG (Susanna and Vessani, 2007). In healthy eyes, the NRR width follows a characteristic 'ISNT' configuration as previously mentioned, and an ONH of normal shape which does not obey the ISNT rule must be viewed as suspected POAG irrespective of cup size. A recent study has shown that the ISNT rule holds true in 78% of

normal eyes and is broken in 72% of glaucomatous eyes (Harizman et al., 2006). In POAG, NRR is lost in all sectors of the disc with regional preferences, depending on the stage and type of disease (Jonas et al., 1999). In early POAG NRR loss occurs predominantly in the infero-temporal and supero-temporal areas, followed later by the temporal area, and finally the nasal area as the disease progresses (Jonas et al., 1999). Figure 2.4 illustrates some of the more common progressions of glaucomatous ONH damage. Pallor of the NRR more often suggests a non-glaucomatous optic neuropathy (Jonas et al., 1999, Susanna and Vessani, 2007).

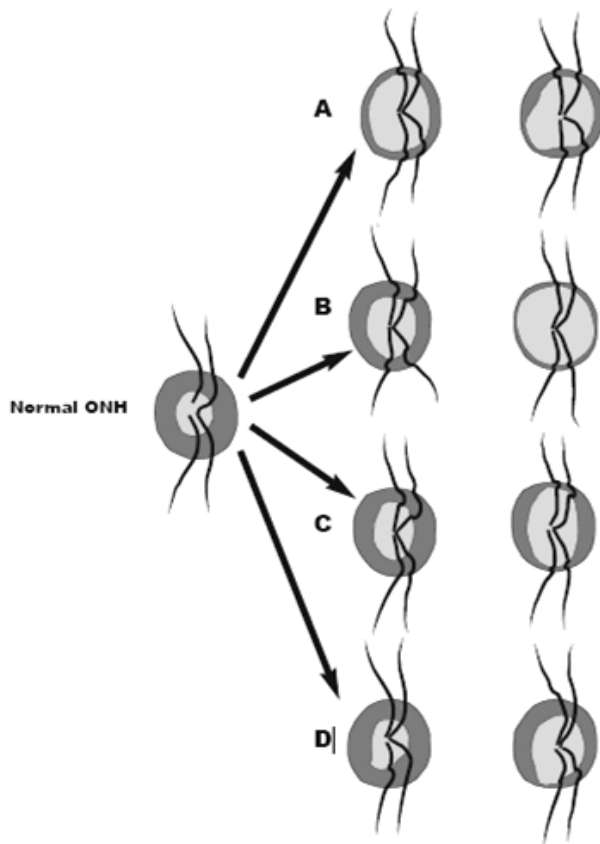


Figure 2.4: Illustration of four common progressions of glaucomatous damage: (A) Combined localized and diffuse NRR loss, (B) Concentric NRR loss, (C) Superior and inferior polar NRR notching, (D) Focal NRR loss/notch (after Traverso et al., 2003)

2.4.3 Blood Vessels

Various changes in ONH blood vessels have been reported as subtle signs of POAG. These include barring of a circumlinear vessel, 'flyover' vessels, 'bayonetting', focal and diffuse thinning of arterioles, and nasalisation of larger blood vessels. These are all non-specific to POAG but

should serve to alert the clinician to the possibility of glaucomatous damage, or aid in the assessment of unusual ONHs.

A far more specific vascular sign of POAG is ONH margin haemorrhage (figure 2.5). These flame or splinter shaped haemorrhages are very rarely found in normal eyes, but are found in 4 to 7% of glaucomatous eyes (Jonas et al., 1999, Susanna and Vessani, 2007). They are often subtle and easily missed but usually occur at the supero- or infero-temporal ONH margins (Jonas et al., 1999, Susanna and Vessani, 2007). Haemorrhages are commonly associated with localised areas of RNFL loss or NRR notching and are 99% specific to POAG, even in cases without measurable visual field loss (Jonas et al., 1999, Susanna and Vessani, 2007).

It has been shown in several studies that the presence of spontaneous venous pulsation (SVP) at the ONH is reduced in POAG (Nicolela, 2007). SVP is present in 98% of healthy subjects and only 50% of those with POAG (Morgan et al., 2004). It has been suggested that the reason for this is an increased resistance to blood flow in the central retinal vein as it exits the eye; this explanation also being applicable to the increased risk of central and hemiretinal vein occlusions, and the ONH haemorrhages observed in POAG (Nicolela, 2007).

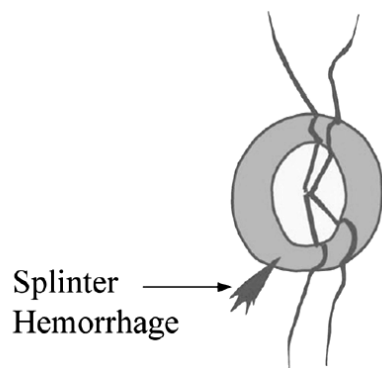


Figure 2.5: Illustration of an inferior splinter haemorrhage (after Traverso et al., 2003)

2.4.4 Lamina Cribrosa

Another non-specific sign of POAG is the visualisation of lamina cribrosa pores. Whilst more common in glaucomatous eyes, these pores are also visible in many normal eyes with large physiological cups (Susanna and Medeiros, 2006). It has also been proposed that the shape of

the pores relates to the severity of visual field damage, with greater ovalisation correlating to more severe visual field loss (Susanna and Medeiros, 2006).

2.4.5 Peripapillary Atrophy

Peripapillary chorioretinal atrophy (PPA) is the thinning and degeneration of the chorioretinal tissue surrounding the ONH. PPA can be divided into two areas, a more peripheral zone α and a central zone β (figure 2.6). α -PPA is characterised by a region of irregular hyper- and hypopigmentation of the retinal pigment epithelium and intimated thinning of the chorioretinal tissue layer. α -PPA is present in many normal eyes as well as glaucomatous eyes, but its size and frequency is increased in POAG, and is related to stage of disease (Jonas et al., 1989, Susanna and Vessani, 2007). β -PPA is characterised by RPE and choriocapillaris atrophy leading to visibility of large underlying choroidal blood vessels and sclera. β -PPA is much more common in glaucomatous eyes than in normals and its extent is again related to stage of disease (Jonas et al., 1989, Susanna and Vessani, 2007). As such, β -PPA can be a sign of POAG, and it is specific to POAG in that non-glaucomatous optic neuropathy is not associated with increased PPA (Susanna and Vessani, 2007). PPA must however be distinguished from the scleral crescent present in highly myopic eyes and those with tilted discs.

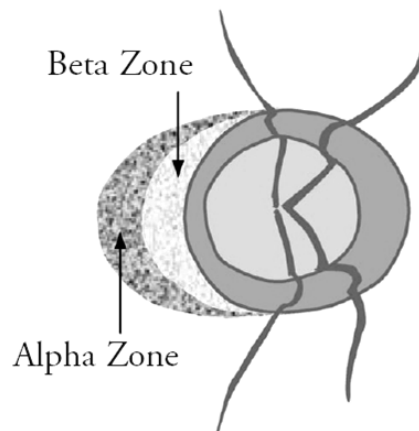


Figure 2.6: Illustration of α - and β -PPA (after Traverso et al., 2003)

2.4.6 Retinal Nerve Fibre Layer

As the RNFL is damaged in POAG a general decrease in brightness can be seen by ophthalmoscopy, associated with an increased clarity of underlying retinal blood vessels. Localised loss of RNFL occurs in around 20% of glaucomatous eyes and appears as wedge-

shaped dark areas emanating from the ONH (Susanna and Vessani, 2007). These signs are, however, non-specific and can occur due to non-glaucomatous optic neuropathy. It should also be noted that there is a physiological decrease in RNFL visibility with age (Susanna and Vessani, 2007).

2.5 The Optic Nerve Head in Glaucoma 3 -Types of Damage

It has been suggested that there are different types of glaucomatous ONH damage, each caused by slightly different mechanisms with commensurate variations in functional loss. Whilst the majority of glaucomatous discs appear to have features of two or more disc types, possibly as a result of combined pathological processes, four types of glaucomatous optic disc have been proposed: focal, myopic, senile sclerotic, and generalised optic cup enlargement (Broadway et al., 1999).

2.5.1 Focal Glaucomatous Optic Disc (Type 1)

Discs of this type are characterised by focal loss of tissue leading to 'notching' of the NRR. Notching tends to occur in smaller discs, emanates from the optic cup, and may or may not reach the disc margins (Broadway et al., 1999). Eyes with this type of glaucomatous damage usually have associated localised visual field defects (although these may be in combination with diffuse defects) and flame haemorrhages (Broadway et al., 1999). The predominance of superior field defects in glaucoma corresponds to a predominance of infero-temporal focal notching (Broadway et al., 1999). It has been suggested that focal damage of this type may occur due to a localised area of weakness in the lamina cribrosa, or a localised vascular event such as might cause an associated flame haemorrhage (Fechtner and Weinreb, 1994). Figure 2.7 shows an example of a typical focal glaucomatous optic disc with infero-temporal loss of NRR.

Figure 2.7: Focal Glaucomatous (Type 1) ONH showing inferior focal NRR loss (after Broadway et al., 1999)



2.5.2 Myopic Glaucomatous Optic Disc (Type 2)

Discs of this type are tilted due to oblique entry of the optic nerve to the eye, have a temporal crescent of PPA, and usually show superior or inferior thinning of the NRR (Broadway et al., 1999). Myopic glaucomatous discs also show localised visual field loss which is often associated with a diffuse loss, however the localised defects do not show the same degree of superior predominance as in focal glaucoma (Broadway et al., 1999). Figure 2.8 shows a typical myopic glaucomatous optic disc, tilted with a temporal crescent of PPA, the disc exhibits thinning of the superior and inferior NRR.

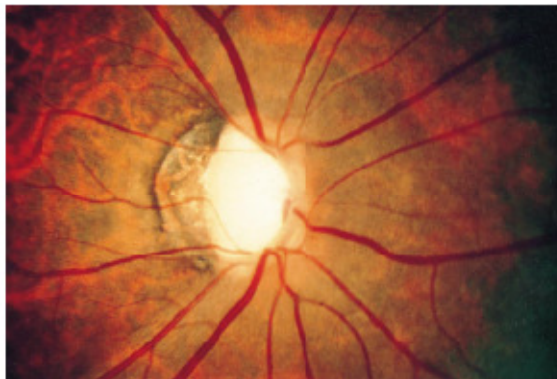


Figure 2.8: Myopic glaucomatous (Type 2) ONH with polar notching, tilted appearance and temporal PPA (after Broadway et al., 1999)

2.5.3 Senile Sclerotic (Atrophic Glaucomatous) Optic Discs (Type 3)

In this type of disc, which occurs mainly in older patients, diffuse NRR tissue loss results in a reduction of rim tissue density without rim area or volume loss (Broadway et al., 1999). Typically a 'moth-eaten' appearance is visible, along with saucerisation of the cup (enlargement of a shallow cup with sloping margins). These discs are usually associated with a complete ring of PPA and are usually larger in size (Broadway et al., 1999). Non-specific visual field loss

results, but this is rarely dense and does not commonly threaten fixation (Broadway et al., 1999). It is possible that this type of damage occurs as a result of a generalised reduction in blood flow to the ONH (Fechtner and Weinreb, 1994). Figure 2.9 shows a typical senile sclerotic glaucomatous optic disc. It has a complete ring of PPA and a shallow, saucerised cup.

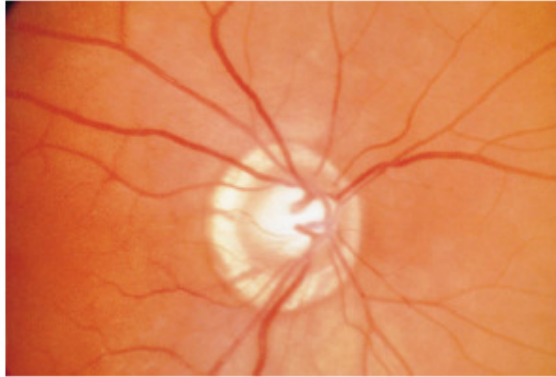
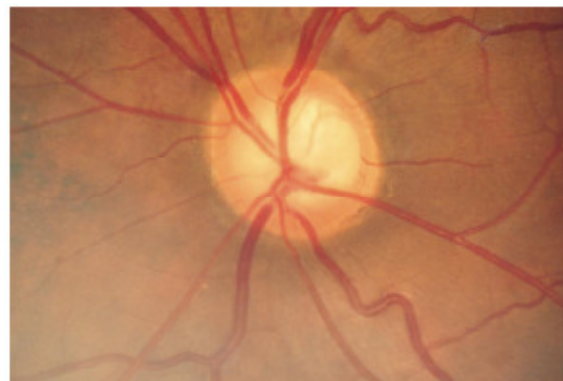


Figure 2.9: Senile sclerotic (Type 3) glaucomatous ONH with diffuse thinning of NRR and complete ring of PPA (after Broadway et al., 1999)

2.5.4 Generalised Enlargement of the Optic Cup (Type 4)

These discs are characterised by enlarged, round cups, without moth-eaten appearance of the remaining NRR tissue (Broadway et al., 1999). This tends to occur in moderate to large discs, and those with larger physiological cups (Broadway et al., 1999). This type of disc damage results in variable and often ill-defined field loss, and is associated with significantly higher pre-treatment IOP than other types (Broadway et al., 1999). It has been proposed that this type of damage occurs due to the mechanical effect of raised IOP causing distortion of the lamina cribrosa, which impinges on retinal ganglion cell axons (Fechtner and Weinreb, 1994). Figure 2.10 shows a glaucomatous disc with generalised, concentric enlargement of the optic cup.

Figure 2.10 Glaucomatous ONH with generalised cup enlargement (Type 4) (after Broadway et al., 1999)



3. Current Optic Nerve Head Imaging Methods in Glaucoma

3.1 Traditional Methods

3.1.1 Direct and Binocular Indirect Ophthalmoscopy

Traditionally the direct ophthalmoscope has been the most popular instrument for examination of the ONH. It provides an easy and accessible way for clinicians to view the ONH, usually without pupil dilation, and it can be used on any patient including those unable to reach table-mounted instruments such as slit lamp biomicroscopes. Direct ophthalmoscopy provides an upright and magnified non-stereoscopic image of the ONH and the projected size of the ophthalmoscope aperture onto the retina can be used as a reference for subjective evaluation of ONH size. In many situations such as domiciliary visits and most general medical practitioner's surgeries the direct ophthalmoscope may be the only practical method of viewing the ONH.

More recently slit lamp binocular indirect ophthalmoscopy, whereby a slit lamp biomicroscope is used in conjunction with a high powered convex lens to view the retina has become the standard method for ONH examination. The view obtained by this method is inverted and magnified, but importantly, through a dilated pupil it is binocular, allowing stereoscopic evaluation of the ONH. As the ONH is a three-dimensional structure this is a great advantage and widely regarded as the most accurate method of disc assessment. The vertical slit height adjustment in conjunction with the graticule on the slit lamp can also be used with a correction factor for magnification to estimate the size of structures such as the ONH.

3.1.2 Fundus Photography

Modern fundus cameras are indirect ophthalmoscopes with a photographic capability that gives high-resolution images of the ONH and surrounding retina creating a permanent record for future comparison, useful in detecting change. By taking two photographs from slightly different angles it is possible to create a stereo pair which can be viewed using binocular

techniques to obtain a three-dimensional image. With the latest software, magnification corrected measurements can be taken from photographs but evaluation of images is still subjective.

3.2 Newer Technologies

The ability of clinicians to discriminate between healthy and glaucomatous eyes based solely on the subjective evaluation of ONH appearance is limited (Abrams et al., 1994), yet this assessment is essential in the diagnosis of POAG, especially as ONH changes often precede detectable visual field loss (Sommer et al., 1991a, Chauhan et al., 2001). As a result of this, the use of imaging systems to aid diagnosis and follow-up of POAG is becoming more widespread. Studies have shown that whilst none of these systems are likely to perform better than a glaucoma specialist clinician viewing stereo-photographs, they can all perform at a similar level, and have the potential to aid detection and monitoring of POAG (Reus et al., 2007, Medeiros et al., 2004, Lin et al., 2007). Unfortunately methodological differences between studies in an area that is fraught with potential biases make direct comparisons of diagnostic ability between instruments very difficult. Furthermore, whilst very high sensitivity and specificity estimates are quoted for these instruments it is often the case that studies only include those with marked structural or functional damage. This means that those cases where diagnosis is difficult and where these instruments could be most useful are excluded, and as such these estimates of diagnostic performance are probably not applicable to general clinical use. Objective techniques such as these may be more useful in detection and monitoring of progressive structural damage (Artes and Chauhan, 2005), however evidence for this is currently limited due to the difficulty of collecting and interpreting longitudinal data in a rapidly evolving field (Artes, 2008).

3.2.1 Optical Coherence Tomography

Optical Coherence Tomography (OCT) is a non-invasive method of producing high definition, two or three dimensional images at high speed, and can be thought of as analogous to ultrasound but using light rather than sound. Low-coherence interferometry is used to measure echo time delay and magnitude of reflected or backscattered light. Transverse scanning then allows false-colour or greyscale cross-sectional imaging of tissues. The latest commercial ultra-

high resolution OCT scanners are capable of imaging to an axial resolution of less than 5µm, though transverse resolution is far inferior to standard fundus photography. The glaucoma algorithm built-in to the latest models measures RNFL thickness along a 3.4mm diameter circle centred on the ONH, which can be presented graphically, as well as in a spreadsheet format where measurements are given for each quadrant and clock hour. For this analysis, studies have shown the superior and inferior quadrants to be the most useful in detecting glaucomatous damage, and comparison of the symmetry between superior and inferior RNFL thickness to have 95% sensitivity at 100% specificity for detection of POAG with visual field loss or clear glaucomatous ONH damage (Hougaard et al., 2004). The OCT also produces 3-dimensional images and topographic measurements of the ONH itself, based on 6 radial scans for which the most sensitive analysis appears to be the 'integrated rim volume', which performs at a similar level to RNFL analysis (Lin et al., 2007). Area under receiver operating characteristic (ROC) curves for detection of glaucomatous visual field damage has been reported as 0.90 to 0.96 in various studies using the highest performing OCT measurements (Lin et al., 2007).

3.2.2 Scanning Laser Polarimetry

Scanning laser polarimetry is currently commercially available as the GDx VCC (Carl Zeiss Meditec, USA). The instrument measures peripapillary RNFL thickness by assessing the change in polarisation of a laser beam reflected back from the retina. This change in polarisation occurs due to the birefringent properties of the RNFL, and transverse and longitudinal scanning with a 780nm wavelength laser produces an image of the ONH and peripapillary retina. The device measures RNFL thickness across the entire image, and thickness along a 3.2mm diameter annulus around the ONH is represented graphically. Consecutive scans can be assessed for progression, based on the RNFL thickness measurements across the entire image, and RNFL thickness in single scans is compared to a normative database. One advantage of the GDx VCC is that one of the measurements provided (the nerve fibre indicator) is a single number which aims to give the likelihood of glaucomatous RNFL damage. This is based on the entire image and allows for easy interpretation.

The main problems with scanning laser polarimetry are poor axial resolution (approx 100µm) and corneal birefringence which contributes to the change in polarisation of the laser signal. Early versions of the GDx had fixed compensation for this but there is significant variation in corneal birefringence between individuals, as well as change over time. The GDx VCC (variable corneal compensation) incorporates individual compensation to counter corneal birefringence.

In the majority of studies of the GDx VCC the highest performing parameter was the nerve fibre indicator, with area under ROC curves quoted from 0.87-0.94 (Lin et al., 2007). Sensitivity for detecting glaucoma has been quoted as high as 91.7% at 95% specificity, which was slightly better than glaucoma specialist clinicians viewing stereo-photographs in the same study (Reus et al., 2007), although images were selected on the basis of subjectively 'normal' or 'glaucomatous' discs, thus eliminating discs which may be difficult to classify .

3.2.3 Confocal Scanning Laser Ophthalmoscopy

In confocal scanning laser ophthalmoscopy (CSLO) the reflected image of a 670nm diode laser scanned across an area of the fundus, is captured as a 2-dimensional scan. The laser beam focus and a confocal aperture are moved in the anterior-posterior direction to obtain a series of 32 images that are then aligned to form a 3-dimensional image of the ONH and surrounding area. Changes in reflectance intensity are used to create a topographic map and produce ONH parameters, most of which also require the manual input of a user-defined ONH margin.

CSLO is commercially available in the Heidelberg Retina Tomograph (HRT), currently in its third incarnation (Heidelberg Engineering GmbH, Heidelberg, Germany). Algorithms which aim to aid glaucoma diagnosis such as Moorfields Regression Analysis (MRA) and the more recently developed Glaucoma Probability Score (GPS) are included in the instrument's software package. MRA compares the neuroretinal rim area in six sectors of the optic disc to a normative database (Garway-Heath and Hitchings, 1998) after taking into account subject age and ONH area, reporting on whether the NRR is within (larger than 95th percentile of normative data), borderline (between 95th and 99.9th percentile of normative data) or outside (less than 99.9th percentile of normative data) normal limits. GPS uses a machine-learning classification system

based on the three-dimensional shape of the ONH and peripapillary RNFL, compared to databases of healthy and glaucomatous eyes, reporting probability of damage in ONH sectors similar to MRA. For MRA the reported sensitivity in various studies varies from 58-80% at 95% specificity (Lin et al., 2007), with the wide variation being due to difficulties in defining inclusion criteria as well as outcome measures in study populations. Diagnostic performance of GPS is similar to that of MRA, however results sometimes differ in the same eye due to the different parameters measured (Coops et al., 2006). MRA and GPS have also been reported as varying widely with variations in optic disc size, producing a high number of false positives in larger discs, and having low sensitivity for detection of POAG in smaller discs (Coops et al., 2006) however this disc size dependence can be reduced through the use of quantile regression to set normative limits (Artes and Crabb, 2010). However, HRT diagnostic parameters are comparable to glaucoma specialist clinicians viewing stereoscopic photographs in their ability to differentiate between normal and glaucomatous discs (Reus et al., 2007).

The HRT also incorporates a dedicated tool for detection of progression which has been shown to detect glaucomatous change in ONHs not detectable by perimetry (Chauhan et al., 2000, Chauhan et al., 2001, Artes and Chauhan, 2005). Whilst there is considerable overlap, visual field measurement may also detect progression not detectable by HRT, and so used together, the two instruments complement each other in the clinical detection of POAG progression.

3.3 Techniques for measurement of optic nerve head blood flow and oxygenation

Due to the associations between vascular changes and glaucoma discussed in section 2.3.2 there is considerable interest in measuring ONH perfusion and oxygenation in glaucoma. Many techniques have been used, and there is no single technique able to provide all the relevant information. Since there are so many techniques, and since different techniques measure different aspects of ocular perfusion at different points in the eye making comparisons difficult, only the most pertinent techniques for measurement of ONH perfusion in glaucoma will be discussed here.

3.3.1 Angiography

Fluorescein Angiography photographically records the passage of fluorescent dye through ocular blood vessels. Due to the presence of tight junctions in the endothelium of retinal vessels the injected fluorescein is unable to pass out of the vessels in the healthy eye enabling visualisation of retinal circulation in detail and ONH circulation to some extent (Flammer et al., 2002). Some quantification of arterial-venous passage time is possible but this may not be well related to ocular blood flow (Tomic et al., 2001). As such angiography is infrequently used in glaucoma studies.

3.3.2 Laser Doppler Velocimetry and Flowmetry

The Doppler effect describes the frequency shift of a light wave emitted from an object which is moving relative to the observer. Wavelength increases as objects move away from the observer ('red-shift') and decreases as objects move towards an observer ('blue-shift'). Using lasers it is possible to detect Doppler shifts with high resolution, and the technique has been used for many years for measurement of red blood cell velocity in ocular blood vessels (Riva et al., 1972).

Laser Doppler Velocimetry measures blood flow velocity by measurement of the Doppler shift in a laser directed at a blood vessel. Along with a measurement of vessel diameter blood flow can be calculated (Mendel et al., 1993), however this technique is limited as the data from a single vessel may not be representative of the entire eye .

Laser Doppler Flowmetry measures relative velocities, red blood cell count and flux at a fixed spot (Riva et al., 1992). By directing the laser at areas between vessels blood flow in capillary beds can be measured, although it is important to know the depth of penetration of the light used in order to know which tissue is being measured. Tissue at different depths can be studied by varying the wavelength of the laser used. Measurements are, however, limited to small selected areas and it is difficult to know the exact volume of the tissue measured making comparisons between patients difficult. The Heidelberg Retina Flowmeter combines this technique with confocal scanning laser tomography, however reproducibility is poor due to its

high sensitivity to changes in illumination and small changes in sample window placement (Flammer et al., 2002).

3.3.3 Multispectral Imaging

Multispectral imaging (also called spectral or hyperspectral imaging) is a technique whereby tissue is imaged using multiple different wavelengths of light. The technique has been widely used in neuroscience for functional brain imaging of animal models, directly measuring changes in brain tissue oxygenation in response to sensory stimuli (Malonek and Grinvald, 1996, Mayhew et al., 1999, Berwick et al., 2005). The technique relies on the wavelength-dependency of light absorption by retinal blood components (chromophores, oxy- and deoxyhaemoglobin, figure 3.1) to calculate oxygenation of the imaged tissue. One common way to do this is to use a Beer-Lambert law model (equation 1).

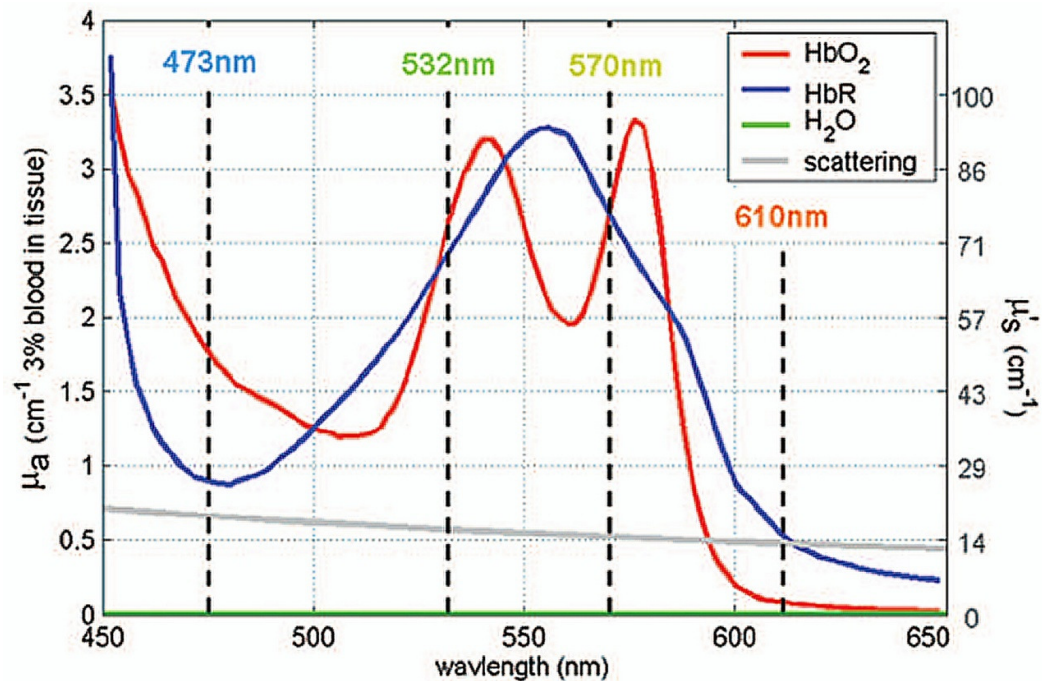


Figure 3.1: Absorption spectra of oxyhaemoglobin (HbO₂), deoxyhaemoglobin (HbR), water (H₂O) and tissue scattering components of blood (after Hillman, 2007).

$$A(\lambda) = c_1\varepsilon_1(\lambda) + c_2\varepsilon_2(\lambda) + c_3\varepsilon_3(\lambda) + c_4\varepsilon_4(\lambda) \dots$$

Equation 1: The Beer-Lambert Law. $A(\lambda)$ =absorption at wavelength λ , c_1 =concentration of chromophore 1, $\varepsilon_1(\lambda)$ =absorbance of chromophore 1 at wavelength λ (known constant), etc.

By imaging at different wavelengths where the contribution to overall absorption by each chromophore is different, the above equation can be solved to find the concentration of each chromophore (oxyhaemoglobin, deoxyhaemoglobin and tissue scattering in this case). The Beer-Lambert law makes several assumptions however, two of which are broken in the eye. The law assumes that the absorbing medium is homogeneously distributed, which it is not, and that the incident light at each wavelength is parallel and travels the same length in the absorbing medium, which it does not as longer wavelengths penetrate deeper (Delori et al., 1977).

Despite these limitations, multispectral imaging provides reasonable estimates of relative oxygenation of imaged tissues, and as such, variations on the technique described have been used with some success in measuring relative oxygenation of retinal blood vessels (Beach et al., 1999, Hardarson et al., 2006), parapapillary and ONH structures (Khoobehi et al., 2004, Beach et al., 2007, Ito et al., 2008), and oxygenation changes in response to medication (Siesky et al., 2008, Traustason et al., 2009).

4. The Visual Field in Glaucoma

4.1 The Normal Visual Field

The visual field is defined as the portion of space that one eye can see at any given instant. For a bright stimulus the extent of the normal visual field, assuming no restrictions due to facial structure etc, is: 60 degrees superiorly, 75 degrees inferiorly, 100 degrees temporally and 60 degrees nasally (Henson, 2000).

The visual field has classically been likened to an island of vision in a sea of darkness. The sensitivity of the eye varies across the visual field. This can be likened to the elevation of the island, or 'hill of vision'. Stimuli whose parameters place them above the hill are too weak to be seen, and stimuli who fall outside the island are outside the field of view and cannot be seen no matter how bright or large they are (Henson, 2000). Under photopic conditions there is a gradual rise in elevation from the edge to the centre of the island which represents increasing sensitivity of the retina from the periphery to the fovea. There is also a physiological blind spot in the temporal field which represents the projection of the ONH where there are no photoreceptors. The main difference between a geographical island and the visual field is that visual field sensitivity varies with light adaptation, whereas geographical islands are fixed (Henson, 2000). With age there is a generalised loss of visual field sensitivity which affects the central field and periphery more than the paracentral area, meaning that the slopes of the island of vision become more convex (Haas et al., 1986). This is partly due to pre-retinal factors such as decreased pupil size and clouding of ocular media, but it has been shown to be primarily due to neural factors such as the decline of photoreceptors and retinal ganglion cells (Johnson et al., 1989). A visual field defect could be described as a deviation (depression in sensitivity) from the normal age-corrected island of vision. Figure 4.1 shows the hill of vision and the seen visual field projection for a number of scenarios.

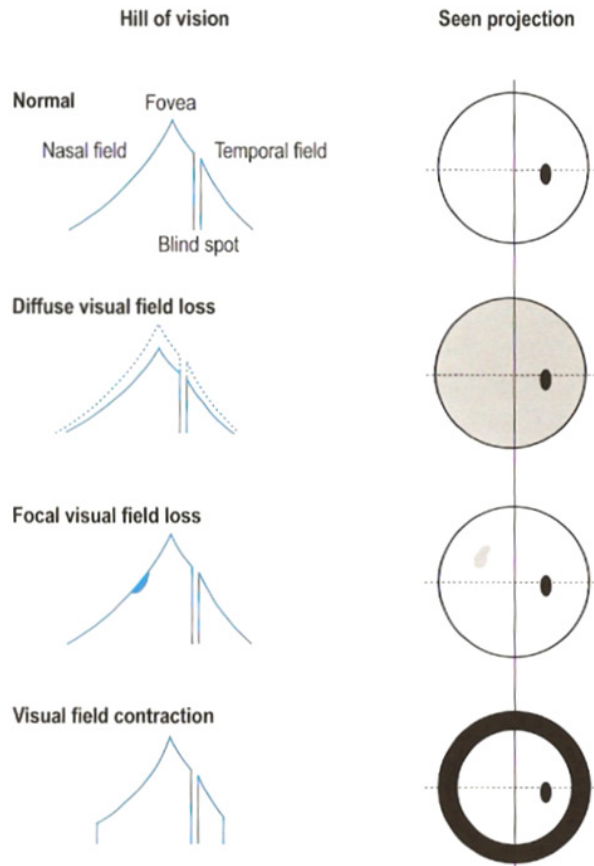


Figure 4.1: Illustration of the hill of vision (sensitivity profile) and corresponding seen visual fields (after Cubbidge, 2005)

4.2 Perimetry

Perimetry is the measurement of the visual field and is a direct measure of visual function. It is one of the few techniques which evaluate peripheral retina and the neural pathways responsible for relaying information from the peripheral retina to the visual cortex (Henson, 2000). Perimetry is used in both detection/diagnosis and monitoring of glaucoma. Glaucoma often causes characteristic visual field defects which can aid detection and diagnosis of the disease, and subsequent management aims to preserve visual function as measured by perimetry.

4.3 Patterns of Glaucomatous Damage

The classically described (initially by Bjerrum in the 19th Century (Bjerrum, 1889)) 'characteristic' patterns of visual field loss in POAG are governed by the retinotopic distribution and arrangement of the retinal nerve fibres, as shown in figure 4.2.

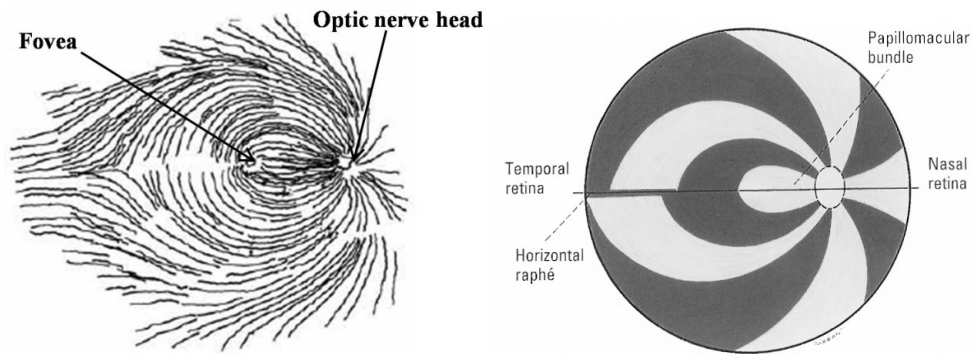


Figure 4.2: (Left) The anatomical distribution of retinal nerve fibres as traced from a silver-stained retina (after Fitzgibbon and Taylor, 1996) and (Right) a schematic diagram of the same (after Kanski, 2003)

Repeatable visual field defects are often preceded by an increase in variability and fluctuation in the visual field (Flammer et al., 1984) and a small diffuse loss in sensitivity across the visual field (Henson et al., 1999). Visual field defects commonly associated with POAG are as follows (Henson, 2000, Henson and Harper, 2007, Rudnicka and Edgar, 2007) and a typical progression of visual field damage in glaucoma is shown in figure 4.3.

4.3.4 Paracentral defects

Paracentral defects are isolated scotomata which may be relative or absolute and most commonly affect the superior visual field. These defects follow the arcuate pattern of the retinal nerve fibres.

4.3.5 Arcuate defects

Arcuate defects are formed by coalescence of paracentral scotomata. These defects are specific to optic nerve head lesions (most commonly POAG) in the absence of other pathology such as branch retinal vein occlusion or arcuate-shaped chorioretinal lesion.

4.3.6 Nasal step

A 'nasal step' is an asymmetry in contrast sensitivity either side of the horizontal midline in the nasal visual field. This occurs because retinal nerve fibres do not cross the horizontal midline and is a highly specific sign of POAG.

4.3.7 Overall depression in sensitivity

This is non-specific to POAG and can commonly be caused by cataract and physiological ageing. The extent of purely glaucomatous diffuse loss is often slight and difficult to detect clinically, although it is very often present alongside localised loss.

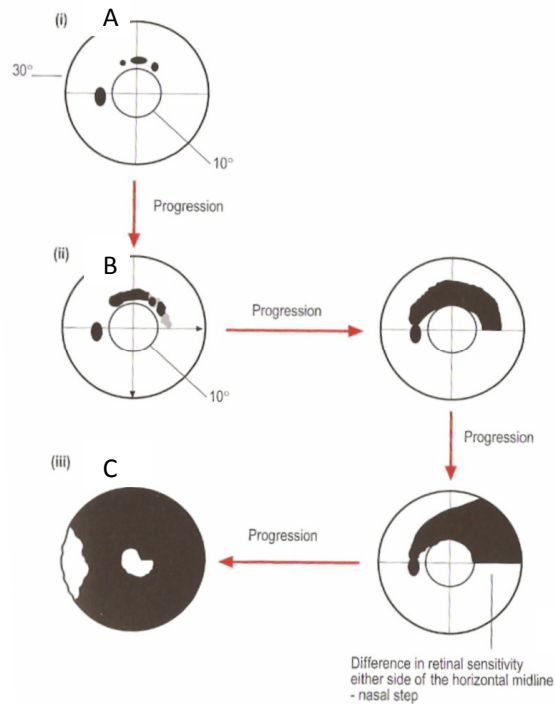


Figure 4.3: Illustration of typical progression of visual field damage patterns in glaucoma (after Rudnicka and Edgar, 2007)

(A) Isolated paracentral scotomata following the course of RNFL bundles

(B) Paracentral scotomata coalesce to form an arcuate defect

(C) Arcuate defects break through to periphery.

In advanced disease only the macular area is spared, sometimes together with a small island in the temporal periphery. In extreme cases complete visual field loss may occur.

4.4 Statistical Indices of Visual Field Damage

4.4.1 Total and Pattern Deviation Probability Maps

Total deviation (TD) is the deviation in sensitivity at a particular test location from that of an age-matched healthy subject, where a negative TD indicates a loss of sensitivity. In most perimetric software a map is produced of the probability of the measured sensitivity occurring in the healthy sample when compared to the percentiles of a normative distribution.

Pattern deviation (PD) represents the deviation in sensitivity at a particular location relative to the rest of the visual field. This measure aims to separate localised loss from diffuse sensitivity

changes by correcting the visual field for generalised changes which are most likely caused by factors such as refractive error, pupil size or cataract. Again, in many software packages a PD probability map is produced for a measured visual field, plotting the probability of the PD of each tested location belonging to a normal distribution of healthy subjects.

4.4.2 Global Visual Field Indices

Whilst not retaining any topographical information, global indices yield a single number, sometimes useful for statistical analysis of visual field data or to give an overall clinical impression of the visual field.

Mean deviation (MD) is a weighted (according to between-subject variance) mean of deviation in sensitivity at each test location. MD gives an indication of the overall state of the visual field, with negative values representing a loss of sensitivity. It is sensitive to diffuse loss and moderately advanced localised loss, but insensitive to small areas of reduced sensitivity.

Pattern standard deviation (PSD) is a weighted (according to between-subject variance) standard deviation of the TD values. It is larger in localised field loss where the variance of deviation within the visual field is larger.

Short-term fluctuation (SF) is an estimate of within-test variability, obtained by repeat determination of thresholds at various points. SF assumes uniform variability across the visual field but this is not the case so the value is of dubious clinical use.

Corrected pattern standard deviation (CPSD) is the PSD corrected for the SF and is sensitive to focal loss, due to separation of true deviations from variability. Both SF and CPSD are only available in full-threshold algorithms and are not reported in the widely-used SITA algorithms.

Visual field index (VFI) is a newer index (Bengtsson and Heijl, 2008) which expresses the visual field as a single percentage where 100% represents a perimetrically normal field, and 0% represents a perimetrically blind field. The VFI is age-corrected and based on pattern deviation

values (except in severely depressed fields) in order to reduce the effect of cataract. A strength of this index is the ease with which it is understood by patients concerned about the progression of their visual field loss.

4.4.3 Glaucoma Hemifield Test

The Glaucoma Hemifield Test (GHT) (Asman and Heijl, 1992) aims to help clinicians decide whether measured visual field loss is compatible with a diagnosis of glaucoma, or within the normal limits of the healthy population. It tests for asymmetry between the superior and inferior hemifields which is suggestive of glaucoma. The sum of PD probability scores in ten sectors of the nasal visual field is calculated. Five of the sectors are in the superior field, and these are mirrored by five sectors in the inferior field for comparison. Asymmetry between any of the sectors which falls outside of the central 99.5% range of a database of healthy subjects is classed as 'outside normal limits'. Any sector pair falling within this range but outside the central 97% range is classed as 'borderline', and if the overall sensitivity of the visual field is below the 99.5% limit GHT reports a 'general reduction in sensitivity'.

4.4.4 Reliability Indices

Reliability indices give an indication of the fixation and response behaviour of the patient in a particular visual field test. However, if we take reproducibility of test results as a measure of their reliability then the strongest performing factor in determining variability in a series of tests is level of visual field loss, i.e. MD and the following reliability indices make little contribution (Bengtsson, 2000).

False positive responses (FP) give an indication of the patient's response criterion. Catch trials are commonly used where no stimulus is presented in a period of time where usually there would be one. If the patient presses the response button during this time a false positive is reported. In some algorithms such as the Swedish Interactive Threshold Algorithm (SITA), FP is estimated from response time data, i.e. if a response is unusually quick for the patient then it is noted as a false positive.

False negative responses (FN) give an indication of the patient's concentration. Stimuli are presented at an intensity brighter than that which has already been seen at a certain location, if the patient fails to respond it may indicate a lack of concentration.

Fixation losses give an indication of the consistency of the patient's eye position through the test. At the start of the test the physiological blind spot is estimated, so that during the test bright stimuli can be presented in this area. If the patient responds to these stimuli then their eye must have moved and a fixation loss is reported.

5. The Structure-Function Relationship in Glaucoma

As the relationship between RGC damage and visual field loss appears to be one of cause and effect it would seem reasonable to assume a relationship between the amount of RGC loss and the extent of visual field loss.

5.1 Early Work

A very common quote amongst clinicians is that up to 50% of optic nerve fibres have already been lost before a visual field defect can be detected. This figure initially came from early work aiming to relate glaucomatous structural and functional changes (Quigley et al., 1982). The study compared the visual fields, as manually assessed by Goldmann kinetic perimetry, to the histological count of RGC axons *post-mortem*. The sample sizes used in this study were very small, with only five normal eyes being used to establish the normal number of RGC axons, and only three 'glaucoma suspect' eyes who were without Goldmann visual field loss. It was only one of these patients who had an RGC count of 50% of the somewhat loosely established norm. Whilst the limitations of this study are obvious: The small sample sizes, the insensitive method used to detect visual field damage, the elapsed time between visual field measurement and optic nerve histological assessment; this paper provided a basic method for future studies.

In later work by the same group, a similar experiment was performed but using more modern standard automated perimetry. This study was also limited by a small sample size (6 glaucomatous eyes, one of which also had uveal melanoma, and 4 of which were a fellow eye to one with other ocular pathology, 5 healthy control eyes to establish normal range). The study concluded that a 10dB decrease in visual field sensitivity corresponded to 40% less RGCs than their established normal number (Quigley et al., 1989). A later paper also by the same group (Kerrigan-Baumrind et al., 2000) described another similar study but with slightly larger sample sizes (17 normal eyes, 17 glaucomatous eyes) and the use of the Humphrey Field Analyzer (HFA). The study reported that areas of visual field loss with Humphrey Total Deviation

Probability of $p < 0.5\%$ ¹ corresponded to 28.5% loss of RGCs. It is, however, important to note that within the $p < 0.5\%$ category are absolute scotomas, which one would logically associate with areas of no remaining RGCs. The value of 28.5% loss is not, therefore, surprising being the average of a series of test locations ranging from losses that are just below $p = 0.5\%$ to absolute scotomas. What is surprising is that the paper concludes that “at least 25% to 35% RGC loss is associated with statistical abnormalities in automated visual field testing”. Re-analysis of the mean RGC counts in the control eyes in this study shows wide 95% confidence intervals of $\pm 42\%$ of the mean RGC count, likely due to the small sample size. This means that there was a large degree of overlap in RGC counts between glaucoma patients and controls in the study such that even the upper limit of 35% RGC loss in their conclusion is not a statistically significant loss in their sample (it is within the range that can be considered feasibly normal according to their measurements) and as such the data presented does not support this conclusion (Hood and Kardon, 2007). Indeed, looking at the figures presented, those with 100% of the “normal” RGC axon count have, on average a visual field Mean Deviation of worse than -6dB and Pattern Standard Deviation of worse than 2.5dB, which probably would be statistically significant. The data presented by Kerrigan-Baumrind *et al* therefore seems to support the opposite conclusion that visual field loss occurs before RGC loss equally as well as the conclusion made.

5.2 Behavioural Experiments

In order to better establish the relationship between RGC count and visual function in glaucoma, Harwerth *et al* carried out an elegant series of experiments using behavioural perimetry in rhesus monkeys (Harwerth *et al.*, 1999, Harwerth *et al.*, 2004, Harwerth *et al.*, 2005, Harwerth *et al.*, 2002). The monkeys were trained to perform visual field tests using an HFA, modified only in ways which did not affect the test outcomes. The monkeys were seated in a custom-made chair in a primate testing cubicle attached to the perimeter. This allowed their eyes to be correctly aligned for testing, their mouths to be positioned on a juice spout

¹ In the paper the authors stated $p = 0.5\%$ rather than $p < 0.5\%$. The Humphrey perimeter does not give values for $p = 0.5\%$ only $p < 0.5\%$.

used to deliver behavioural rewards, and for them to hold a response switch. The monkeys were trained to press and hold down the response switch to initiate a trial, and subsequently to release the switch in the presence of a visual stimulus. The stimulus would be presented at a random time within 5.5 seconds interval and if the monkey's response was within 900ms of stimulus presentation then it was recorded as a true-positive response and the monkey rewarded. Alternatively if the response was not within this time it was recorded as a miss and the monkey was neither rewarded nor punished.

Once the monkeys were trained to perform perimetric tests, glaucoma was surgically-induced in one eye. This was achieved through argon laser treatment to the trabecular meshwork which resulted in intraocular pressure raised consistently above 40mmHg leading to glaucomatous damage similar in many ways to that in human patients (Harwerth et al., 1997). The fellow eye served as a control eye, allowing measures of glaucomatous loss with greater confidence than previous studies. Once the visual fields had been accurately measured at the desired stage of damage, the eyes were enucleated for histological analysis, giving a direct and almost immediate comparison between structural and functional measures.

Early results, plotted on log-linear axes (figure 5.1) were taken in partial support of previous work, in that visual sensitivity loss appeared small and constant until around 30-50% of RGCs were lost after which a more steady relationship between RGC and visual sensitivity loss appeared (Harwerth et al., 1999). Whilst the results appear to suggest either that clinical perimetry is insensitive to early neural loss, or that there is some redundancy in the visual system such that a proportion of RGCs can be lost before vision is affected, account needs to be taken of the log-linear scaling used which emphasises larger losses to the detriment of smaller, early losses.

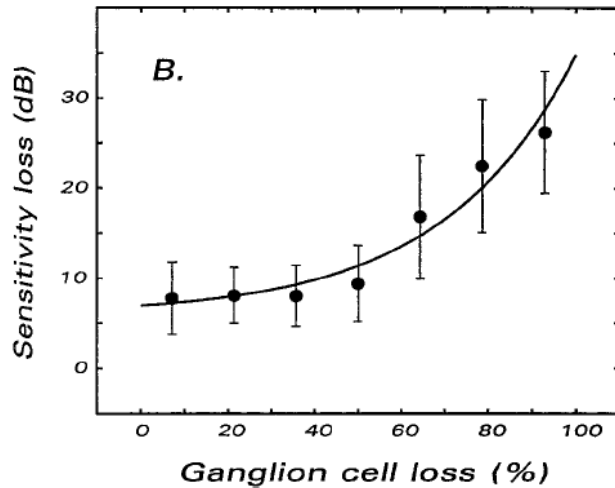


Figure 5.1: Primate RGC loss vs. visual sensitivity loss plotted on log-linear axis (after Harwerth et al, 1999)

In later work, Harwerth *et al* addressed the issue of variability in the structure-function relationship by taking into account retinal eccentricity as a factor in expected RGC axon count, eliminating a proportion of the scatter in the model (Harwerth *et al.*, 2004). The issue of scaling was also addressed, finding that plotting RGC loss on a logarithmic scale (dB) produced a linear relationship between RGC loss and visual sensitivity loss (also measured in dB) with varying gradient depending on retinal eccentricity (figure 5.2) (Harwerth *et al.*, 2004, Harwerth *et al.*, 2005).

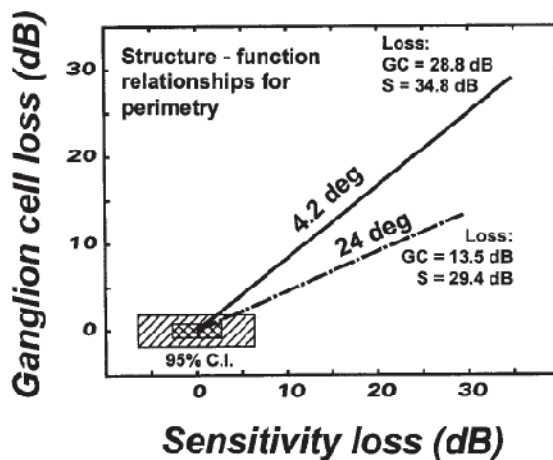


Figure 5.2: Primate RGC loss correlated with visual sensitivity plotted on log-log axes to produce a linear relationship, with retinal eccentricity taken into account (after Harwerth *et al*, 2004)

The structure-function model derived from primate data was then applied in a re-analysis of the data from the study by Kerrigan-Baumrind *et al* (2000). The model was used to predict RGC axon counts from measured visual sensitivities of glaucoma patients, and the results compared

to *post-mortem* histological cell counts. The results showed that clinical perimetry is, in fact, a direct expression of glaucomatous neural loss and as such a good measure of stage of disease (Harwerth and Quigley, 2006). The application of the model to human data revealed a slightly less precise relationship between structure and function. This may be due to the elapsed time between the visual field being measured and the patient's death and subsequent histological RGC count, but may also be due in part to reduced variability in visual field measurements obtained from well-trained primates compared to clinical measurements obtained from patients without extensive perimetric experience (Harwerth et al., 1993).

5.3 The Topographic Structure-Function Relationship

In order to establish a relationship between functional measures and currently available *in-vivo* measures of retinal and ONH structure it is essential to first establish a proper topographic relationship between these. That is, to establish a relationship between the locations tested in clinical perimetry and the corresponding areas of RNFL and ONH.

One such model, which has since been widely used, was derived from fundus photographs obtained during routine clinical examination of normal-tension glaucoma patients (Garway-Heath et al., 2000). Photographs featuring visible, well-defined RNFL bundle defects (so-called "wedge defects") or prominent nerve fibre bundles were selected, and the defects manually traced back to the ONH. A scaled HFA 24-2 visual field matrix was then superimposed onto the photographs and the relationship of visual field test locations to the ONH circumference was estimated by observing the proximity of test locations to nerve fibre defects/bundles. The resulting map divided the ONH into six sectors, each with a corresponding area of visual field test locations (figure 5.3).

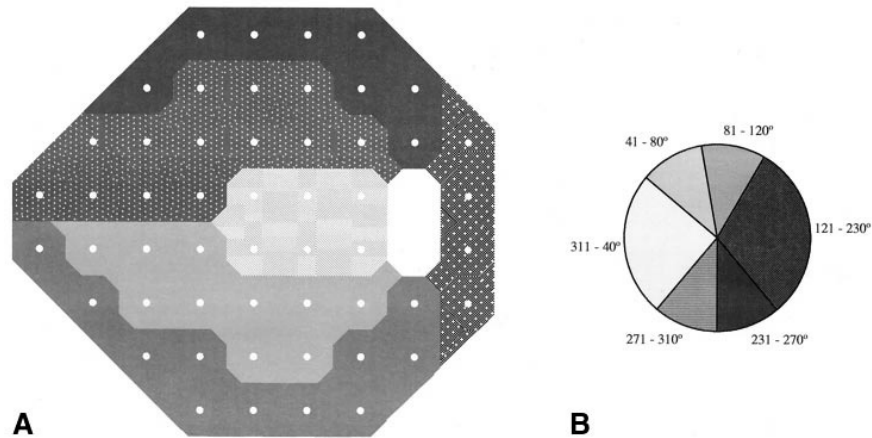


Figure 5.3: Visual field divisions (A) and corresponding optic nerve head sectors (B) (after Garway-Heath et al, 2000)

This model has been incorporated, with some small modification (Garway-Heath et al., 2002), into the HRT software and used in several studies aiming to correlate NRR measurements or peripapillary RNFL thickness (measured by OCT) to visual field sensitivities. The model does have some clear limitations. It assumes a consistent retinotopic organisation of RGC axons travelling in bundles, which is not well established. For example, it may be possible that there is some tendency of RGC axons to move between adjacent bundles, and some controversy exists over the relative position of ONH insertion of long (peripheral) and short (central) RGC axons which may affect the resultant map (Ogden, 1974, Radius and Anderson, 1979, Minckler, 1980, Ogden, 1983, Fitzgibbon and Taylor, 1996). The relatively large sectors used in the map were a product of large between-subject variability, much of which can be explained by variations in ONH position (Garway-Heath et al., 2000). The map has not been verified by examination of corresponding visual field data and therefore remains an essentially theoretical, albeit useful, representation of the topographic structure-function relationship. These limitations increase variability and, therefore, limit the precision of subsequent *in-vivo* quantitative studies which make use of the model.

Later work by Gardiner *et al* (2005) used cross-sectional HFA 24-2 visual field and HRT structural data in an attempt to refine the map. The resultant map divided the ONH into 36 10° sectors (thereby increasing resolution) and assessed the correlation of each sector to each visual field

test location (Gardiner et al., 2005). The measures correlated were individual threshold sensitivities at each visual field test location and the ONH 'sector rim area measure' which was the deviation in sector NRR area from a healthy population after normalisation for overall NRR area. However, the correlations were mostly very weak, with the mean best correlation found for each ONH sector being 0.28 (range 0.12-0.52). This, combined with the increased complexity of the map, means it has not been widely adopted and as such the map produced by Garway-Heath *et al* (2000) is still the most often used.

5.4 In-vivo measurements

Garway-Heath *et al* (2002) compared visual sensitivity at HFA 24-2 visual field test locations and pattern electroretinogram response amplitudes to checkerboard stimuli to NRR thickness as measured by HRT using the topographic map proposed earlier by their own group (Garway-Heath et al., 2000). They found a weak but significant linear relationship between NRR area and both pattern electroretinogram amplitudes and visual field sensitivity values when plotted on linear scales (Garway-Heath et al., 2002). The study provided further evidence that structural and functional changes in glaucoma occur concurrently, and there is no RGC functional reserve.

Studies using OCT to measure RNFL thickness have also used the above spatial models to correlate sensitivity at HFA 24-2 visual field test locations in the arcuate areas to RNFL thickness in corresponding para-papillary areas (figure 5.4). In agreement with the primate and human studies previously mentioned, a linear model was found to be the best fit to the data obtained from human glaucoma patients (Hood et al., 2007, Hood and Kardon, 2007). In using OCT data however, it must be remembered that the entire RNFL thickness is measured, which contains not only RGC axons, but also glial cells, capillaries and efferent fibres. As such there is a certain minimum thickness in every patient, beyond which no amount of glaucomatous damage will thin the RNFL. This minimum thickness manifests itself as the intercept with the y-axis (RNFL thickness), or as the asymptote to the curve when results are plotted on log-linear axis (Hood et al., 2007, Hood and Kardon, 2007).

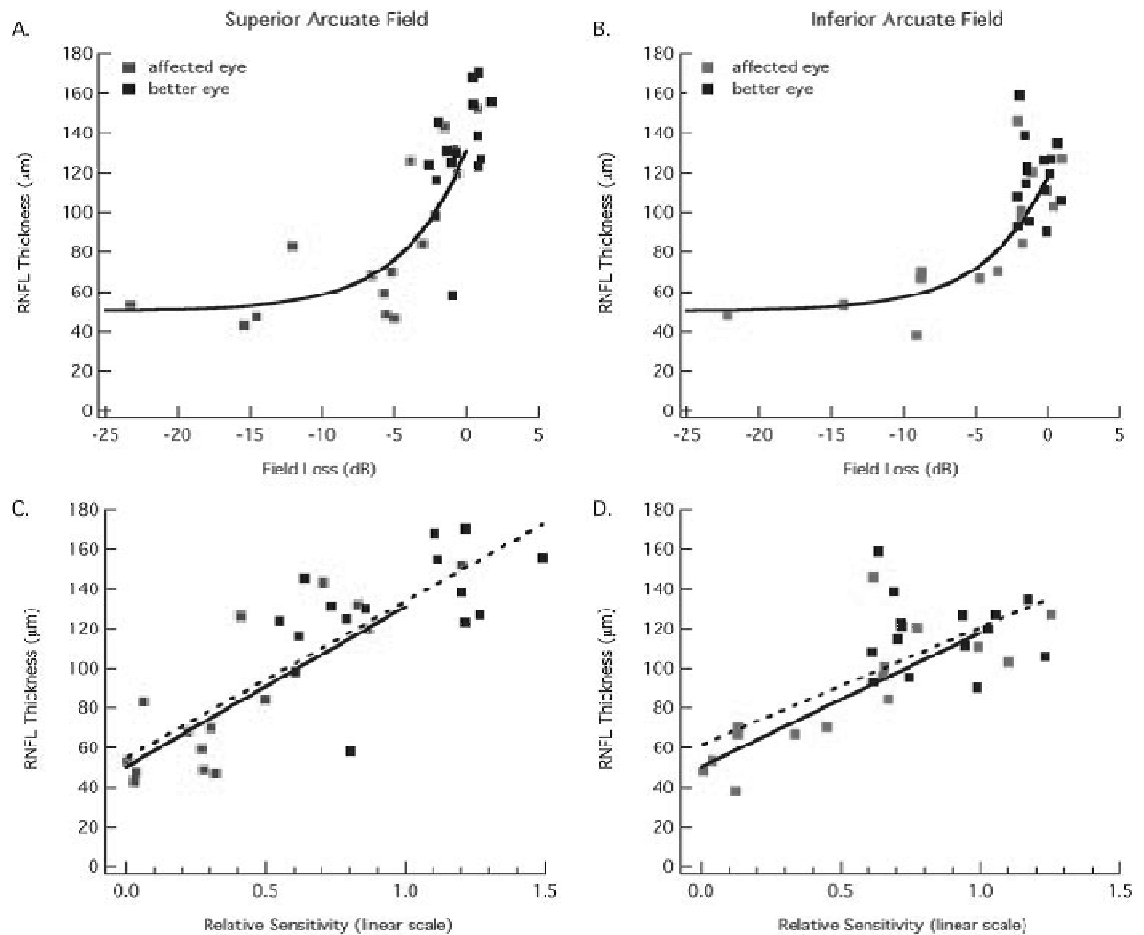


Figure 5.4: Visual sensitivity vs. RNFL thickness for superior and inferior arcuate areas of the visual field, plotted on log-linear (A,B) and linear axes (C,D) (after Hood et al, 2007)

In-vivo structural measurements using OCT have also been taken in primates and correlated with visual field sensitivity measurements from behavioural perimetry as described above. The linear model was again the best fit to the data, which was in this case presented as percentage loss thus avoiding the above issue of residual measured thickness (100% loss does not mean zero thickness) (Harwerth et al., 2007). This study shows good agreement with those on human data, confirming the validity of the primate model used.

These linear models, whilst being the best fit to the data, do not account for all of the variability in the studied populations, i.e. the data are still quite scattered around the regression line. Much of the scatter is probably due to the variability in the measurements taken, especially perimetry where response variability has been shown to be inversely correlated to sensitivity

(i.e. as the sensitivity worsens, variability increases) (Henson et al., 2000). Another potential method of improving the model for *in-vivo* measurements is to improve the precision of the topographic models used, as variability within these is reflected in the results of any quantitative study using them.

5.6 Future Direction in Structure-Function Relationships

Improvements in the structure-function relationship model in the form of reduced scatter and more precise estimates of the slope may come via improved precision in topographic structure-function maps and reduced variability in testing methods, especially perimetry where patient factors as well as physiological and technological factors affect results. Psychophysical developments in visual field testing, whether through new techniques which selectively examine certain neural pathways, or through improved testing of peripheral locations by altering the stimuli used may also help to reduce scatter in structure-function models (Anderson, 2006).

Another area which has been given little consideration in the past is that of spatial *types* of glaucomatous ONH and visual field damage. It is widely accepted that glaucoma is not actually one disease, but rather a group of diseases with similar characteristics, and so it follows that these slightly different diseases may have slightly different patterns of structural and functional damage. It has already been demonstrated clinically that many glaucoma patients can be placed into categories based on ONH appearance, who then have other similar disease characteristics such as spatial patterns of visual field loss to those within the same category (Broadway et al., 1999). Similar work has been carried out with visual field data to attempt to classify patients based on spatial patterns of sensitivity loss (Brusini and Johnson, 2007, Keltner et al., 2003). These may be important findings as it is possible that these distinct disease types may have different underlying mechanisms which progress and respond to treatments differently. Unfortunately it is difficult to know exactly how many categories there should be, and it seems likely that if these distinct disease mechanisms exist, many patients will be affected by more than one. Broadway *et al* (1999) found it impossible to classify the majority of

their patients into one of their 4 ONH categories. Whilst more categories may help somewhat, it may be more likely that increased understanding of these types could come through objective statistical mapping techniques of ONH (Yan et al., 2005) and visual field data (Twa et al., 2008).

5.7 Structure-function summary

Current evidence suggests that glaucomatous structural change and functional loss occur concurrently and linearly throughout the progression of the disease. There appears to be little or no redundancy in the visual system in the form of any RGC functional reserve, such that small losses of RGCs cause small losses in visual sensitivity, however these are not necessarily noticed by the patient or detected by current methods.

6. Discus – Investigating subjective judgement of glaucomatous damage in optic disc photographs.

Contribution

This project was carried out with Paul Artes (PHA) and followed on from the work carried out by an MSc student, Damien Echendu (DE). PHA collected the images from the OLGA clinic database, and DE carried out the image quality grading and selection of images to be incorporated into the software, which was written by PHA. I performed final checks on the images and associated visual fields to ensure suitability for the project. The data from expert observers in the UK was collected by myself, and the data from expert observers in Canada was collected by PHA. I carried out the statistical analysis of the data and authored the published paper (and this chapter) with help from PHA and David Henson.

Publications

Denniss J, Echendu D, Henson DB, Artes PH (2010) Discus –Investigating subjective judgment of glaucomatous damage in optic disc photographs. *Optometry & Vision Science (glaucoma special edition, in press)*

Conference Presentations

Denniss J, Echendu D, Henson DB, Artes PH (2008) The Interpretation of Optic Disc Images for Glaucomatous Damage by Specialist Clinicians. ARVO 2008 Annual Meeting, Fort Lauderdale, FL, USA (poster)

Denniss J, Echendu D, Henson DB, Harper RA, Harding, AK, Artes PH (2008) Interpretation of Optic Disc Images for Glaucomatous Damage: Reference Data from Specialists. IPS Congress 2008, Nara, Japan (paper)

Henson DB, **Denniss J**, Echendu D, Artes PH (2007) *Discus* –a software package for analysing the clinical grading of glaucomatous optic discs. UK & Eire Glaucoma Society Annual Meeting 2007, Cardiff, UK (paper)

6.1 Abstract

6.1.1 Purpose

To describe a software package (Discus) for investigating clinicians' subjective assessment of optic disc damage, and to provide reference data from a group of expert observers.

6.1.2 Methods

Optic disc images were selected from patients with manifest or suspected glaucoma or ocular hypertension who attended the Manchester Royal Eye Hospital. Eighty images came from eyes without evidence of visual field (VF) loss in at least 4 consecutive tests (VF-negatives), and 20 images from eyes with repeatable VF loss (VF-positives). Software was written to display these images in randomized order, for up to 60 seconds. Expert observers (n=12) rated optic disc damage on a 5-point scale (definitely healthy, probably healthy, not sure, probably damaged, definitely damaged).

6.1.3 Results

Optic disc damage as determined by the expert observers predicted VF loss with less than perfect accuracy (mean area under receiver-operating curve (AUROC), 0.78; range 0.72 to 0.85). When the responses were combined across the panel of experts, the AUROC reached 0.87, corresponding to a sensitivity of ~60% at 90% specificity. While the observers' performances were similar, there were large differences between the criteria they adopted ($p < 0.001$), even though all observers had been given identical instructions.

6.1.4 Conclusions

Discus provides a simple and rapid means for assessing important aspects of optic disc interpretation. The data from the panel of expert observers provide a reference against which students, trainees, and clinicians may compare themselves. The program and the analyses described in this paper are freely accessible from www.discusproject.blogspot.com.

6.2 Introduction

In clinical practice, decisions often have to be made under considerable uncertainty, and there is often no perfect test that can give a “correct” answer against which such decisions can be compared and evaluated. In glaucoma, a pertinent example is subjective optic disc assessment.

Subjective optic disc assessment is, arguably, one of the most important clinical procedures in glaucoma (Fingeret et al., 2005, Susanna Jr and Vessani, 2007, Broadway et al., 1999, Caprioli, 1994, Jonas et al., 1999, Lin et al., 2007). Optic nerve damage is often the first clinically detectable sign of the disease (Weinreb and Khaw, 2004, Garway-Heath, 2008) as shown in the Ocular Hypertension Treatment Study where almost 60% of patients who converted to glaucoma developed optic disc changes before they showed reproducible visual field damage (Gordon et al., 2002, Keltner et al., 2006). In the European Glaucoma Prevention Study optic disc changes were recognised before visual field changes in approximately 40% of the patients who developed glaucoma (EGPS Group, 2007). However, healthy optic discs cover a large spectrum of appearances such that even highly experienced observers may find it difficult to identify early damage unambiguously (Broadway et al., 1999, Jonas et al., 1999). Although imaging tools such as confocal scanning laser tomography or optical coherence tomography can provide precise measurements of the optic nerve and the nerve fibre layer, they do not distinguish perfectly between healthy eyes and those with early glaucomatous optic disc damage. Visual field loss provides a functional measure of optic disc damage but may not be sensitive to early damage. In short, there is no ideal reference standard for optic disc damage and no simple rule that can tell with certainty whether a given disc is damaged or not. Without a ‘correct’ answer, however, it is difficult to investigate clinicians’ subjective decisions.

Given that subjective optic disc assessment is of such paramount importance in clinical practice, it is somewhat surprising that little work has previously been done to establish a framework for measuring clinicians’ skills, attitudes and decision criteria in the context of this task. A tool to measure an individual observer’s skill at judging optic disc damage would be useful, for example, for monitoring the progress of junior clinicians through the different stages of a training programme. Similarly, it would be interesting to investigate how clinicians’ attitudes

and decision criteria depend on the “framing” (Kahneman et al., 1982) of the task, i.e. what information is available on the prior likelihood of damage and on the cost/benefit of high sensitivity or high specificity.

The objective of this paper is to suggest a “first stab” approach for conducting subjective classification experiments and for interpreting the data. We describe a freely accessible software package (“Discus”) which observers can use to view and rate a set of selected optic disc images under controlled conditions, to assess their skill at interpreting these photographs. We suggest that data from such experiments can be interpreted, even in the absence of a true “gold standard”, by comparison to a reference panel of expert observers, and discuss data from such a panel. Ultimately, we would like to stimulate further research into the important topic of subjective decision-making and how it applies to clinical practice in glaucoma.

6.3 Methods

6.3.1. Selection of Images

To obtain a set of optic disc images with a wide spectrum of early glaucomatous damage, data were selected from patients who had attended the Optometrist-led Glaucoma Assessment (OLGA) clinics at Manchester Royal Eye Hospital (Manchester, UK) between June 2003 and May 2007. This clinic sees patients who are deemed at risk of developing glaucoma, for example due to ocular hypertension, or who have glaucoma but are thought of as being at low risk of progression and are well controlled on medical therapy. Patients undergo regular examinations (normally in intervals of 6 months) by specially trained optometrists. During each visit, visual field examinations (Humphrey Field Analyzer program 24-2, SITA-Standard) and non-stereoscopic fundus photography are performed (Topcon TRC-50EX, field-of-view 20 degrees, resolution 2000×1312 pixels, 24 bit colour). All data were anonymised prior to use and as such the study was deemed by the NHS Central Manchester Research Ethics Committee to not require ethical approval.

In order to establish two clearly distinct and well defined groups, images were selected from patients who had undergone at least 4 visual field tests on each eye within a period of 2 to 5 years. From these patients, visual field (VF) positive and VF-negative groups were established based on the visual fields' Mean Deviation (MD) and Pattern Standard Deviation (PSD) (Table 6.1). The cut-offs here were chosen to dichotomise the patients into those with likely glaucomatous visual fields, and those with clinically normal visual fields.

Table 6.1: Inclusion criteria for VF-positive and VF-negative groups. Criteria had to be met on all 4 examinations. For inclusion in the VF-negative group, the criteria had to be met with both eyes. In addition, the between-eye differences in MD and PSD had to be less than 1.0 dB

	MD	PSD
VF-positive	between -2.5 and -10.0 dB	between 3.0 and 15.0 dB
VF-negative	better than [$>$] -1.5 dB ¹	better than [$<$] 2.0 dB ¹

If both eyes of a patient met these criteria, a single eye was randomly selected. A small number of eyes (n=17) were excluded owing to clearly non-glaucomatous visual field loss (for example, hemianopia) or non-glaucomatous lesions visible on the fundus photographs (e.g. chorioretinal scars).

To eliminate any potential clues other than glaucomatous optic disc damage, we matched the image quality in VF-negative and VF-positive groups. One of the authors (DE) viewed the images on a computer monitor in random order and graded each one on a five-point scale for focus and uniformity of illumination. During grading, the observer was unaware of the status of the image (VF-positive or -negative), and the area of the disc had been masked from view. A final set of 20 VF-positive images and 80 VF-negative images was then created such that the distribution of image quality was similar in both groups (Table 6.2). The total size of the image set (100), and the ratio of VF-positive to VF-negative images (20:80), had been decided on beforehand to limit the duration of the experiments (such that the task could reasonably be completed without losing concentration) and to keep the emphasis on discs with early damage whilst still including enough VF-positive images to allow for estimation of sensitivity for their detection

Table 6.2: Characteristics of VF-positive and VF-negative groups. Image quality was scored subjectively on a scale from 1 to 5. Differences between groups were tested for statistical significance by Mann-Whitney U (MWU) tests.

	Image Quality	Age, y	MD, dB	PSD
VF-positive (n=20)	1.82 (1.20)	66.0 (13.1)	-6.20 (1.76)	5.58 (2.15)
VF-negative (n=80)	1.68 (1.33)	61.3 (9.3)	+0.60 (0.4)	1.50 (0.16)
p-value (MWU)	0.67	0.35	<0.001	<0.001

6.3.2 Expert Observers

For the present study, 12 experts (either glaucoma fellowship-trained ophthalmologists working in glaucoma sub-specialty clinics (n=10) or scientists involved in research in the optic disc in glaucoma (n=2) were selected as observers. They were approached ad-hoc during scientific meetings or contacted by e-mail or letter with a request for participation.

Prior to the experiments, the observers were given written instructions detailing the selection of the image set. The instructions also stipulated that responses should be given on the basis of apparent optic disc damage rather than the perceived likelihood of visual field damage.

6.3.3. Experiments

In order to present images under controlled conditions, and to collect the observers' responses, a software package Discus (3.0E, figure 6.1) was developed in Delphi (CodeGear, San Francisco, CA). The software is freely available from <http://www.discusproject.blogspot.com> for users of Windows operating systems.

The software displayed the images, in random order, on a computer monitor. After the observer had triggered a new presentation by hitting the "Next" button, an image was displayed until the observer responded by clicking one of 5 buttons (definitely healthy, probably healthy, not sure, probably damaged, definitely damaged). After a time-out period of 60 seconds the image would disappear, but observers were allowed unlimited time to give a response. To guard against occasional finger-errors, observers were also allowed to change their response, as long as this occurred before the "Next" button was hit.

To assess the consistency of the observers, 26 images were presented twice (2 in the VF-positive group (10%) and 24 in the VF-negative group (30%)). A larger rate of repetitions in the VF-negative group (30% compared to 10%) was chosen to reduce the prevalence of VF-positive presentations in the session. No feedback was provided during the sessions.

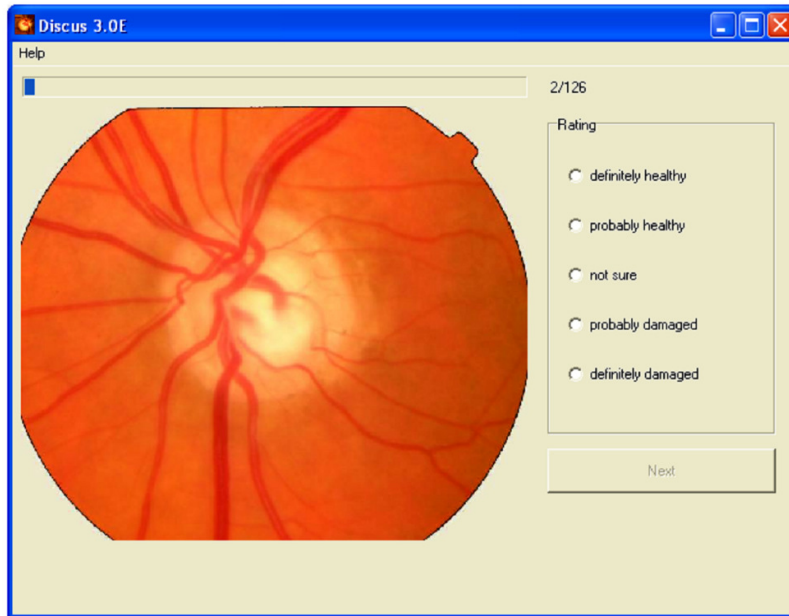


Figure 6.1: Screenshot of Discus software.

Images remained on display for up to 60 seconds, or until the observer clicked on one of the 5 response categories. A new presentation was triggered by hitting the “Next” button.

6.3.4 Analysis

The responses were transformed to a numerical scale ranging from -2 (“definitely healthy”) to +2 (“definitely damaged”). The proportion of repeated images in which the responses differed by one or more categories was calculated, for each observer. For all subsequent analyses, however, only the second of the two responses was used. All analyses were carried out in the freely available open-source environment *R*, and the *ROCR* library was used to plot ROC curves (Ihaka and Gentleman, 1996, Sing et al., 2005).

6.3.4.1 Individual observers’ ROC curves

To obtain an objective measure of individual observers’ performance at discriminating between eyes with and without visual field damage, ROC curves were derived from each set of responses. For this analysis, the visual field status was the reference standard, and responses in the “not sure” category were interpreted as between “probably healthy” and “probably

damaged". If an observer had used all five response categories, the ROC curve would contain 4 points (A – D). Point A, the most conservative criterion (most specific but least sensitive) gave the sensitivity and specificity to visual field damage when only the "definitely damaged" responses were treated as test positives while all other responses ("probably damaged", "not sure", "probably healthy", "definitely healthy") were interpreted as test negatives. For point D, the least conservative criterion (most sensitive but least specific), only "definitely healthy" responses were interpreted as test negatives, and all other responses as test positives.

6.3.4.2 Individual observers' criteria

When using a subjective scale, as in the current study, the responses are dependent on the observer's interpretation of the categories and their individual attitude to respond with "probably damaged" or "definitely damaged" (response criterion). A cautious observer, for example, might regard a particular disc as "probably damaged" whilst an equally skilled but less cautious observer might respond with "not sure" or "probably healthy". To investigate the variation in response criteria within our group, we compared the observers' mean responses across the entire image set.

6.3.4.3 Combining responses of expert observers

To estimate the performance of a panel of experts, and to obtain a reference other than visual field damage for judging current as well as future observer's responses, the mean response of the 12 expert observers was calculated for each of the 100 images.

To estimate if the expert group (n=12) was sufficiently large, we investigated how the performance of the combined panel changed depending on the number of included observers. Areas under the ROC curve were calculated for all possible combinations of 2, 3, 4...11 observers to derive the mean performance, as well as the minimum and maximum.

6.3.4.4 Relationship between responses of individual observers and expert panel

As a measure of overall agreement between the expert observers, independent of their individual response criteria, the Spearman rank correlation coefficient between the 12 sets of responses was computed. The underlying rationale of this analysis is that, by assigning each image to one of five ordinal categories, each observer had in fact ranked the 100 images. If two

observers had performed identical ranking, the Spearman coefficient would be 1, regardless of the actual responses assigned.

6.4 Results

The experiments took between 13 and 46 minutes (mean 29 minutes) to complete. On average, the observers responded 7 seconds after the images were first presented on the screen, and the median response latencies of individual observers ranged from 4 to 16 seconds. The reproducibility of individual observer's responses was moderate; on average, discrepancies of one category were seen in 44% (12) of 26 repeated images (range 23 – 62%).

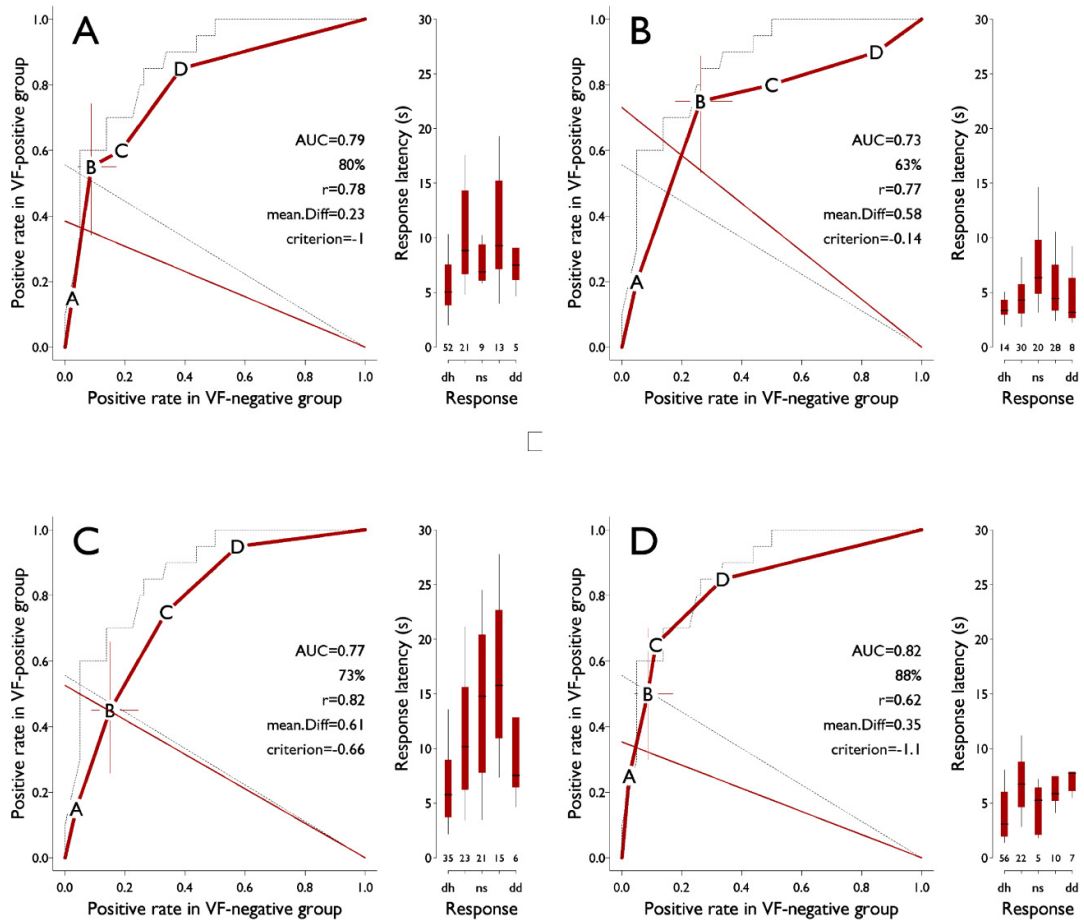
Individual observers' results are shown in figure 6.2A-L. The points labelled A, B, C, and D represent the trade-off between the positive rates in the VF-positive (vertical axis) and VF-negative groups (horizontal axis) achieved with the four possible classification criteria. Point A, for example, shows the trade-off when only discs in the "definitely damaged" category are regarded as test-positives. Point B gives the trade-off when discs in both "definitely damaged" and "probably damaged" categories are regarded as test-positives. For D, the least conservative criterion, only responses of "definitely healthy" were interpreted as negatives. To indicate the precision of these estimates, the 95% confidence intervals were added to point B.

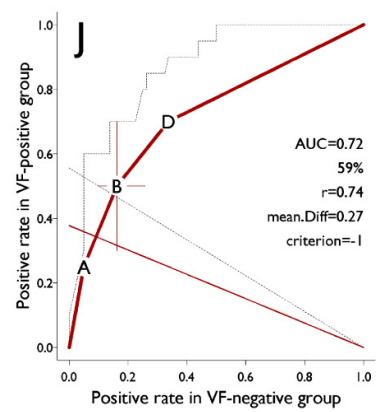
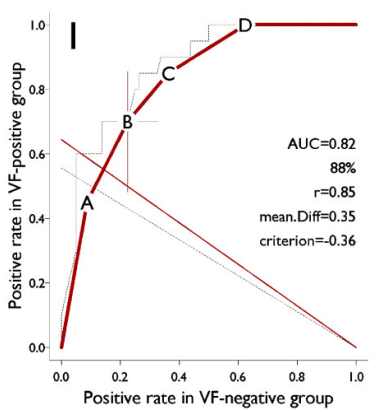
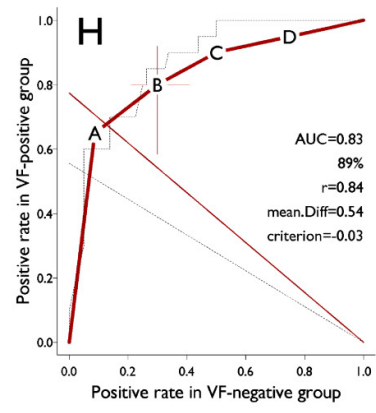
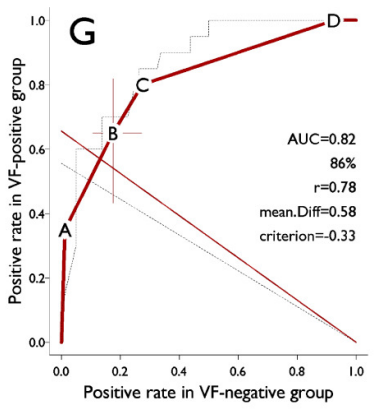
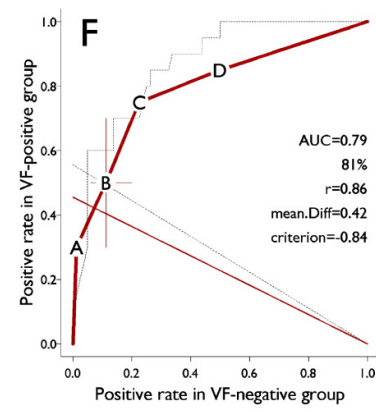
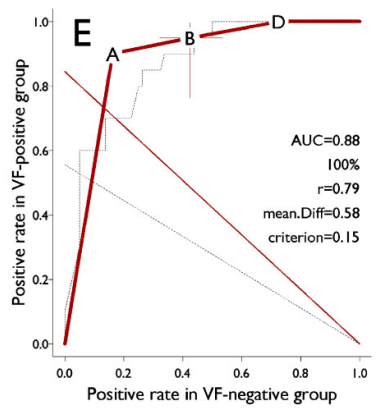
Areas under the curve (AUROC) ranged from 0.71 (95% CI 0.58-0.85) to 0.88 (95% CI 0.82-0.96), with a mean of 0.79. There was no relationship between observers' overall performance and their median response latency (Spearman's $r=0.34$, $p=0.29$).

In contrast to their similar overall performance, the observers' response criteria differed substantially ($p<0.001$, Friedman test). For example, the proportion of discs in the VF-positive category which were classified as "definitely damaged" ranged from 17% to 63% between observers, while the proportion of discs in the VF-negative category classified as "definitely healthy" ranged from 8% to 68%. In figure 6.2A-L, the response criterion is represented by the inclination of the red line with its origin in the bottom right corner. If the responses had been

exactly balanced between the “damaged” and “healthy” categories, the inclination of the line would be 45 degrees. A more horizontal line represents a more conservative criterion (less likely to respond with “probably damaged” or “definitely damaged”, while a more vertical line represents a less conservative criterion. There was no relationship between the observers’ performance (AUROC) and their response criterion (Spearman’s $r=0.41$, $p=0.18$).

To derive the “best possible” performance as a reference for future observers, the responses of the expert panel were combined by calculating the mean response obtained for each image. The ROC curve for the combined responses (grey curve in figure 6.2A-L) enclosed an area of 0.87.





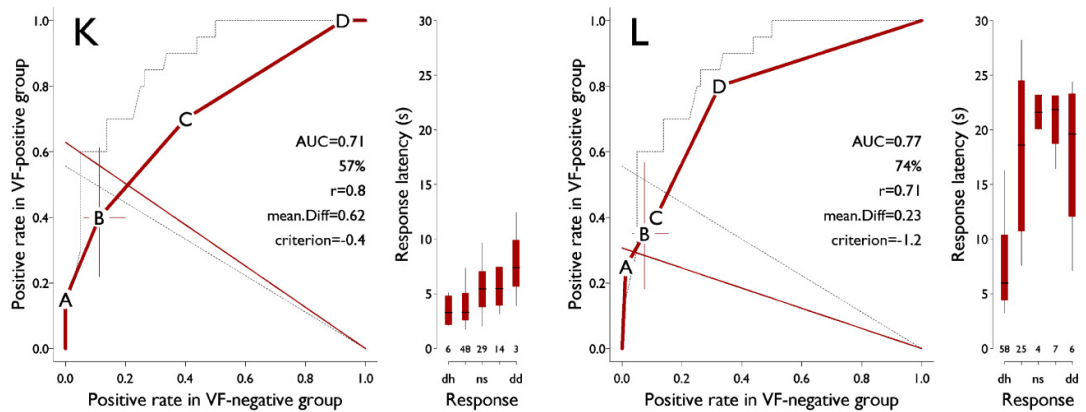


Figure 6.2: Receiver-operating characteristic (ROC) curves for the classification of optic disc photographs by the 12 expert observers (A-L), with a reference standard of visual field damage. The x-axis (positive rate in VF-negative group) measures specificity to visual field damage, while the y-axis (positive rate in the VF-positive group) gives the sensitivity. Point A (most conservative criterion) shows the trade-off between sensitivity and specificity when only “definitely damaged” responses are interpreted as test positives. Point D (the least conservative criterion) shows the trade-off when all but “definitely healthy” responses are interpreted as test positives. Boxplots (right) give the distributions of response latencies, and the number of times each response was selected.

To facilitate comparison, the grey ROC curve, and the dotted grey line, represent the performance and the criterion respectively of the group as a whole. Results provided in numerical format are the area under the ROC curve (AUC), the percentage of the AUC as compared to that of the entire group (individual ROC area–0.5) / (expert panel ROC area–0.5), the Spearman rank correlation of the individual’s responses with those of the entire group, the mean difference between repeated responses, and the average response as a measure of criterion (-2=“definitely healthy”, -1=“probably healthy”, 0=“not sure”, 1=“probably damaged”, and 2=“definitely damaged”).

To investigate how the performance of an expert panel varies with the number of contributing observers, the area under the ROC curve was derived for all possible combinations of 2, 3, 4, etc, up to 11, observers (figure 6.3). The limit of the ROC area was approached with 6 or more observers, and it appeared that a further increase in the number of observers would not have had a substantial effect on the performance of the panel.

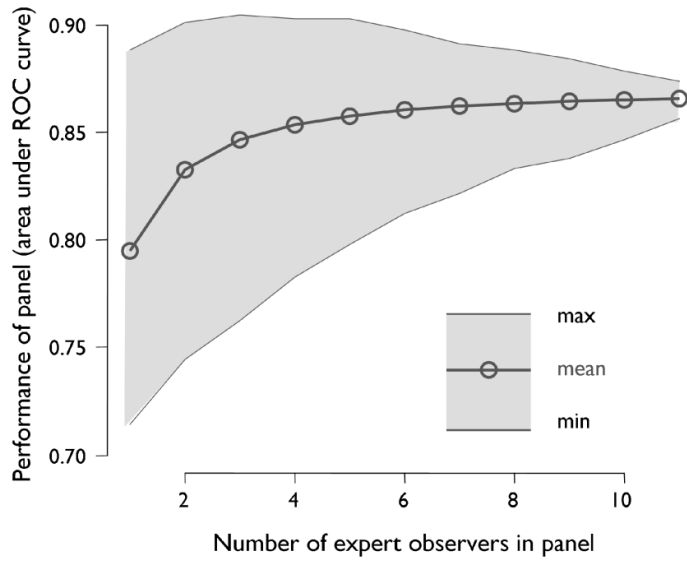


Figure 6.3: Performance (area under ROC curve) of combined expert panel as a function of number of included observers.

All possible combinations of 2 to 11 observers were evaluated. The mean area under the ROC curve approaches its limit with approximately 6 observers.

Individual observers' Spearman rank correlation coefficient with the combined expert panel ranged from 0.62 to 0.86, with a median of 0.79. There was no relationship between the Spearman coefficient and the area under the ROC curve ($r = 0.09$, $p = 0.78$).

6.5 Discussion

Several authors have previously investigated how clinicians agree with each other in diagnosing glaucoma, differentiating between different types of optic disc damage, or in estimating specific parameters such as cup/disc ratios (Lichter, 1976, Tielsch et al., 1988, Nicolela et al., 2001, Spalding et al., 2000, Harper et al., 2000b, Harper et al., 2001, Spry et al., 1999, Abrams et al., 1994, Varma et al., 1992, Azuara-Blanco et al., 2003, Sung et al., 2002) but there is little previous work on accuracy and biases in diagnostic decisions (e.g. healthy vs. damaged optic discs) and the factors that may influence it. The objective of this paper was to describe the design of the Discus software, to discuss how data obtained with it might be analyzed, and to provide data from a panel of experts as a reference for future observers.

The image sample for the current report was highly selected, being drawn from a population of patients who were being followed in a glaucoma clinic and who either had established disease or were deemed to be at high risk of developing glaucoma. Consequently, there are many

patients suspected of having glaucoma who do not (or do not yet) have visual field loss. Therefore, many of the VF-negative optic discs in this sample show features of damage, and unequivocally healthy discs are likely to be under-represented compared to an unselected population. Likewise, the image sample does not contain optic discs with end-stage damage, because patients with MDs worse than -10dB were not selected. Because our image sample is not representative of an unselected population, the ROC curves are likely to underestimate clinicians' performance at detecting glaucoma by ophthalmoscopy in an epidemiological screening scenario. However, the use of a "difficult" data set may also be seen as an advantage as it allows observers' performance to be assessed on the type of optic disc more likely to cause diagnostic problems in clinical practice.

With the visual field as the reference standard, all 12 expert observers in this study had ROC areas significantly smaller than 1, and even when the judgments of the observers were combined, this "best possible" panel response did not discriminate perfectly between optic discs in the VF-positive and VF-negative groups. These findings are not surprising, given the lack of a strong association between structure and function in early glaucoma that has been reported by many previous studies (Anderson, 2006, Garway-Heath et al., 2002, Johnson et al., 2000, Harwerth and Quigley, 2006, Caprioli, 1989, Caprioli and Miller, 1988). However, the experiments provide a vivid illustration of how difficult it can be to make diagnostic decisions in glaucoma based solely on the optic disc.

Estimated at a specificity fixed at 90%, the combined panel's sensitivity to visual field loss was 60%. This is similar to data previously reported for clinical observers and objective imaging tools (Sharma et al., 2008, Deleon-Ortega et al., 2006, Mardin and Jünemann, 2001, Greaney et al., 2002, Harper and Reeves, 2000). Unfortunately, objective imaging data are not available for the patients in the current dataset and we are therefore unable to perform a direct comparison. However, the methodology developed in this paper may prove useful for future studies that compare diagnostic performance between clinicians and imaging tools in different clinical settings.

One limitation of our study was the relatively small size of the expert group ($n = 12$). However, by averaging every possible combination of 2 to 11 observers within the group, we demonstrated that the response of the combined panel was likely to have attained near-maximum performance, and that a larger group of observers was unlikely to have changed our findings substantially.

One challenging issue is how to derive complete and easily interpretable summary measures of observer performance, in the absence of a reference standard of optic disc damage. To avoid biases, the images in this study were not selected based on optic disc appearance (Whiting et al., 2004, Medeiros et al., 2007, Harper et al., 2000a). We therefore used visual field data as the criterion to separate optic disc images into VF-positive and VF-negative groups, and the ROC areas therefore measure the statistical separation between an observer's responses to optic discs in eyes with and without visual field damage (Hanley, 1989, Hanley and McNeil, 1982). However, owing to the lack of a strong correlation between structure and function, visual field loss is not an ideal metric for optic disc damage in early glaucoma. For example, it is likely that a substantial proportion of the VF-negative images show early structural damage, whereas some optic discs in the VF-positive group may still appear healthy.

We have attempted to address the problem of a lacking ideal reference standard in two complementary ways. First, a new observer's ROC area can be compared to that of the expert panel, such that the statistic is re-scaled to cover a potential range from near zero (corresponding to chance performance, AUROC = 0.5) to around 100% (AUROC = 0.87, performance of expert panel). Second, we suggest that the Spearman rank correlation coefficient may be useful as a measure of agreement between a future observer's responses and those of the expert panel (Svensson, 1997). Because this coefficient takes into account the relative ranking of the responses rather than their magnitude, it is independent of the observer's attitude, i.e. their inclination to call a disc damaged. Consider, for example, three images graded as "probably damaged", "probably healthy", and "definitely healthy" by the expert panel. An observer responding with "definitely damaged", "not sure", and "probably healthy" would differ in attitude but agree perfectly on the relative ranking of damage, and

their rank correlation with the expert panel would be 1.0. Our data suggest that observers may achieve similar ROC areas with rather different responses (consider observers D and F as an example), and the lack of association between the ROC area and the rank correlation means that these statistics measure somewhat independent aspects of decision-making.

A surprising finding was that individual observers in our study adopted very different response criteria, even though they had been provided with identical written instructions and identical information on the source of the images and the distribution of visual field damage in the sample (compare observers A and E, for example). It is possible that we might have been able to control the criteria more closely, for example by instructing observers to use the “probably damaged” category if they believed that the chances for the eye to be healthy were less than, say, 10%. More importantly, however, our findings underscore the need to distinguish between differences in diagnostic performance, and differences in diagnostic criterion, or attitude, whenever subjective ratings of optic disc damage are involved. This is the principal reason for why we avoided the use of kappa statistics which measure overall agreement but do not isolate differences in criterion (Fleiss, 1971, Feinstein and Cicchetti, 1990).

In addition to the source of our images, here are several other reasons for why the performance on Discus should not be regarded as providing a truly representative measure of an observer’s real-world diagnostic capability. First, we used non-stereoscopic images. Stereoscopic images would have been more representative of slitlamp biomicroscopy, the current standard of care. There is also evidence that many features of glaucomatous damage may be more clearly apparent in stereoscopic images (Morgan et al., 2005). However, the diagnostic improvement over non-stereoscopic images is probably not large (Hrynchak et al., 2004, Parkin et al., 2001, Vingrys et al., 1994, Rumsey et al., 1990). Second, Discus does not permit a comparison of fellow eyes which often provides important clues in patients with early damage (Harasymowycz et al., 2004). Third, the display of images on a computer monitor does not assess an observer’s aptitude at obtaining an adequate view of the optic disc in real patients. Notwithstanding these limitations, we believe that Discus provides a useful assessment of some important aspects of recognising glaucomatous optic disc damage.

Further studies with Discus are now being undertaken to examine the performance of ophthalmology residents and other trainees as compared to our expert group. These studies will also provide insight into which features of glaucomatous optic disc damage are least well recognised, and how clinicians use information on prior probability in their clinical decision-making. A large dataset of responses from a more diverse range of observers will also provide us with the opportunity to apply more powerful techniques of analysis, for example Item Response Theory (Lord, 1980) to optimise the psychometric properties and the utility of this tool.

The Discus software is freely available from www.discusproject.blogspot.com and interested users may submit their results for instant analysis to an automated web server on this site.

6.6 Acknowledgements

Robert Harper, Amanda Harding and Joanne Marks of the OLGA clinic at the Manchester Royal Eye Hospital supported this project and contributed ideas. Jonathan Layes (Medicine) and Bijan Farhoudi (Computer Science) of Dalhousie University, Halifax, NS helped to improve the software and to implement an automated analysis on our server. We are most grateful to all 12 anonymous observers for their participation.

7. Evaluating the strength of the topographic structure-function relationship in glaucoma

Contribution

The data for this project was taken from the databases of previous studies in Manchester and Halifax, Canada. I carried out the selection of suitable patients from these databases and built the patient database studied. The idea to map locations of disc damage to locations of visual field loss came from Ingo Schiessl (IS) and the idea of generating a large number of random maps to test was my own. I carried out all the MATLAB programming and statistical analysis for this project myself, with supervision from IS and David Henson (DBH). I also wrote the manuscript (currently under review) and this thesis chapter myself with helpful comments provided by IS and DBH.

Publications

Denniss J, Henson DB, Schiessl I (2010) Evaluating the strength of the topographic structure-function relationship in glaucoma (*manuscript currently under peer-review*)

Conference Presentations

Denniss J, Henson DB, Schiessl I (2010) Evaluating the strength of the topographic structure-function relationship in glaucoma. IPS Congress 2010, Puerto de la Cruz, Tenerife, Spain (paper)

7.1 Abstract

7.1.1 Purpose

To evaluate the strength of the relationship between topographical areas of structural and functional damage in glaucoma.

7.1.2 Methods

Visual field (VF) and HRTII sectoral Moorfields Regression Analysis (sMRA) optic nerve head (ONH) data from 185 eyes of 185 patients with clinically diagnosed glaucoma based on both optic disc and visual field damage were taken from the de-identified databases of previous studies in Manchester, UK (n=93) and Halifax, Canada (n=92).

VF test points were divided into 6 groups to form topographic maps. VF Total Deviation values were split into 3 grades, and the mode grade of points within a group taken to represent the group. A discordance measure was devised whereby a VF group whose grade did not equal the corresponding sMRA grade for a particular map was marked a discord. Proportion of discordance in all 6 corresponding VF/ONH areas across all patients was calculated for each map (0=perfect relationship, 1=no relationship). Discordance was compared for all permutations of 10000 computer-generated maps and an existing structure-based map (SBM).

7.1.3 Results

The SBM discordance was 0.4468, less than all other permutations of itself (n=720). Lowest discordance from the 10,000 randomly generated maps was 0.4297. 22.68% of randomly generated maps had one or more permutation with discordance less than or equal to the SBM.

7.1.4 Conclusions

The topographic structure-function relationship found was weak. Anatomical and measurement variation may partially account for this, though variation in disease process between patients cannot be excluded. The application of such maps to individual patients may be limited.

7.2 Introduction

Open-angle glaucoma is an optic neuropathy which leads to functional loss in the visual field and structural changes at the optic disc and/or retinal nerve fibre layer (RNFL). It is an age-related and commonly progressive disease which is one of the leading causes of blindness in the developed world (Quigley, 1996).

Whilst there have been many investigations going back many years into the temporal sequence of structural and functional changes in glaucoma, the topographic relationship between areas of optic disc damage and corresponding areas of visual field damage is less well-tested.

Particularly, though there have been several papers which attempt to define this topographical relationship (Anton et al., 1998, Boden et al., 2002, Danesh-Meyer et al., 2006, Gardiner et al., 2005, Garway-Heath et al., 2000, Turpin et al., 2009, Yamagishi et al., 1997) (described later), there is a dearth of information relating to how strong the relationship is, and how applicable it is to larger populations of patients with glaucoma.

Determining the topographic relationship between structural and functional changes in glaucoma is clinically important in cases where structural or functional measures alone are not sufficient for a diagnosis of glaucoma (or glaucomatous disease progression) to be confirmed or excluded. Concordance or discordance between the two measures, such as a visual field defect in an area known to correspond to an area of focal neuroretinal rim (NRR) loss, may help the clinician to decide on a particular treatment or follow-up regime for a patient. Combining test data in this way is routinely carried out mentally by clinicians, but even without automation accurate decision making relies on the existence of an applicable topographic relationship. Understanding of this relationship is also important when investigating the temporal sequence of structural and functional changes in glaucoma. Whilst this is dependent on the tests used to measure the changes, the subject attracts continued interest both for its implications for disease detection with new and existing instruments and also for its importance in development of clinical guidelines for the treatment and follow-up of patients with glaucoma.

With the development and application of diagnostic imaging devices such as scanning laser ophthalmoscopy and optical coherence tomography comes a new potential for more targeted, patient-specific functional testing. It has been suggested, for example, that placement of stimuli in visual field tests may be informed by topographic maps relating objective structural measurements to areas of the visual field. This technique may allow the time available to conduct a visual field test to be better weighted towards areas where a defect is expected and/or more clinically relevant (Turpin et al., 2009).

The general idea of a topographic structure-function relationship has been accepted in clinical practice for many years. The association between loss of inferior NRR tissue and visual field loss in the superior hemifield or *vice versa* is a typical example. Several attempts have been made to precisely define this relationship by linking spatial locations of functional losses in the visual field with corresponding structural changes in the NRR or RNFL in order to produce more detailed topographic maps (Anton et al., 1998, Boden et al., 2002, Danesh-Meyer et al., 2006, Gardiner et al., 2005, Garway-Heath et al., 2000, Turpin et al., 2009, Yamagishi et al., 1997).

Figure 7.1 shows the map published by Garway-Heath *et al* (2000) which links each test location of the 24-2 visual field test to one of six optic disc sectors. This map, which from this point will be referred to as the Garway-Heath map, was produced by superimposing the 24-2 test pattern onto fundus photographs showing prominent RNFL bundles or visible RNFL bundle defects which could be manually traced back to insertion at the optic disc. The map produced is consistent with what would be expected from the neural layout of the retina (Fitzgibbon and Taylor, 1996, Ogden, 1974, Ogden, 1983, Radius and Anderson, 1979) but is based solely on structural data, no visual field data were used. Despite this the map has been widely accepted and used in studies of the relationship between retinal light sensitivity and optic disc or RNFL structure in glaucoma.

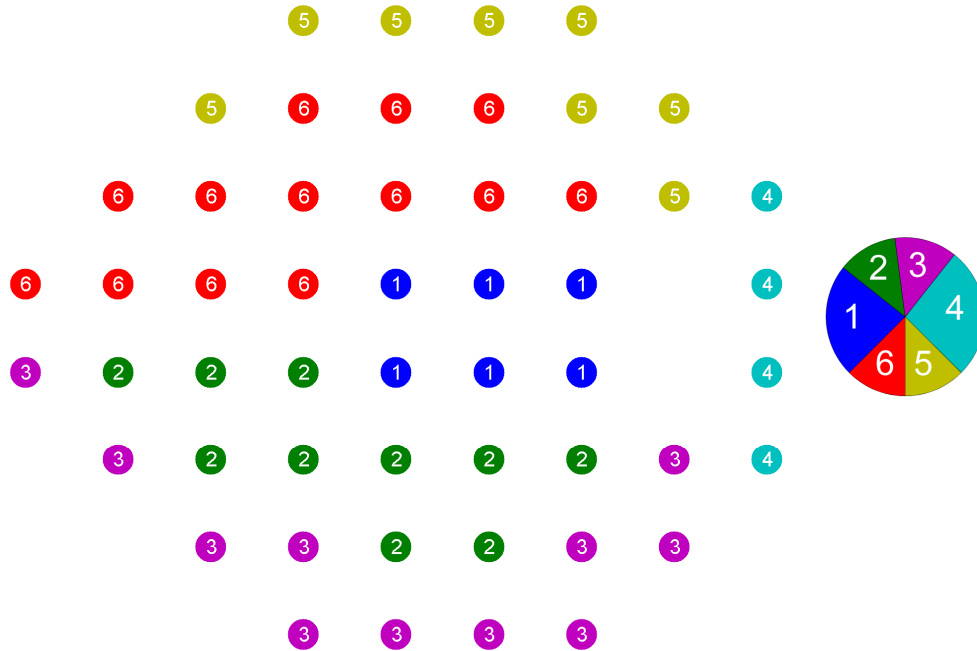


Figure 7.1: Representation of the 24-2 visual field sectors (left) as defined by Garway-Heath (2000) with colour and numerically-coded corresponding optic disc sectors (right) for a right eye. Optic disc sectors are numbered sequentially from 1 to 6 with 1 being the temporal sector, 2 the superior-temporal sector etc.

More recently, papers by Gardiner *et al* (2005) and Turpin *et al* (2009) have described maps based on visual field sensitivity data and HRT optic disc measurements from patients with glaucoma. Gardiner *et al* based their map on whichever of 36 optic disc sectors best correlated with each test location of the 24-2 pattern within their sample. The correlations found were, however, very weak with the best correlation between each test location and an optic disc sector ranging from 0.120 to 0.520 (mean 0.277) and only 27 of the 52 non-blind spot test locations exhibiting a correlation greater than 0.2 with at least one optic disc sector. Similar weak relationships were found by Turpin *et al* albeit with a smaller dataset. Their results showed that 67% of visual field locations could be mapped to one of six optic disc sectors with statistical significance after both the visual field and optic disc measurements had been normalised with the fellow eye. The mean correlation between a visual field location and corresponding optic disc sector was 0.35.

One reason for this weak topographic structure-function relationship is the large amount of between-subject variation exhibited in the temporal sequence of structural and functional changes as found in previous cross-sectional studies (Harwerth and Quigley, 2006, Hood et al., 2007). Whilst this is a limitation of using cross-sectional data it cannot exclude the possibility that the topographic structure-function relationship may not follow the anatomically expected pattern, or may simply be weak. The use of a large cross-sectional dataset should minimise this problem by averaging, making it unlikely that this variability could fully explain a lack of a strong relationship. Variations in disease process may offer another explanation for measurements taken from patients with glaucoma not following the anatomically expected pattern.

In this paper we evaluate the strength of the topographic relationship between clinical measures of optic disc structure and functional measures of the visual field in glaucoma. We test both a published structure-based map (the Garway-Heath map) and a large sample of computer-generated maps in which visual field test points are randomly grouped and assigned to corresponding optic disc sectors without any clinical or scientific preconceptions. Our hypothesis is that if a strong relationship does exist between locations of optic disc and visual field damage, then the computer-generated maps which show the strongest relationship in the sample should approximate to the true relationship, irrespective of the absolute correlation.

7.3 Methods

7.3.1 Study population

SITA 24-2 (Humphrey Field Analyzer, Carl Zeiss Meditec, Ca) visual field and HRTII (Heidelberg engineering GmbH, Germany) optic disc data from 185 patients with primary open-angle glaucoma and previous visual field test experience were taken from the de-identified databases of previous studies in Manchester, UK (Coops et al., 2006) (n=93) and Halifax, Canada (Artes and Chauhan, 2005) (n=92). All patients provided written informed consent in agreement with the tenets of the Declaration of Helsinki at the time of the original studies. The studies were approved by the ethics committees of the respective institutions.

All patients had clinically-diagnosed glaucoma based on both optic nerve head and visual field damage confirmed over at least 4 visits to the glaucoma clinics of either the Manchester Royal Eye Hospital (Manchester patients) or the Eye Care Centre at the Queen Elizabeth II Health Sciences Centre (Halifax patients). In addition, patients were selected who had both visual field mean deviation (MD) worse than (<) -2.5dB and pattern standard deviation (PSD) worse than (>) 2.5dB. All included visual field plots and corresponding HRT topography data were also examined by one author (JD) to confirm compatibility with a diagnosis of glaucoma (for example to rule out clear non-glaucomatous visual field loss such as hemianopia).

Where both eyes of a patient were eligible for the study, one eye was selected randomly, and all data from left eyes were converted to right for analysis. Table 7.1 shows the age and visual field global characteristics of the studied population.

Table 7.1: Age and visual field global characteristics of subjects from Manchester (n=93), Halifax (n=92) and overall (n=185). Most patients had early to moderately advanced glaucoma.

		Median	Range
Age (years)	Overall	71	40 to 96
	Manchester	71	42 to 96
	Halifax	71	40 to 96
Mean Deviation (dB)	Overall	-7.6	-29.0 to -2.6
	Manchester	-5.7	-26.1 to -2.6
	Halifax	-10.0	-29.0 to -3.1
Pattern Standard Deviation (dB)	Overall	6.7	2.5 to 12.6
	Manchester	5.8	2.5 to 12.5
	Halifax	7.8	2.5 to 12.6

Optic discs were analysed by Moorfields Regression Analysis (MRA, described elsewhere (Garway-Heath and Hitchings, 1998)). Table 7.2 shows the distribution of MRA grades assigned to individual optic disc sectors (n=6x185=1110) from the HRT.

Table 7.2: Distribution of assigned Moorfields Regression Analysis (MRA) grades to individual optic disc sectors from the HRT (n =6x185 =1110)

MRA Sector grade	Overall		Manchester		Halifax	
	Number of sectors	%	Number of sectors	%	Number of sectors	%
0: Within normal limits	484	44	291	52	193	35
1: Borderline	232	21	107	19	125	23
2: Outside normal limits	394	35	160	29	234	42

7.3.2 Grading and grouping of visual field points

Visual field sensitivities are reported as a continuous variable in the 24-2 test whereas optic disc sectors are discretely classified by MRA as in Table 7.2. To facilitate comparison of visual field sensitivities to the HRT optic disc data, we split the visual field total deviation (TD) values into three grades, 0, 1 and 2. Our method for doing this is described below.

7.3.2.1 *Minimum discordance method for grading of visual field sensitivities*

This method set the visual field grade boundaries so that we had the best possible outcome for the Garway-Heath map (figure 7.1) given our patient data set, meaning that any bias induced by the grading of the visual field points is in favour of the Garway-Heath map. This method was chosen as all grading methods had potential to introduce some bias into the results, and it was decided that by biasing towards the structure-based Garway-Heath map, any stronger alternative topographic relationships found were more likely to be genuinely stronger relationships, rather than simply the result of biased visual field grading. Also, this method was not influenced by any preconceptions of what constitutes a particular severity of defect.

In order to find which boundaries generated the maximum relationship using the Garway-Heath map an algorithm was written in MATLAB (R2008a, MathWorks Inc, USA) which set the lower boundary at every value between 0.0dB and 10.0dB in 0.1dB steps, and the upper boundary at every value between [lower boundary + 0.1dB] to [lower boundary +10dB] in 0.1dB steps. This gave 10100 possible combinations of boundaries, each of which was tested with the Garway-Heath map. In order to assess the strength of the relationships we grouped the visual field points into the six groups described by Garway-Heath *et al* (2000) and took the mode grade

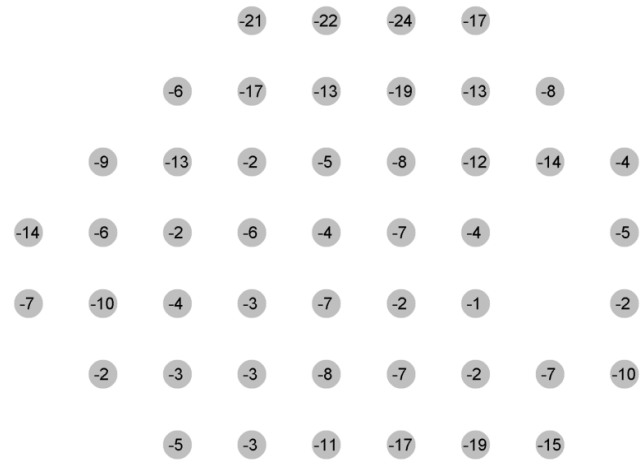
within each group to represent the overall level of damage in the group. Figure 7.2 shows an example of how a visual field is graded and grouped. We chose to take the mode grade within the group rather than other measures (median, mean rounded to nearest integer) for the following reasons: The median, whilst potentially more closely related to retinal ganglion cell count, was trialled and found to result in weaker relationships (albeit the differences were small). The grades in the groups were generally not normally distributed therefore the mean would be a poor representation. Each group was then compared to its corresponding optic disc sector (taken directly from the HRT sectoral MRA, see 'Optic disc sectors' later) using a simple discordance measure which is described later (see 'Discordance measure' section). This process was repeated for all 185 patients in our sample.

The final grade boundaries chosen were:

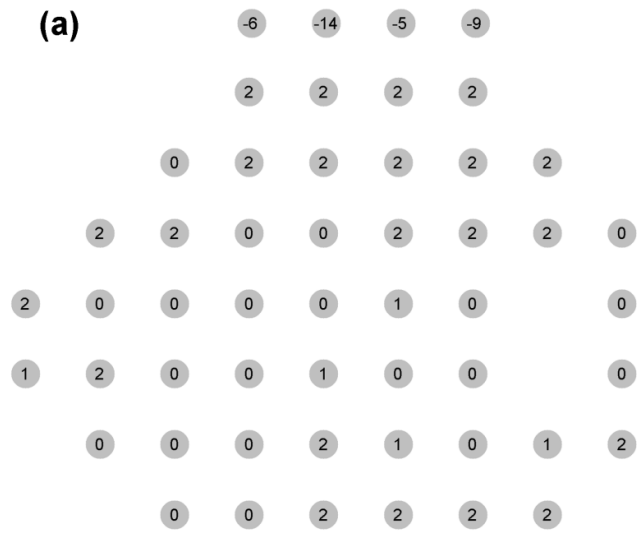
'0' = $TD > -6.8\text{dB}$,

'1' = $-6.8\text{dB} < TD < -7.9\text{dB}$,

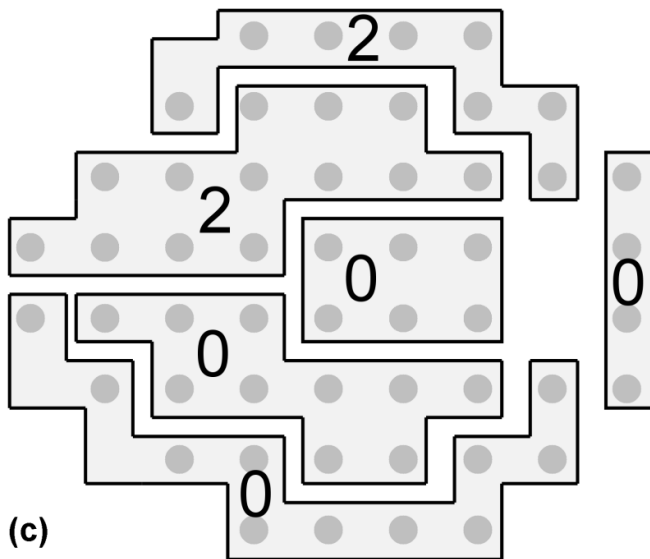
'2' = $TD < -7.9\text{dB}$.



(a)



(b)



(c)

Figure 7.2: Example of how visual field points were graded and grouped, in this case according to the Garway-Heath map. Individual total deviation values (a) are graded either 0, 1 or 2 (b) then the mode value of points within a group is taken to represent the group (c). Blind spot points are ignored for this analysis. See Figure 7.1 for how these groups relate to the optic disc sectors.

7.3.3 Optic disc sectors

The optic disc sectors were taken directly from the 6 MRA sectors used in the HRTII software. In this study 'sector grades' are designated as in table 7.2.

These optic disc sectors differ slightly from those described by Garway-Heath *et al* (2000) as shown in table 7.3. These differences are not likely to affect the results of our study due to the mean standard deviation of assigned optic disc position to visual field test locations being 7.2° in the study by Garway-Heath *et al* (2000). This means that for 95% of patients a given visual field test location corresponds to a point on the optic disc within an almost 30° range.

Table 7.3: Differences in optic disc sectors between those described by Garway-Heath *et al* (2000) and those used in the HRT Moorfields Regression Analysis. These differences are not likely to affect our results due to the large variability in the data used in the study by Garway-Heath *et al*

Sector	Garway-Heath <i>et al</i> (2000) (degrees)	HRT-MRA (degrees)
Temporal	311-40	315-45
Superior temporal	41-80	45-90
Superior nasal	81-120	90-135
Nasal	121-230	135-225
Inferior nasal	231-270	225-270
Inferior temporal	271-310	270-315

Figure 7.3 shows the distributions of grades at each optic disc sector and corresponding visual field sector (according to the Garway-Heath map) for all 185 subjects.

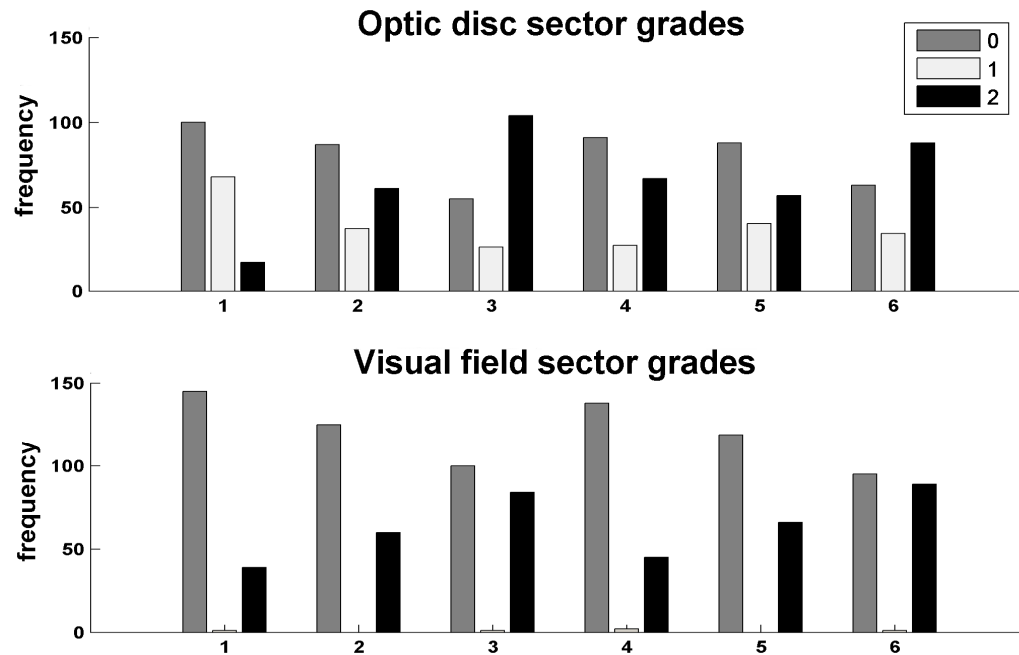


Figure 7.3: Distribution of grades assigned to sectors of optic discs (top) and corresponding visual field sectors according to the Garway-Heath map for all subjects (bottom). Sectors numbered sequentially as in Figure 7.1.

7.3.4 Discordance measure

In this section we introduce the use of a simple measure of discordance. We consider a discord to have occurred when the grade assigned to a visual field group and corresponding optic disc sector of a patient do not exactly match, for example if the visual field sector is graded '2' and the optic disc sector is graded '1' then there is a discordance. In this way each of the six corresponding visual field and optic disc sectors for each patient is considered and the proportion of discordance in the entire population calculated. The resultant discordance score lies between zero and one, with scores closer to zero representing less discordance i.e. stronger match between visual field and optic disc sectors. The simplicity of this measure becomes apparent when displayed in a graphical form. If we plot the grade of the visual field sector against the grade of the corresponding optic disc sector (see figure 7.4) the result is 9 locations representing the 9 possible combinations of matching the grades 0, 1 and 2. If there was a perfect match of grades between the visual field groups and corresponding optic disc sectors all points would lie on the diagonal and discordance would be 0. The measure is represented by

the following formula where n is the total number of points and $\sum exactmatch$ is the number of points on the diagonal:

$$discordance = 1 - \frac{(\sum exactmatch)}{n}$$

Visual field sector grade	0	393	153	176
	1	0	4	1
	2	91	75	217
		0	1	2
		Optic disc sector grade		

Figure 7.4: Number of individual optic disc sectors and corresponding visual field groups (according to the Garway-Heath map) given each grade for all subjects. 'Σexactmatch' in the discordance formula above refers to the sectors within the grey line. All sectors outside of the grey line are considered discords in the calculation. In this example 614 of 1110 sectors are within the grey line so discordance is $1 - (614/1110) = 0.4468$.

In order to evaluate what discordance could be expected by a chance relationship between optic disc structure and visual field sensitivity in our dataset, a dataset of equal size to the patient dataset was generated, in which for each visual field test location and each optic disc sector the distribution of grades '0', '1' and '2' exactly matched the equivalent distribution in the patient dataset, but with random assignment to 'subjects'. Discordance calculated from this dataset can be considered the discordance due to chance topographical correspondence in our dataset and used as a reference against which the discord measures from the real patient data may be compared.

Discordance was calculated for the Garway-Heath map in both its standard form and also for every possible permutation of the six sectors ($n=720$).

7.3.5 Generation of random structure-function maps

To explore the possibility of a strong topographic structure-function relationship existing within our dataset which does not conform to the Garway-Heath map, 10,000 maps were generated in MATLAB in which visual field test locations were randomly assigned to one of six groups. The six groups consisted of the same numbers of points as the groups in the Garway-Heath map such that the numbers of points in each group were as follows: 4, 6, 8, 10, 11, 13. These points could be spread anywhere in the visual field.

As the groups were random, there was no expected correspondence between any particular group and optic disc sector. For this reason discordance was calculated for every possible permutation of the six groups and six optic disc sectors ($n=720$). Therefore we calculated discordance from 7.2 million different projections from the visual field points to the optic disc sectors with our patient dataset.

If a strong topographic structure-function relationship existed within the dataset it would be expected that the best performing (lowest discordance) maps from these 10,000 randomly-generated maps would at least approximate to this.

7.4 Results

For the Garway-Heath map discordance was 0.4468, which was less than all other permutations of the map (median discordance 0.4982, range 0.4468–0.5360).

These results may be compared to the dataset generated as a reference containing the same distribution of optic disc and visual field sector grades at each location but with random assignment of these to 'subjects'. Discordance for all permutations of the Garway-Heath map was measured in the range 0.5477 – 0.6261 (median discordance 0.5838). The distribution of discordance measurements from the patient dataset was significantly lower than this distribution (Mann-Whitney U test, $p<0.01$). For the Garway-Heath map in its standard form discordance was 0.5631.

The best projection from all 7.2 million calculations is shown in figure 7.5. The minimum discordance found was 0.4297 (figure 7.5). This map appears to be a completely random pattern with no likely anatomical foundation and no respect for the horizontal midline as would be expected if this were the case. 22.7% of the randomly generated maps had at least one permutation with discordance the same as or lower than the Garway-Heath map.

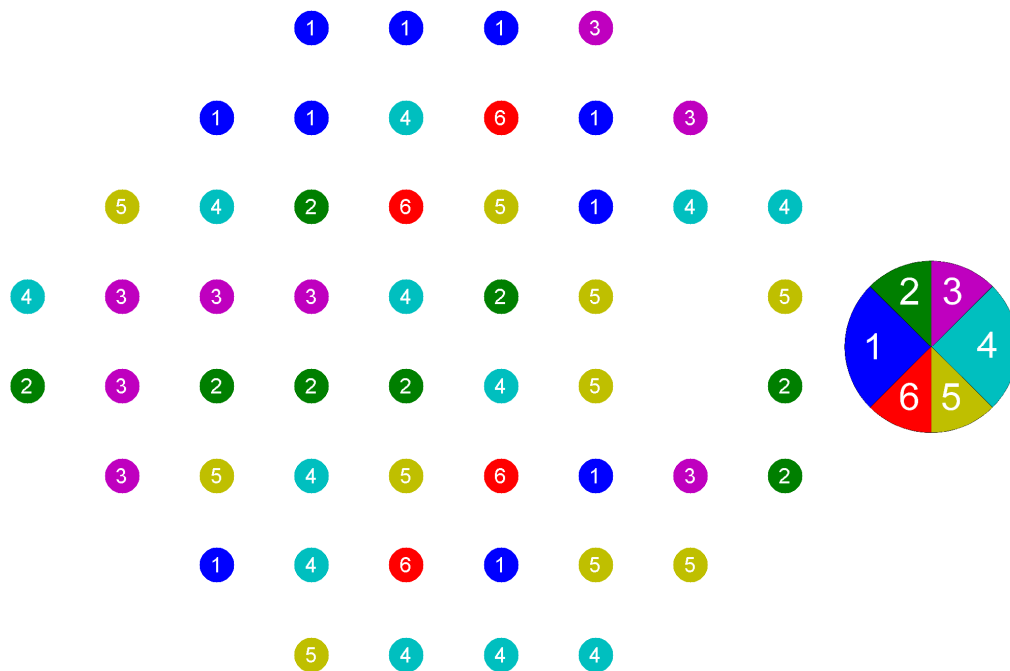


Figure 7.5: The computer-generated map which produced minimum discordance (0.4297) from a sample of 10,000 with colour and numerically-coded corresponding optic disc sectors (right) for a right eye. Optic disc sectors are numbered sequentially from 1 to 6 with 1 being the temporal sector, 2 the superior-temporal sector etc. The visual field points in all groups appear to be randomly distributed with little respect for the horizontal midline as would be expected should the pattern be of anatomical foundation.

7.5 Discussion

The topographic structure-function relationship measured using the structure-based Garway-Heath map was weak. However, the clear distinction between discordance measured with the random dataset and with the patient dataset shows that the relationship found is not likely to be due to chance. The large proportion (22.7%) of computer-generated maps with equal or stronger topographic relationships than the Garway-Heath map suggests that, despite our results being averaged across a large number of patients, the Garway-Heath map does not well represent the topographic relationship in our sample. The strongest topographically-related maps produced do not approximate to the relationship expected based on RNFL anatomy, and their points do not appear to cluster significantly or even respect the horizontal midline as would be expected if a strong topographic structure-function relationship existed. These results suggest that the weak relationships found are not simply due to anatomical and measurement variability, but may actually be a feature of the disease itself.

There are several possible explanations as to why a stronger relationship was not shown. For example, some variation in the layout of ganglion cell axons in the RNFL and their insertion into the optic disc does occur, (Garway-Heath et al., 2000) and variations in axial length, global shape, location of blood vessels and optical properties of the eye add to this, weakening the relationship in cross-sectional data. However, this is unlikely to be the sole factor limiting the strength of this relationship. Anatomical variations are likely to be small, and would be expected to result in clustered areas of visual field points relating to the optic disc sectors, albeit in slightly different positions for different patients. One would expect that by generating a large number of maps using data from a large number of patients these effects would average out such that the best maps would at least approximate to that expected based on RNFL anatomy (i.e. the Garway-Heath map), yet this was not the case.

Similarly, if a physiologically perfect relation existed in the data, with the addition of measurement variability alone we would expect the measurement variability to be approximately evenly distributed around the true values and so by averaging across a large

dataset, and testing such a large number of topographic maps, the best performing map would at least approximate the true relationship. We can clearly see that this does not occur by the lack of any noticeable clustering of points in the best performing map. Also, variability in terms of defect depth in the visual field is reduced by the grading of TD values, which means we are testing a more gross relationship which is less affected by measurement variability than if we had compared absolute values from the optic disc and visual field.

Whilst we know from previous studies that the relationship between ganglion cell loss and loss of visual field sensitivity is approximately linear (when visual field sensitivities are plotted on a linear scale), (Harwerth and Quigley, 2006, Hood et al., 2007, Harwerth et al., 2005, Hood and Kardon, 2007) there is considerable variability in the data and this is another potential factor limiting the strength of the topographic relationship we measure here. Again, however, this variation would be minimised as a result of the large number of patients in our sample.

It seems likely, therefore, that the lack of a strong topographic structure-function relationship in glaucoma may actually be a characteristic of the disease process or processes. For example, one possible theory that would explain why some visual field defects do not correspond topographically to optic disc changes is the occurrence of intermittent or partially mobile visual field defects. These could occur due to localised vascular events or failures of axoplasmic flow at any point along the length of a retinal ganglion cell, which may not affect optic disc structure in the first instance. It has previously been suggested that in some cases reversible visual field damage caused by vascular insufficiency can precede more permanent loss, (Flammer et al., 2002) and it seems reasonable that in these cases there may be no measurable structural change to the optic disc. Another situation which has been proven to occur in experimental glaucoma in primates (Weber and Harman, 2005) is that of dysfunctional ganglion cells which have reduced function (and so produce a visual field defect) yet are still present so structural measures such as the HRT will not detect a change, limiting the strength of any structure-function relationships in glaucoma.

The lack of a strong topographic structure-function relationship in glaucoma is consistent with previous reports. Broadway *et al* (1999) investigated the different patterns of optic disc damage which occur in glaucoma, and the patterns of visual field damage associated with each. It was found that only 7% of patients could be considered to have a 'pure' example of one type of optic disc damage, with most patients having a mix of types. In patients who did exhibit purely focal optic disc damage, nearly all had a focal visual field defect, but in 50% of these cases this was in combination with a more diffuse loss. Conversely in those patients with more generalised optic disc damage 58% had localised visual field damage, which occurred in isolation in 37%. The occurrence of localised visual field defects with generalised optic disc damage and *vice versa* suggests that the spatial patterns of visual field and optic disc damage in glaucoma may not be intimately linked.

Our findings are also consistent with previous studies by Gardiner *et al* (2005) and Turpin *et al* (2009) which also found only weak correlation between spatial locations of optic disc and visual field damage as described in our introduction.

The visual field-grade boundaries generated may be compared to the clinically-derived visual field classifications of Hodapp, Parrish, and Anderson, (Hodapp *et al.*, 1993) although these are for mean deviation rather than individual TD values (MD, weighted mean of all TD values across the whole field), see table 7.4. Whilst our boundary for the most extreme category of loss is lower than that of Hodapp, Parrish and Anderson it is worth noting that our sample contains mostly early to moderate glaucoma, therefore it is perhaps beneficial that we split our dataset into 3 groups which better reflect the distribution of defects within the sample.

Table 7.4: Comparison of chosen visual field grade boundaries with those suggested by Hodapp et al (1993)

	Hodapp et al	Present study
Early '0'	MD>-6dB	TD>-6.8
Moderate '1'	-6dB>MD>-12dB	-6.8<TD<-7.9
Advanced '2'	MD<-12dB	TD<-7.9

An interesting finding of this study is that when the visual field grade boundaries were adjusted to minimise the discordance produced by the Garway-Heath map, very few '1's resulted. This implies that the strongest relationship between the two measures is achieved when the 'borderline' HRT values are considered 'within normal limits'. A possible explanation is that the topographic relationship is stronger in more advanced disease, so a stronger relationship results when early losses are ignored. This is consistent with a theory of intermittent visual field losses preceding permanent losses in early glaucoma.

An alternative approach to the analysis of these data could avoid the pitfalls of grading the visual field and optic disc sectors into discrete categories. Mean visual field sensitivity within each visual field group could be compared to the log neuroretinal rim area within each corresponding optic disc sector by Spearman correlation, and the correlation coefficients summed to obtain an overall measure of association for the map tested. This could be done for each permutation of the Garway-Heath map and the randomly generated maps as in this study. A re-analysis by this method of the data reported here may be carried out in a future study.

One difference between this study and some previous studies is that we did not apply any further analysis to the optic disc data beyond that carried out by the standard software supplied with the instruments, such as normalising against the fellow-eye or adjusting for the exact position of the optic disc. Whilst this could be seen as a limitation of our study in that we may have found a slightly stronger relationship had we done this, it must be remembered that for topographic structure-function maps to be of clinical use they must be applicable to clinical

data. By using optic disc and visual field measures which are readily available to clinicians our results are more applicable to clinical scenarios where such further analysis is not feasible at present.

Previous studies have also divided the optic disc into more sectors than the six used in this study in order to link areas of the NRR with visual field test locations with greater resolution.

However in our study this would only weaken the relationship found. Because of this, our results may be considered a 'best-case' for unmodified clinical data from patients with early to moderately advanced glaucoma. In more advanced cases of glaucoma visual sensitivity tends towards zero across the entire visual field and the optic disc tends towards total cupping so it is unlikely that inclusion of such cases in our dataset would improve the relationship found.

In conclusion the application of topographic structure-function maps to individual patients with glaucoma may be limited, possibly as a consequence of the disease process itself. This reduces the clinical and scientific utility of these maps such as in combining topographical information from the optic disc and visual field to aid glaucoma diagnosis in uncertain cases or in targeted patient-specific perimetric tests. It is possible that the weak relationship found is not simply a result of measurement and anatomical variation between patients but is also contributed to by the disease process itself, and further research is required to ascertain the mechanisms behind sensitivity losses in the visual field which are not explained by corresponding optic disc change.

7.6 Acknowledgements

We would like to thank Dr Paul H Artes and Dr Balwantray C Chauhan, Dalhousie University, Canada for use of their dataset, and Dr Anna Kwartz who collected the Manchester data.

8. Testing of a high-resolution multispectral fundus imaging system for measurement of optic disc tissue oxygenation

8.6 Contribution

This work was carried out by our multispectral imaging group; myself, David Henson (DBH), Ingo Schiessl (IS) and Vincent Nourrit (VN) in collaboration with an MSc student working with us, Mikhail Ponomarenko (MP). MP was conducting his MSc project on the topic of test-retest variability of optic disc oxygenation measured by multispectral imaging.

The modification of the fundus camera and construction of the multispectral system were carried out mainly by VN with help from myself and DBH. Initial informal testing of the system was carried out by myself and VN with help from DBH and IS. The method of converting the multispectral image data to oxygenation maps was previously developed by IS for brain imaging and modified for these image series by IS.

The repeatability study was designed by myself and DBH, and subjects were recruited by MP. Monochromatic image series were collected by MP under my supervision/instruction. MP also carried out (under my supervision/instruction) the alignment of the monochromatic images using a series of MATLAB routines written by VN, and computed the oxygenation maps from the aligned images using a MATLAB script written by IS. MP then carried out the segmentation of the optic discs from surrounding tissue and the masking of the blood vessels using a series of MATLAB routines written by myself.

The division of the optic discs into 8 sectors relevant to use in glaucoma, evaluation of test-retest variability of the oxygenation measurements in these sectors and statistical analysis was then carried out by me. This was done with a view to using these sectors in my next projects (reported in chapters 9 and 10). MP independently carried out his own analysis of generic test-retest variability which was less specific to glaucoma and is not reported here. Finally I wrote the chapter featured here.

8.1 Abstract

8.1.1 Purpose

To describe a high-resolution multispectral fundus imaging system and the production of spatial oxygenation maps of the optic disc using the system. To evaluate the test-retest variability of the oxygenation maps in healthy subjects when analysed with relevance to glaucoma.

8.1.2 Methods

Eight eyes of 8 healthy volunteers were imaged with a multispectral system consisting of a modified fundus camera incorporating a Peltier-cooled CCD array and a 250W halogen lamp filtered by a fast-tuneable liquid crystal filter. Eight images were captured sequentially over ~1.5s at wavelengths selected according to absorption properties of blood components (range 496- 700nm), and a Beer-Lambert law model was used to produce oxygenation maps of the optic disc from the aligned images. Subjects were imaged 12 times in 4 sets of 3 images over two visits to the department. After segmentation of the optic disc and masking of visible blood vessels from the oxygenation maps, the disc was divided into eight 45° sectors. Test-retest variability was evaluated both within- and between-sets of images by coefficient of variation, estimated within-subject standard deviation and Bland-Altman analysis.

8.1.3 Results

Coefficients of variation in oxygenation for all sectors were below 5% both between images within a set and between averaged values from different sets. No significant differences were found in coefficients of variation ($p=0.21$) or estimated within-subject standard deviation ($p=0.07$) when comparing images within a set or comparing averaged values between sets. Limits of repeatability between averaged values from sets taken both ten minutes and one week apart were well within the measured range of the system in these healthy eyes.

8.1.4 Conclusions

Good quality oxygenation maps of the optic disc can be produced using the multispectral system. Measurements of oxygenation in 45° optic disc sectors are repeatable both on the same day and one week later, and the majority of the current variability is between individual images. Improvements in the image processing techniques may further reduce variability.

8.2 Introduction

Ocular blood flow and blood flow velocity can currently be measured by a variety of methods and technologies, but this may be considered a somewhat indirect measurement of what is really important in ischaemic disease, the oxygenation of tissue. In glaucoma for example, progressive structural damage to the optic disc is a hallmark of the disease but controversy remains around the exact mechanisms behind this damage. Some theories suggest that ischaemia or vascular dysregulation at the level of the optic disc may play a role in the pathophysiology of the disease, but the extent of this involvement is difficult to ascertain without a direct method of assessing optic disc oxygenation.

Multispectral imaging has been widely used in biomedical research to directly image changes in brain tissue oxygenation in response to sensory stimuli in animal models (Malonek and Grinvald, 1996, Mayhew et al., 1999, Berwick et al., 2005). The technique relies on the wavelength-dependency of light absorption properties of blood components. By imaging tissue at a range of wavelengths tailored to produce maximally different images relating to oxygen levels, relative oxygenation maps of the imaged tissue can be produced.

Several groups have reported on ocular applications of multispectral imaging techniques which promise a more direct measure of tissue oxygenation. Though approaches to image processing and analysis vary between groups, all methods aim to utilise spectral information which is generally ignored by current imaging devices focusing instead on high resolution of structural detail. Khoobehi *et al* (2004) used a slit spectrography technique to measure relative oxygen saturation changes in the optic discs of immobilised healthy non-human primate eyes in response to alterations in intraocular pressure and the oxygen content of inspired air. Ito *et al* (2008) used multispectral imaging to calculate the oxygenation of small areas of juxtapapillary retina in patients with glaucoma and healthy subjects. On average they found a reduction in oxygenation in glaucomatous eyes compared to healthy eyes (albeit with substantial overlap in range).

In this chapter we describe and test a multispectral system based on modifications made to a standard fundus camera. The aim was to allow collection of multispectral images of the retina quickly and comfortably for the subject, and to process these images to produce repeatable oxygenation maps of the imaged tissue. Since we are particularly interested in the application of this technology to glaucoma, we concentrate on the optic disc and describe an analysis for calculating oxygenation in eight 45° sectors of the disc. We evaluate test-retest variability of the oxygenation levels calculated in these sectors with a view to later relating these measurements to visual function.

8.3 Methods

8.3.1 The Multispectral System

The multispectral system was based around a series of modifications to a mydriatic film fundus camera (Zeiss Fundus Flash 3, West Germany). The original flash light source was removed and replaced with an external source coupled to the camera by optical fibre. The external light source was originally based around a 150W xenon lamp (Osram XBO, Osram GmbH, Germany) which was heat filtered and collimated by a custom-built system. This lamp was powered by a dedicated switched-mode power supply (Rofin 7730, Rofin Ltd, Surrey, UK). Later, we replaced this source with a 250W halogen lamp which has an in-built heat filter and projecting lens (Diamator 150 slide projector, AGFA, Mortsel, Belgium). This light source has a reduced emission profile in the UV, does not produce ozone and greatly reduces the cost of replacement lamps. The halogen lamp was powered by a smoothed DC power supply unit (TSX3510, Thurlby Thondar Instruments, Huntingdon, UK) with a voltage ripple of less than 0.01% to ensure light output was as constant as possible.

The output light was filtered by a fast-tuneable liquid crystal filter (Varispec VIS 07-20 STD, Cambridge Research Instrumentation, UK) with a 7nm half width at half maximum. An aspheric condensing lens then gathered the filtered light into the optical fibre (core diameter 5mm, numerical aperture 0.59), the other end of which was fixed at the position of the fundus

camera's original flash light source by a 3-axis translation system which allowed for careful positioning of the fibre for optimum light delivery.

Reflected light from the fundus was captured by a low-noise Peltier-cooled CCD array (Orca C4742-80-12AG, Hamamatsu Photonics, Hamamatsu, Japan) with a spatial resolution of 336x256 pixels (after 4x4 binning). This replaced the original film camera in the imaging plane of the fundus camera. An auxiliary viewing system was removed from the viewing path of the fundus camera, which shortened the path necessitating the addition of a condensing lens to bring the image onto the CCD array. This viewing system was redundant as the CCD array allows us to monitor the image in real time. Images recorded have a horizontal field-of-view of approximately 15° at the fundus. This is smaller than the fundus camera's original field of view due to the use of a 'cropped' CCD array which is smaller than the original photographic film.

Figure 8.1 shows the system with the halogen lamp.

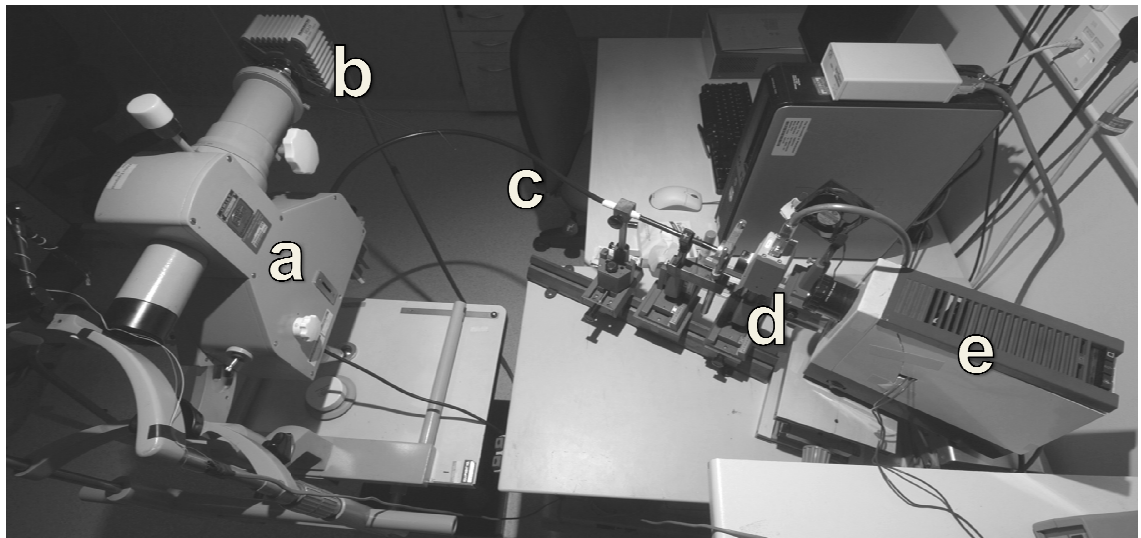


Figure 8.1: The multispectral imaging system incorporating (a) modified fundus camera with (b) Peltier-cooled CCD array, (c) fluid optic, (d) fast tuneable liquid crystal filter and (e) 250W halogen lamp.

8.3.2 Subjects

This study adhered to the tenets of the Declaration of Helsinki and all participants gave written informed consent to take part. The study was approved by the NHS Central Manchester Research Ethics Committee. To formally test the instrument and to evaluate test-retest variability of the oxygenation maps produced (see later) healthy volunteers (n=8, median age 27 years, range 25-61 years) with no ocular disease, clear ocular media and normal visual fields were recruited. Following pupillary dilation subjects were imaged 3 times in succession with the multispectral system (see below), followed by a ten minute break before another 3 image series were collected in succession. Subjects were then asked to return one week later to repeat the same process. Each monochromatic image series was used to produce one multispectral image (see section 8.3.4 later), leaving us with four sets of 3 images (12 monochromatic image series in total) collected on two separate visits to the department. Figure 8.2 describes this process for the purpose of clarity.

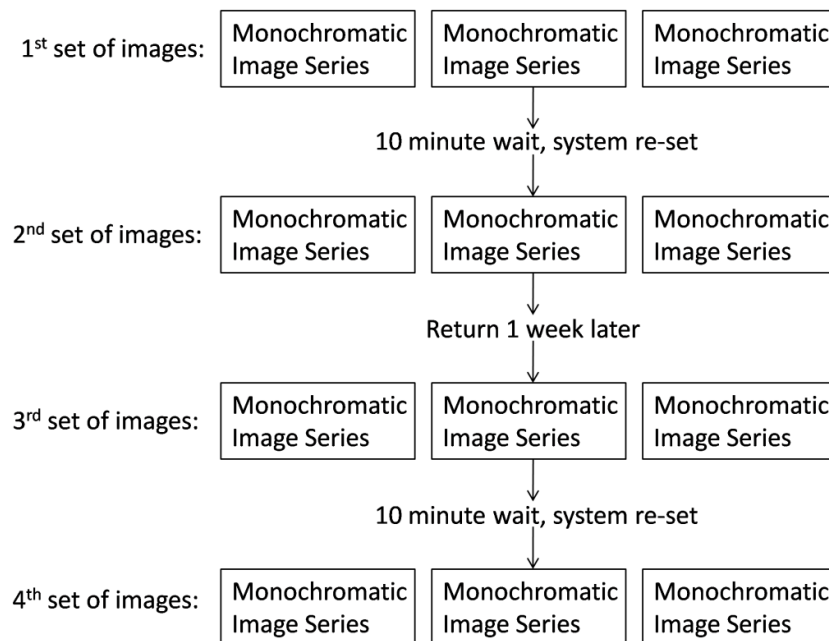


Figure 8.2: Flow chart describing the images captured for each patient. On the first visit 3 monochromatic image series were captured consecutively to form the first set of images. After a ten minute wait a further 3 monochromatic image series were captured consecutively to form the second set of images. The patients then returned one week later and the process was repeated to form the third and fourth sets of images. Each of the 12 monochromatic image series was used to produce an oxygenation map (see section 8.3.4).

8.3.3 Image Capture

Monochromatic images were captured sequentially at 8 different wavelengths (496, 550, 570, 575, 580, 586, 610 and 700nm) selected according to the absorption properties of blood components (OMLC, 1998, van Assendelft and Zijlstra, 1975, Benesch *et al.*, 1973). More specifically, we captured images at 2 isobestic wavelengths (550 and 570nm), at wavelengths where the ratio between light absorption by oxygenated and deoxygenated haemoglobin is maximal (575, 580 and 610nm) and at 700nm, where tissue scattering dominates. We also acquired images at the wavelengths 495nm and 586nm for the future implementation of a path length independent spectroscopic analysis similar to that of Berwick *et al.* (2005).

Total acquisition time for the 8 monochromatic images was <1.5s, with the exposure time for each individual image varying according to wavelength (range 0.03s (610 and 700nm) to 0.6s (496nm)). This variable acquisition time compensated for the emission profile of the light source, the transmission profile of the liquid crystal filter and the sensitivity profile of the CCD array, all of which are lowest at the blue end of the spectrum. Approximately 0.3s of the total acquisition time was attributable to the time taken for the filter to switch between wavelengths. Following capture, all monochromatic images were subjectively reviewed for quality and any poor images, such as those due to eye movement, were discarded and re-captured.

8.3.4 Production of Spatial Oxygenation Maps

The captured monochromatic images were corrected for systematic variations due to the inhomogeneous sensitivity of the system across different wavelengths with a correction factor derived from images taken of a white surface with a flat absorption spectrum.

The monochromatic images were then aligned using a series of MATLAB routines based on the identification of landmarks in the images. Due to the relatively large size of the images and their detailed nature this provides little difficulty. Several approaches to alignment were trialled (combination of translation, rotation and scaling; shearing and/or tilt correction; polynomial fit;

piecewise linear transformation and local weighted mean fit) and a combination of translation, rotation and scaling was deemed best for our images. This was determined simply by direct observation of contrast, resolution of detail and movement artefacts in the aligned images rather than by using arbitrary image quality metrics such as RMS contrast.

Using a Beer-Lambert law model (Malonek and Grinvald, 1996, Mayhew et al., 1999, Berwick et al., 2005) we then calculated pixel-by-pixel oxygenation maps of the imaged tissues from the aligned images. The model used (for each pixel) was as follows:

$$-\log[I_{\lambda}/I_{iso}] = \Delta C_{oxy} \epsilon_{oxy}(\lambda) + \Delta C_{deoxy} \epsilon_{deoxy}(\lambda) + \Delta C_{scattering} \epsilon_{scattering}(\lambda)$$

In the model I_{λ} is the pixel intensity at wavelength λ , I_{iso} is the pixel intensity at the isobestic wavelength 570nm, ΔC_{oxy} and ΔC_{deoxy} are the changes of chromophores (oxygenated and deoxygenated haemoglobin) and ϵ_{oxy} and ϵ_{deoxy} are extinction coefficients for the same. $\Delta C_{scattering}$ and $\epsilon_{scattering}$ are the components for tissue scattering. Appendix I gives a detailed description of how the oxygenation maps are produced from the monochromatic images using this model.

Figure 8.3 shows the steps involved in converting a monochromatic image series to a multispectral image (oxygenation map).

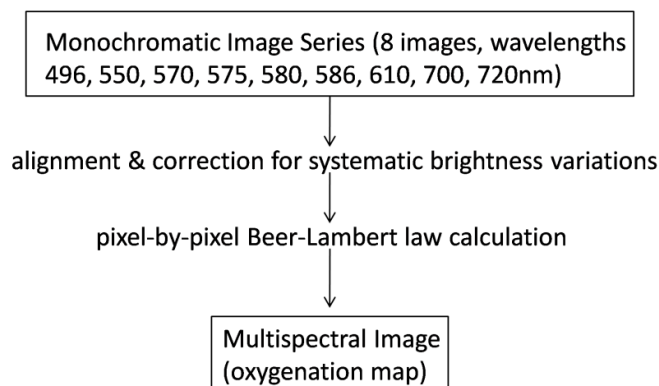


Figure 8.3: Flow chart showing how each monochromatic image series was converted to a single oxygenation map.

8.3.5 Data Analysis

Image processing was carried out in MATLAB (R2008a, The Mathworks Inc, Natick, MA, USA) with the Image Processing Toolbox. A mask was applied to each of the spatial oxygenation maps to segment the optic disc from the surrounding retina, and then a second mask was applied to remove visible blood vessels from the maps, leaving only optic disc tissue. Masking was performed manually on each oxygenation map with reference to the original monochromatic images at each wavelength. Automated masking methods were tried (thresholding, edge detection) but the results were not satisfactory so manual masking was preferred. Oxygenation levels were then calculated from the masked maps in eight 45° sectors around a user-defined central point, as shown in figure 8.4.

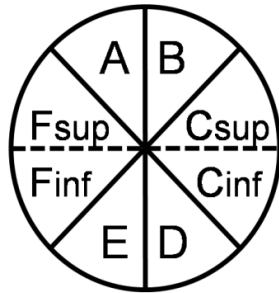


Figure 8.4: The eight 45° sectors (shown for a right eye) into which the optic disc was divided for analysis. In the oxygenation maps the sectors are centred around a user-defined centre point of the optic disc. Sectors in later figures are labelled as in this diagram.

Test-retest repeatability was measured first for each sector across all 12 multispectral images (coefficient of variation, estimated within-subject standard deviation (Bland and Altman, 1996)). Next repeatability within a set of 3 consecutively captured multispectral images was assessed by the same methods. Sector oxygenation values within sets were then averaged (4 sets per patient) to calculate repeatability across different sessions. For these averaged sets repeatability was assessed again by coefficient of variation and estimated within-subject standard deviation. To evaluate repeatability between sessions separated by either ten minutes or one week in more detail Bland-Altman analysis was carried out and limits of repeatability calculated (Bland and Altman, 1986).

8.4 Results

The optic discs of all 8 subjects were successfully imaged 12 times in 4 sets of 3 image series as described above. Anecdotally, all subjects found the imaging process comfortable and no adverse effects were reported. Light measured at the plane of the subject's pupil was below the maximum permissible exposure according to ANSI limits (American National Standards Institute, 2001).

Figure 8.5 shows an example series of monochromatic images from one subject and figure 8.6 shows the oxygenation map produced from these images. In the oxygenation map the brighter areas represent areas of higher oxygenation, and the darker areas represent areas of lower oxygenation. The brightest areas in these maps are generally the blood vessels which are brighter because they have both greater oxygenation and a higher density of the chromophores (haemoglobin) than the surrounding tissue. Oxygenation at each pixel is represented in arbitrary relative units, though because images are scaled for display they do not show the full dynamic range of measurement available.

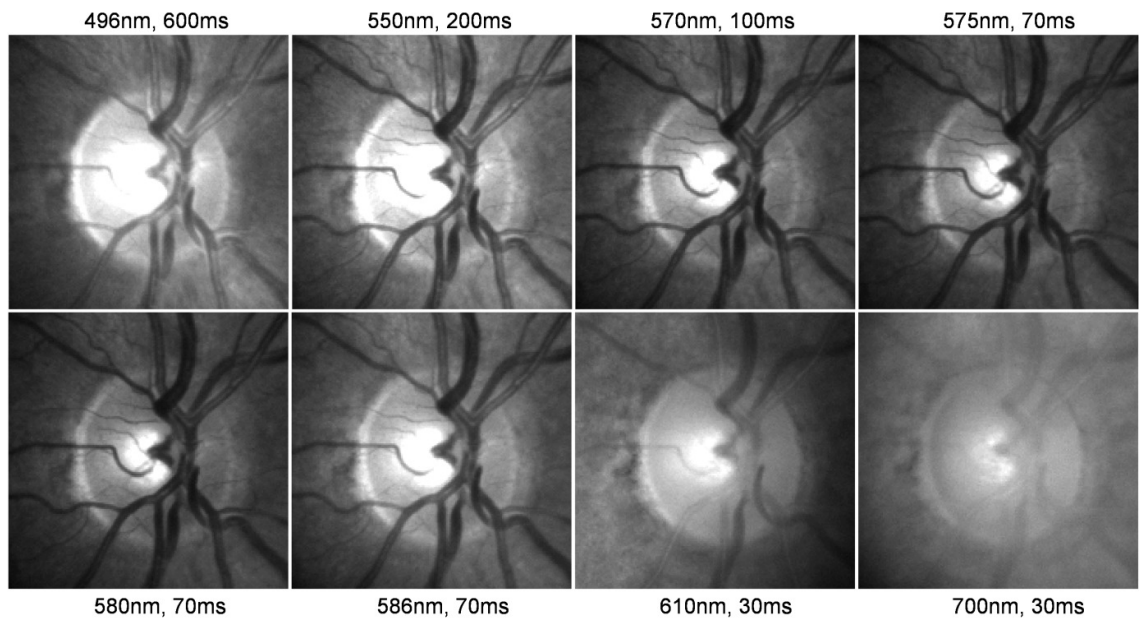
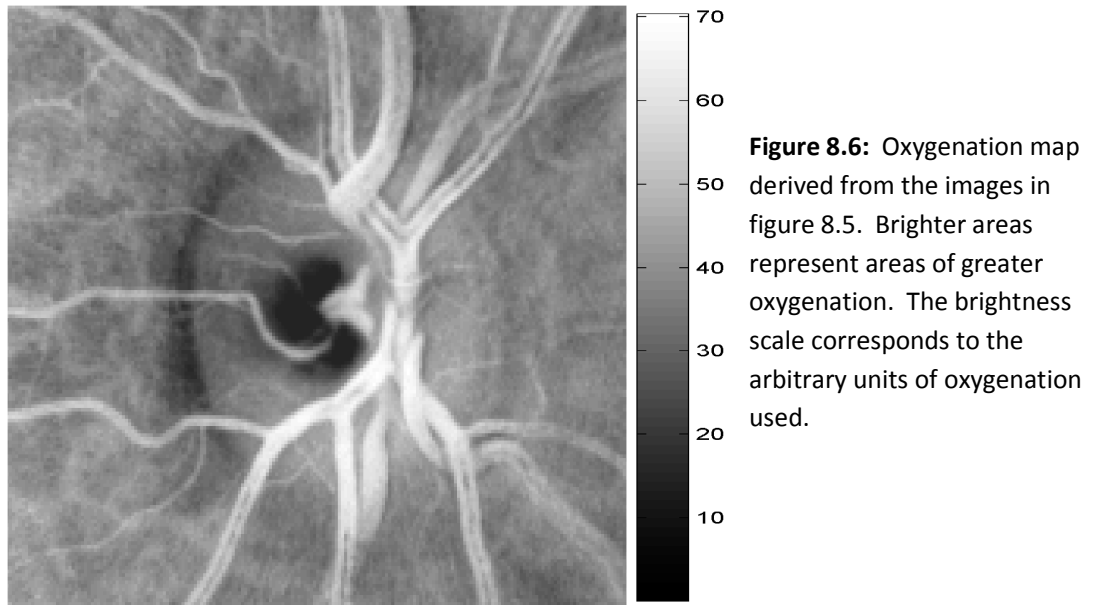


Figure 8.5: Monochromatic images of one subject's optic disc taken at 8 different wavelengths. Images are labelled with wavelength and exposure time.



The manual masking of blood vessels and segmentation of the optic disc from the surrounding retina in the oxygenation maps were potential sources of variability. This can be seen in figure 8.7 which shows six images of one optic disc taken on the same day. Although this may be a somewhat extreme example it highlights the potential for human error to affect the repeatability of the masking done this way. Further potential for variability was added by variations in placement of the user-defined centre point around which the 8 45° sectors were arranged.



Figure 8.7: Six masked oxygenation maps of the same optic disc taken on the same day. Variability can be seen in the manual masking of blood vessels, and also in the manual segmentation of the optic disc from the surrounding retina.

Figure 8.8 shows the coefficients of variation in oxygenation of each optic disc sector (as defined in figure 8.4) for each patient across all 12 images. Each subject is individually represented by a

black circle, and the red circles represent the mean values across all subjects. The red triangles in the plot represent the mean coefficient of variation in optic disc sector oxygenation within sets of 3 consecutively captured images and the red crosses represent the same measure between average values from these sets (for all subjects).

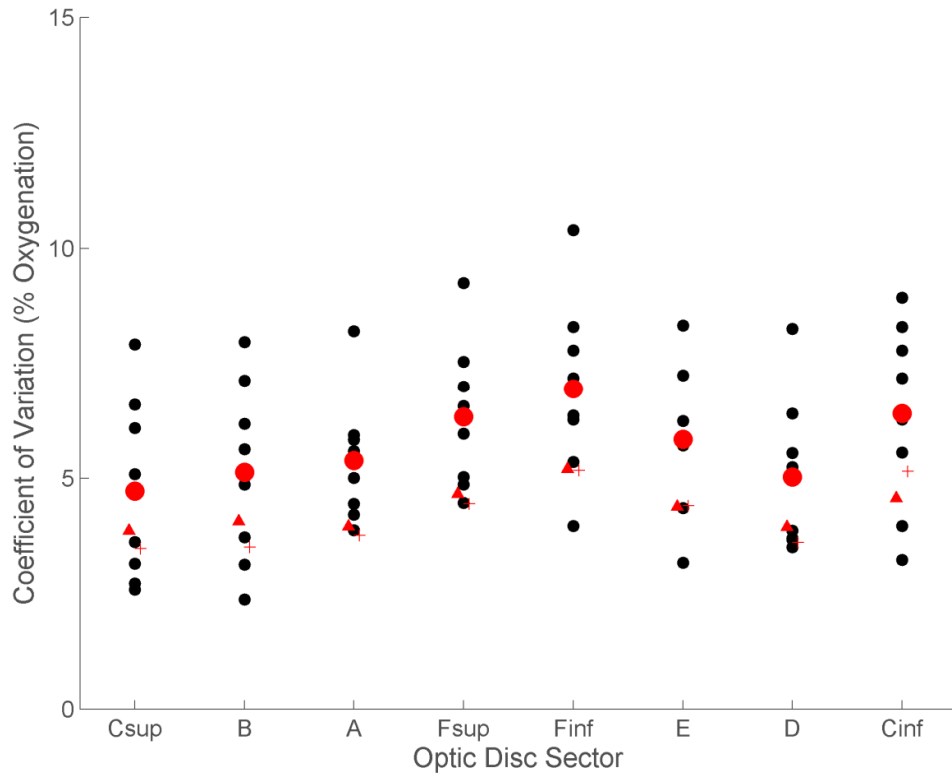

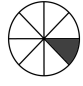


Figure 8.8: Coefficients of variation in optic disc sector oxygenation across all 12 images for all subjects. Each subject is individually represented by a black circle. Red circles represent the mean values across all patients. Red triangles represent the mean coefficient of variation in optic disc sector oxygenation within sets of 3 consecutively captured images, and red crosses represent the same measure between average values from sets (for all subjects). Optic disc sectors are labelled as in figure 8.4.

From figure 8.8 it is apparent that the majority of the variability is between individual images. Variability is similar (no significant difference, Wilcoxon signed ranks test, $p=0.21$) whether comparing images within a set taken consecutively, or comparing images taken in different sessions. Table 8.1 gives the estimated within-subject standard deviations (Bland and Altman, 1996) of optic disc sector oxygenation for all subjects. Again, the majority of variability is between individual images and there is no significant difference in variability within- or between-sets (Wilcoxon signed ranks test, $p=0.07$).

Table 8.1: Estimated within-subject standard deviations (arbitrary units) of optic disc sector oxygenation for all 12 images, within sets of 3 consecutively captured images, and between average values from sets (all patients).

								
All 12 images	1.89	2.14	1.92	1.80	1.86	1.92	1.86	2.12
Within-sets	1.65	1.94	1.62	1.46	1.46	1.61	1.62	1.69
Between-sets	1.38	1.50	1.48	1.44	1.53	1.48	1.38	1.73

Bland-Altman analysis (Bland and Altman, 1986) was used to assess in more detail the variability between sets of averaged oxygenation values for each optic disc sector. Figure 8.9 shows an example Bland-Altman analysis of sector B (superior-temporal) for sets taken 10 minutes and 1 week apart. In a perfectly repeatable test all points would lie on the solid grey line in all the plots. The dashed grey lines in plots (b) and (d) give the limits of repeatability of the test, and the mean difference (mean distance above or below the solid grey line in these plots) represents the systematic bias in the test i.e. whether oxygenation is systematically higher or lower in the second session.

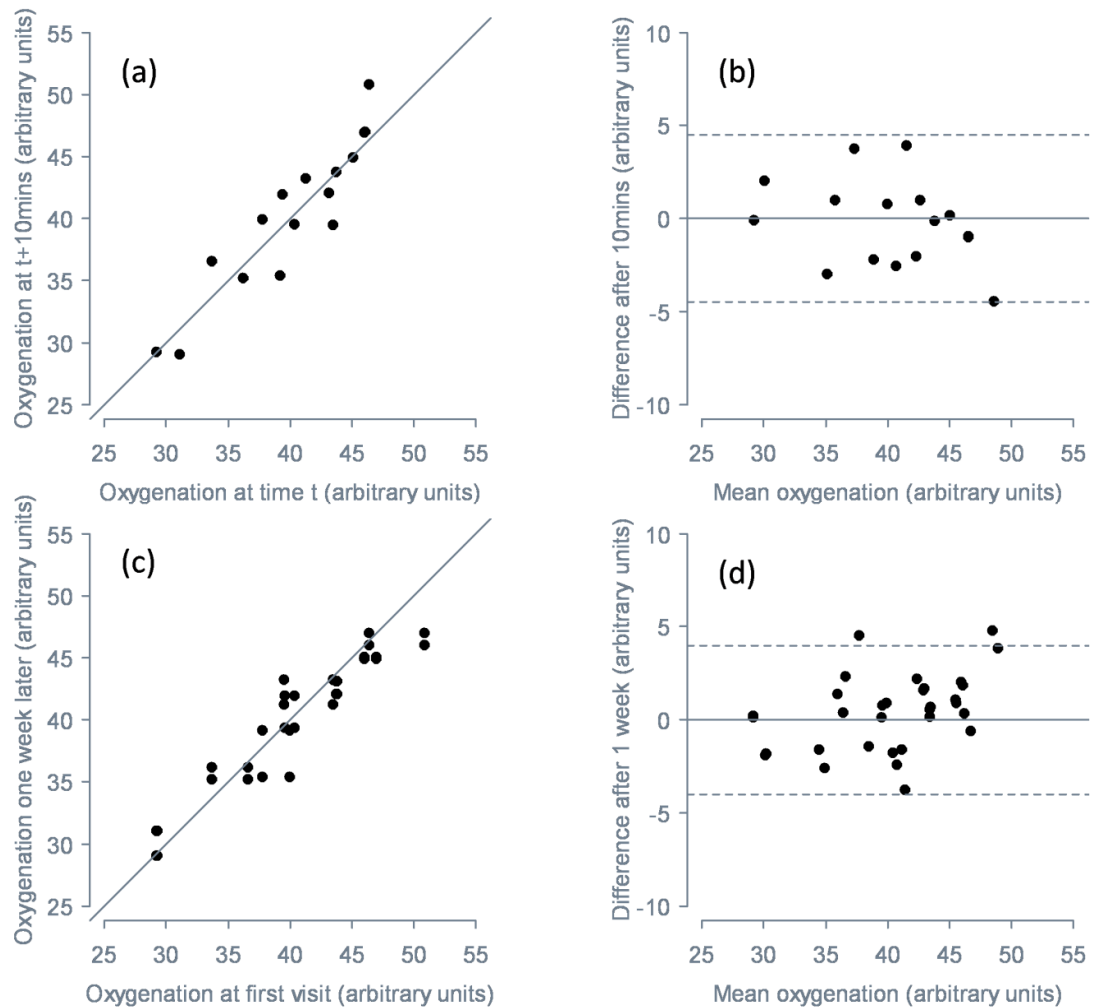


Figure 8.9: Example Bland-Altman analysis of between-session test-retest variability for sector B (superior-temporal sector). (a) and (c) are scatter plots of the data from the first set vs. the second set taken 10 minutes and 1 week later respectively. The grey line in these scatter plots is a 1:1 line for reference. (b) and (d) show the mean oxygenation from the 2 tested sets plotted against the difference in oxygenation between the 2 sets taken 10 minutes and 1 week apart respectively. In these plots the solid grey line is the line of no systematic bias, and the dotted grey lines represent the upper and lower limits of repeatability. (a) and (b) have 16 points representing each of the 8 subjects on 2 visits, whilst (c) and (d) have 32 points representing each combination of the 2 sets taken at each visit (therefore 4 points per subject).

Figure 8.10 shows the mean and 95% range of optic disc sector oxygenation of all images of all subjects and the systematic bias and limits of repeatability of these values for sets re-tested 10 minutes and 1 week apart. The red crosses represent the mean oxygenation with added

systematic bias, which is minimal. The plots show that even in this small sample of healthy subjects the measurement range of the instrument far exceeds the limits of repeatability.

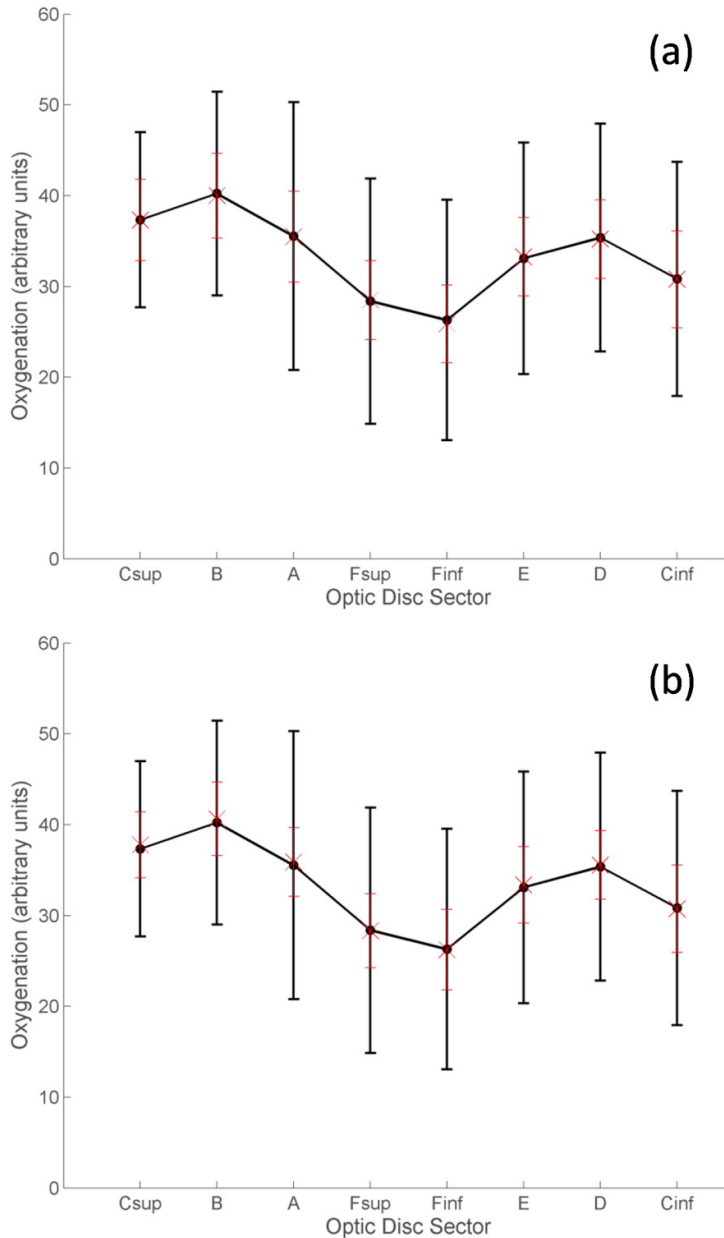


Figure 8.10: Mean and 95% range of optic disc sector oxygenation values across all images of all subjects (black line/whiskers) with mean test-retest difference (systematic bias) represented by the difference between the black circles and red crosses. Red whiskers give the limits of repeatability between sets of images taken (a) 10 minutes apart and (b) one week apart. Optic disc sectors are labelled as in figure 8.4.

Limits of repeatability were significantly narrower between sets of images taken one week apart rather than ten minutes apart (Wilcoxon signed ranks test, $p < 0.05$). Based on the limits of repeatability found for each sector, for a change in sector oxygenation due to disease to be detectable with the current system it would have to exceed 3.8 units on average (range 3.53 to 4.16 units in individual sectors).

8.5 Discussion

Multispectral imaging was performed successfully on a group of healthy subjects. The technique used was non-invasive, safe and comfortable for the subjects. Good quality spatial oxygenation maps of all subjects' optic discs were produced. With the current system the minimum detectable change in optic disc sector oxygenation due to disease is 3.8 units on average.

Coefficients of variation between consecutively captured images within sets were below 5% for all sectors, and between-set repeatability of optic disc sector oxygenation values averaged across sets of three images was similar (figure 8.8). Limits of repeatability and estimated within-subject standard deviations were well within the measured range of the instrument in the healthy subjects imaged (figure 8.10). The true measurement range of the instrument is expected to be much larger in patients with ocular disease affecting optic disc oxygenation. Estimated within-subject standard deviations were also not significantly different within- or between-sets of images, and there was no systematic tendency for increased or decreased measurements in repeat image sets taken ten minutes or one week after the initial set.

It is somewhat surprising that the limits of repeatability were narrower for image sets taken one week apart compared with those taken ten minutes apart. It is possible that this small but statistically significant effect arose as a result of the increased number of comparisons in the one week sets; this would reduce the effect of minor outliers on the data and therefore narrow the limits of repeatability. Nevertheless, the fact the limits of repeatability were not wider for image sets taken one week apart compared to ten minutes apart is promising, as it implies that there is little change in the true oxygenation of the imaged tissue and that the variation found is therefore within the imaging process.

The fact that variation is not increased between image sets compared to within image sets (figure 8.8, table 8.1) also suggests that the vast majority of the variation is between the individual images, the oxygenation values from which were averaged for comparison between

sets. This is again a promising finding as it means that the process of setting-up the instrument for the subject (positioning the subject, aligning and focusing the system etc.) causes little of the variability, since if it did one would expect increased variability between image sets compared to within them. It seems likely therefore, that the majority of the variability is introduced during the image processing stage, that is to say the production of the oxygenation maps from the monochromatic images, the segmentation of the optic disc from the surrounding retina, the masking of blood vessels and the positioning of the centre-point around which the eight sectors are arranged.

Variability in the production of the oxygenation maps could arise from imperfections in the alignment of the monochromatic images, or slight differences in the exposure of certain areas of the monochromatic images caused by slight changes in fixation by the subject. Shifts in the overall brightness in the image series could also induce variability in the oxygenation maps.

Later processing stages seem a more likely major source of variability; figure 8.7 shows an example of the amount of variation in the segmentation of the optic disc from the surrounding retina and the masking of the blood vessels in oxygenation maps of the same optic disc. This is a result of the manual method used to carry out these processes which is a limitation of the current system. As previously mentioned automated methods for both of these processes were trialled, but were not used as the results were not satisfactory. Particularly in the case of masking the blood vessels, automatic methods such as thresholding and edge detection tended to leave areas of vessels unmasked and since the major vessels are much brighter than the surrounding tissue in the oxygenation maps this would cause even greater variability. Masking of blood vessels may always be a problem in analysing these oxygenation maps since even small areas of unmasked vessels may have a large effect on the measured oxygenation in a sector due to their high oxygenation values. The manual method used was deemed better than automated methods as better coverage of the vessels could usually be ensured by the user.

Variability is also added by the manual positioning of the centre-point around which the eight optic disc sectors are arranged. Again, small variations in sector placement can move an area of

particularly high or low oxygenation into a different sector in repeat images. One possible solution to this would be an automated algorithm to define the centre-point of the optic disc based on its outer limits, although this would obviously require repeatable automated segmentation of the optic disc from the surrounding retina.

The system captures the monochromatic images sequentially which holds the advantage over simultaneous capture that exposure time can be adjusted independently for each wavelength, ensuring that all images are correctly exposed. The wide range of exposure times used highlights the value of this. Sequential capture does require alignment of the monochromatic images before oxygenation maps can be produced but this was achieved satisfactorily with a combination of translation, rotation and scaling. This method worked well because image deformation could be well approximated by a global transformation, and this method only requires a small number of landmarks to be manually identified in the images by the user. This is especially important because at the long wavelengths most optic disc features are not visible, making accurate selection of control points difficult.

A potential limitation to the applicability of these methods to future studies lies in the averaging of oxygenation values across sets of consecutively captured images. This obviously requires multiple good quality sets of images to be obtainable, which wasn't a problem in this cohort of mostly young, healthy subjects with clear ocular media but it could prove to be a problem in a more elderly population where media clarity and ability to sit at the instrument for multiple image captures might be reduced. However, since we have shown that the variability between averaged values from sets of images is the same as the variability between individual images it seems that this step may not be necessary for future studies.

Further work to reduce the variability of the oxygenation maps should focus on developing repeatable, automatic methods of segmenting the optic disc from the surrounding retina, masking the blood vessels and defining the centre-point of the optic disc. One way to improve the existing manual segmentation/masking process would be for the user to have an independent image for reference whilst performing the task. This could come from a standard

fundus photograph, or a three dimensional topography image such as from the Heidelberg Retina Tomograph. Improvements in these areas should yield a significant reduction in test-retest variability of sector oxygenation measurements, and reduce the minimum detectable change in optic disc sector oxygenation for longitudinal studies.

In conclusion, the system developed is safe and comfortable for the subject and produces repeatable measures of optic disc sector oxygenation. Variability could be further reduced through improvement in the image analysis techniques.

9.0 The relationship between optic disc oxygenation and visual field sensitivity in glaucoma

Contribution

This project was carried out by our multispectral imaging group comprising of myself, David Henson (DBH), Ingo Schiessl (IS), Vincent Nourrit (VN) and Cecilia Fenerty (CHF). Patient recruitment and image capture was carried out by myself. Alignment of the monochromatic images and generation of the oxygenation maps from the aligned images were carried out by myself using MATLAB routines written by VN and IS respectively. Segmentation of the optic disc from surrounding retina, masking of blood vessels and division of the optic disc into eight sectors was carried out by myself using my own MATLAB routines. The idea to compare superior-inferior differences in optic disc oxygenation to superior-inferior differences in visual field sensitivity was mine following discussion with DBH. All statistical analysis was carried out by myself and the manuscript (currently under review) and this chapter were authored by myself with helpful comments from the rest of the group. CHF and DBH also provided valuable clinical advice on this project.

Publications

Denniss J, Schiessl I, Nourrit V, Fenerty CH, Henson DB (2010) The relationship between optic disc oxygenation and visual field sensitivity in glaucoma. (*manuscript currently under peer-review*)

Conference Presentations

Denniss J, Schiessl I, Nourrit V, Fenerty CH, Henson DB (2010) Spatial Oxygenation Mapping of the Optic Disc in Glaucoma by Multispectral Imaging. ARVO 2010 Annual Meeting, Fort Lauderdale, FL, USA (poster)

Denniss J, Schiessl I, Nourrit V, Fenerty CH, Henson DB (2010) Preliminary results from multispectral imaging of the optic nerve head in glaucoma. College of Optometrists Research Symposium 2010, York, UK (paper)

9.1 Abstract

9.1.1 Purpose

To investigate the relationship between optic disc oxygenation and visual field sensitivity in patients with glaucoma.

9.1.2 Methods

Thirty-three eyes of 18 patients with primary open-angle glaucoma (mean age 73 ± 7 years) were imaged with a multispectral system incorporating a modified digital fundus camera, 250W tungsten halogen lamp and fast-tuneable liquid crystal filter. Eight images were captured sequentially over ~ 1.5 s at wavelengths selected according to absorption properties of blood components (range 496-700nm), and a Beer-Lambert law model was used to produce oxygenation maps of the optic disc from the aligned images. Patients also underwent visual field (VF) testing (Humphrey Field Analyzer, SITA 24-2) and Heidelberg Retina Tomograph (HRT3) imaging of the optic disc. Differences in optic disc oxygenation and neuroretinal rim (NRR) area between both superior/inferior portions and vertically opposing 45° sectors were compared with differences in sensitivity between corresponding VF sectors.

9.1.2 Results

Significant relationships were found between superior-inferior hemifield difference in VF sensitivity and superior-inferior difference in optic disc oxygenation ($r=0.68$, $p<0.001$) and NRR area ($r=0.37$, $p<0.05$). Significant relationships were also found between difference in sensitivity between corresponding VF sectors and: (1) superior-/inferior-temporal oxygenation difference ($r=0.63$, $p<0.001$), (2) superior-/inferior-temporal NRR area difference ($r=0.46$, $p<0.05$) and (3) superior-/inferior-nasal oxygenation difference ($r=0.63$, $p<0.001$) in the optic disc.

9.1.3 Conclusions

Superior-inferior differences in optic disc oxygenation are related to superior-inferior differences in VF sensitivity in patients with glaucoma. Multispectral imaging provides clinically important information on optic disc perfusion which is complementary to structural imaging techniques in predicting glaucomatous functional loss.

9.2 Introduction

Progressive structural changes in the optic disc and functional losses in the visual field are hallmarks of primary open-angle glaucoma, one of the world's leading causes of blindness (Quigley, 1996). The precise mechanisms which lead to these changes are the subject of continued controversy. Whilst the existence of certain secondary, congenital and narrow-angle glaucomas demonstrate that increased intraocular pressure alone can be sufficient to cause glaucomatous optic neuropathy, glaucoma can occur at any intraocular pressure showing that raised intraocular pressure is not always required for development of glaucomatous optic neuropathy.

It has been reported by several authors that reduced ocular blood flow and perfusion is a risk factor for primary open-angle glaucoma (Michelson et al., 1998a, Drance et al., 2001, Yamazaki and Drance, 1997, Flammer et al., 1999, Flammer and Orgul, 1998, Hamard et al., 1994, Leske, 2009, Leske et al., 2008). However, the absolute level of reduction appears unrelated to disease stage measured by functional loss, presumably due to the wide between-subject variation in blood flow measurements from both healthy and glaucomatous eyes (Michelson et al., 1998a). For the interested reader, many studies of ocular blood flow in glaucoma have been reviewed by Flammer *et al* (2002).

Multispectral imaging (also called *hyperspectral* imaging) is a technique that has been widely used in biomedical research for brain imaging of animal models, directly measuring tissue oxygenation and often looking for changes in response to a sensory stimulus (Malonek and Grinvald, 1996, Mayhew et al., 1999, Berwick et al., 2005). The technique relies on the wavelength-dependency of light absorption properties of blood components. By imaging tissue at a range of wavelengths tailored to produce maximally different images relating to oxygen levels, relative oxygenation maps of the imaged tissue can be produced.

Previous studies have applied multispectral imaging techniques to the optic disc and surrounding retina. Khoobehi *et al* (2004) used a slit spectrography technique to measure

relative oxygen saturation changes in the optic discs of immobilised healthy non-human primate eyes in response to alterations in intraocular pressure and the oxygen content of inspired air. Ito *et al* (2008) used multispectral imaging to calculate the oxygenation of small areas of juxtapapillary retina in patients with glaucoma and healthy subjects. On average they found a reduction in oxygenation in glaucomatous eyes compared to healthy eyes (albeit with substantial overlap in range), and a weak relationship between visual field mean deviation and the oxygen saturation of certain areas.

A common feature of both structural and functional damage in glaucoma is vertical within-eye asymmetry (Jonas et al., 1999, Jonas and Budde, 2000, Asman and Heijl, 1992, Mikelberg and Drance, 1984, Hart and Becker, 1982), for example visual field defects tend to affect the superior and inferior hemifields unequally. Because of the large between-subject variability in blood flow/oxygenation it could be beneficial to look at within-eye differences in oxygenation and visual field sensitivity. In this way the eye acts as its own reference, negating the need for normative population data.

In this paper we use multispectral imaging to calculate superior-inferior differences in relative oxygenation of the optic discs of patients with primary open-angle glaucoma. We also measure neuroretinal rim area and visual fields to establish, for the first time, a strong relationship between optic disc oxygenation and visual field sensitivity.

9.3 Methods

9.3.1 Patients

The study adhered to the tenets of the Declaration of Helsinki and was approved by the NHS Central Manchester Research Ethics Committee. All patients provided written informed consent to participate after explanation of the nature and possible consequences of the study. Patients were recruited from the glaucoma clinics of the Manchester Royal Eye Hospital, Manchester, UK. Recruited patients all had a clinical diagnosis of primary open-angle glaucoma and were receiving bilateral treatment for the condition. Patients were aged over 40 years, had

no other ocular disease except mild cataract and had refractive error within ± 5.00 DS equivalent and/or 1.50DC. In order to recruit a wide spectrum of disease from 'suspect' to advanced, both eyes of a patient were included in the study if they met the above criteria and in addition at least one eye had visual field mean deviation (MD) worse than ($<$) -2.00dB and pattern standard deviation (PSD) worse than ($>$) 2.00dB. All visual fields were subjectively examined by one author (JD) to exclude any clearly non-glaucomatous losses such as hemianopia, and all patients had had at least 2 prior visual field tests.

Patients underwent HRT3 (Heidelberg Retina Tomograph, Heidelberg Engineering, Heidelberg, Germany) and multispectral imaging of the optic discs of both eyes in the same visit. Visual field data (SITA Standard 24-2, Humphrey Field Analyzer, Carl Zeiss Meditec, Ca) was collected retrospectively from the clinic database (most recent visual field test). One patient's visual field data was 19 months old due to a spinal problem preventing further testing, though this patient had 'end stage' visual fields with little further progression possible. Another patient's visual field test was done 6 months after imaging, and for the remaining patients tests were done within 3 months of imaging (median 22 days).

Of the 21 recruited patients, 2 patients could not be imaged with the multispectral system in either eye due to poor pupillary dilation, and 1 patient could only be imaged in one eye for the same reason. A further patient could not be imaged in either eye, and another only in one eye with the HRT3. This left a final dataset of 33 eyes of 18 patients (17 left, 15 right eyes, mean patient age 73 ± 7 years).

9.3.2 Multispectral Imaging

Multispectral images were obtained with a custom-modified digital fundus camera system (figure 9.1). Briefly, the system incorporates a 250W tungsten halogen lamp filtered by a fast tuneable liquid crystal filter (Varispec VIS 07-20 STD, Cambridge Research Instrumentation, UK). Images were captured with a low-noise Peltier-cooled CCD array (Orca C4742-80-12AG, Hamamatsu Photonics, Hamamatsu, Japan) with a spatial resolution of 336x256 pixels (with 4x4 binning).

Following pupillary dilation, images were taken sequentially at 8 different wavelengths selected according to the absorption properties of blood components (OMLC, 1998) (range 496-700nm, total acquisition time <1.6s). More precisely, we captured images at 2 isobestic wavelengths (550 and 570nm), at wavelengths where the ratio between light absorption by oxygenated and deoxygenated haemoglobin is maximal (575, 580 and 610nm) and at a wavelength above 650nm, where tissue scattering dominates. Images were subjectively reviewed for eye movement artefacts as they were captured, and any poor images were re-captured.

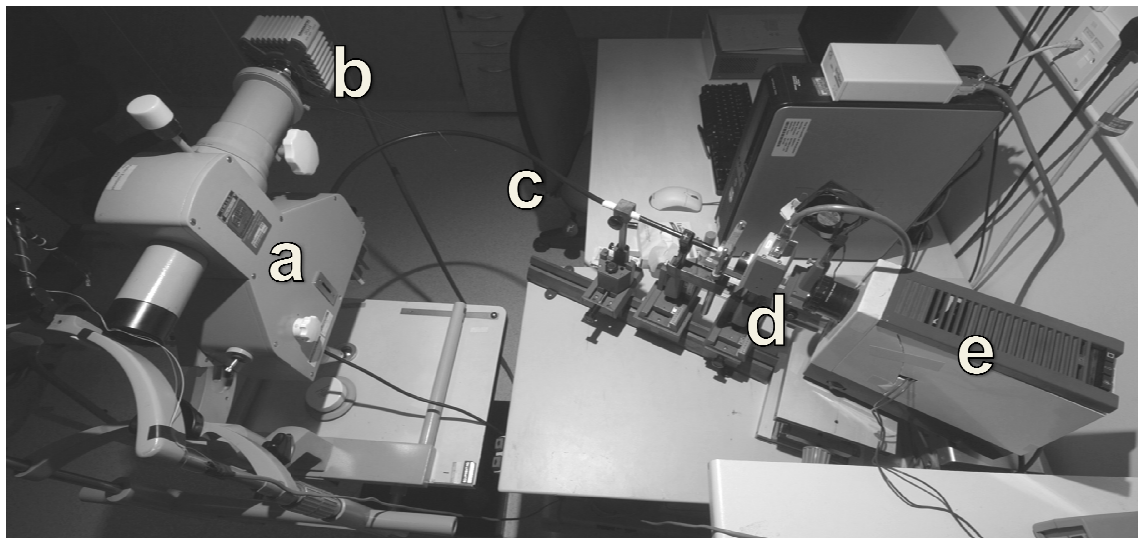


Figure 9.1: The multispectral imaging system incorporating (a) modified fundus camera with (b) peltier-cooled CCD array, (c) fluid optic, (d) fast tuneable liquid crystal filter and (e) 250W tungsten halogen lamp.

9.3.2.1 Production of Spatial Oxygenation Maps

Captured images at each wavelength were corrected for systematic variations due to the inhomogeneous sensitivity of the system across different wavelengths with a correction factor derived from images taken of a white surface with a flat absorption spectrum. The captured monochromatic images were then aligned assuming that degradation due to eye movement can be approximated by a combination of translation, rotation and scaling (Nourrit et al., 2008).

Using a Beer-Lambert law model (Malonek and Grinvald, 1996, Mayhew et al., 1999, Berwick et al., 2005) we then calculated pixel-by-pixel oxygenation maps of the imaged tissues from the aligned images. Appendix I describes this process in more detail.

9.3.3 Data analysis

9.3.3.1 Spatial oxygenation maps

Image processing was carried out in MATLAB (R2008a, The Mathworks Inc, Natick, MA, USA). A mask was applied to each of the spatial oxygenation maps to segment the optic disc from the surrounding retina, and then a second mask was applied to remove visible blood vessels from the maps, leaving only optic disc tissue. Masking was performed manually by one author (JD) with reference to the relevant HRT3 topographies and original monochromatic images at each wavelength. Oxygenation levels were then calculated in eight 45° sectors from the masked maps, as shown in figure 9.2.

9.3.3.2 HRT3 optic nerve head topography

Neuroretinal rim area was calculated in each of the eight 45° sectors shown in figure 9.2 (corresponding to those described above) using the custom sectors feature of the instrument's in-built software (version 3.1.2.0). These data were collected primarily for use as a reference standard against which the relationships between oxygenation and visual field measurements could be judged.

9.3.3.3 Comparison with visual field data

In order to facilitate comparison of altitudinal differences in visual field sensitivity with differences in oxygenation and neuroretinal rim area above and below the horizontal midline of the optic disc, visual field sensitivities were grouped according to a published map (Garway-Heath et al., 2002). The map describes the anatomical relationship between optic disc sectors and 24-2 visual field test locations as found by using fundus photographs to trace visible retinal nerve fibre layer bundles or defects from their insertion at the optic disc to the points of an overlaid 24-2 test grid. For this study, measured sensitivities at points within each group were averaged for comparison to corresponding optic disc sectors. In the cases of sectors Csup, Cinf, Fsup and Finf which are combined into two sectors in the published map, we split the visual

field sectors relating to these two sectors at the horizontal midline (corresponding to the optic disc sectors which are also split at the horizontal midline). For some comparisons we combine sectors ourselves, for example to compare the entire superior and inferior hemifields. The map used is shown in figure 9.2.

All left eyes were converted to right for analysis and statistical analysis was carried out in the open-source environment *R* (version 2.11.1).

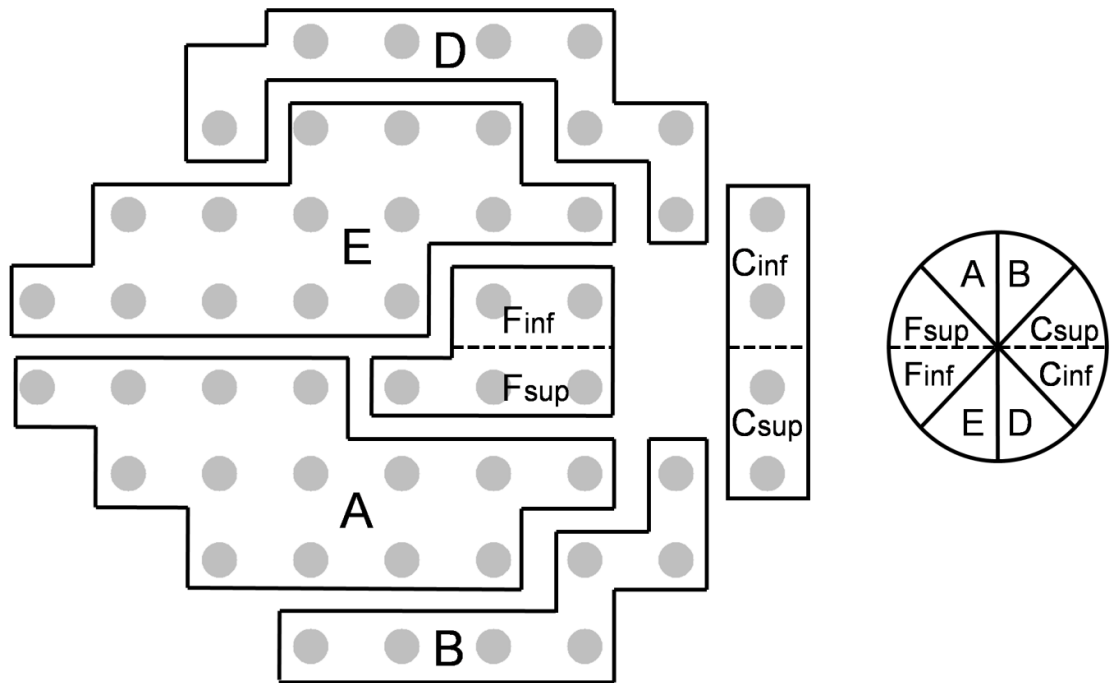


Figure 9.2: Diagram of optic disc (right) and visual field (left) sectors for a right eye, adapted from Garway-Heath *et al* (2002). The dashed lines show where we split the original sectors described by Garway-Heath *et al* at the horizontal midline. Sectors are labelled as they are referred to in the text.

9.4 Results

Visual field mean MD was -6.2dB (range +0.6 to -19.8dB) and mean PSD was 5.0dB (range 1.8 to 10.7dB). Mean optic disc oxygenation (in arbitrary units) was 20.3 ± 6.2 units (range 10.5 to 36.8 units). Mean total neuroretinal rim area was $1.0 \pm 0.5 \text{mm}^2$ (range 0.3 to 2.6mm^2).

Figure 9.3 shows examples of spatial oxygenation maps from 2 patients with their corresponding visual fields. In the oxygenation maps brighter areas represent areas of greater oxygenation and darker areas represent areas of less oxygenation. Anecdotally, all patients were asked whether they found the multispectral imaging process comfortable, and all responded positively.

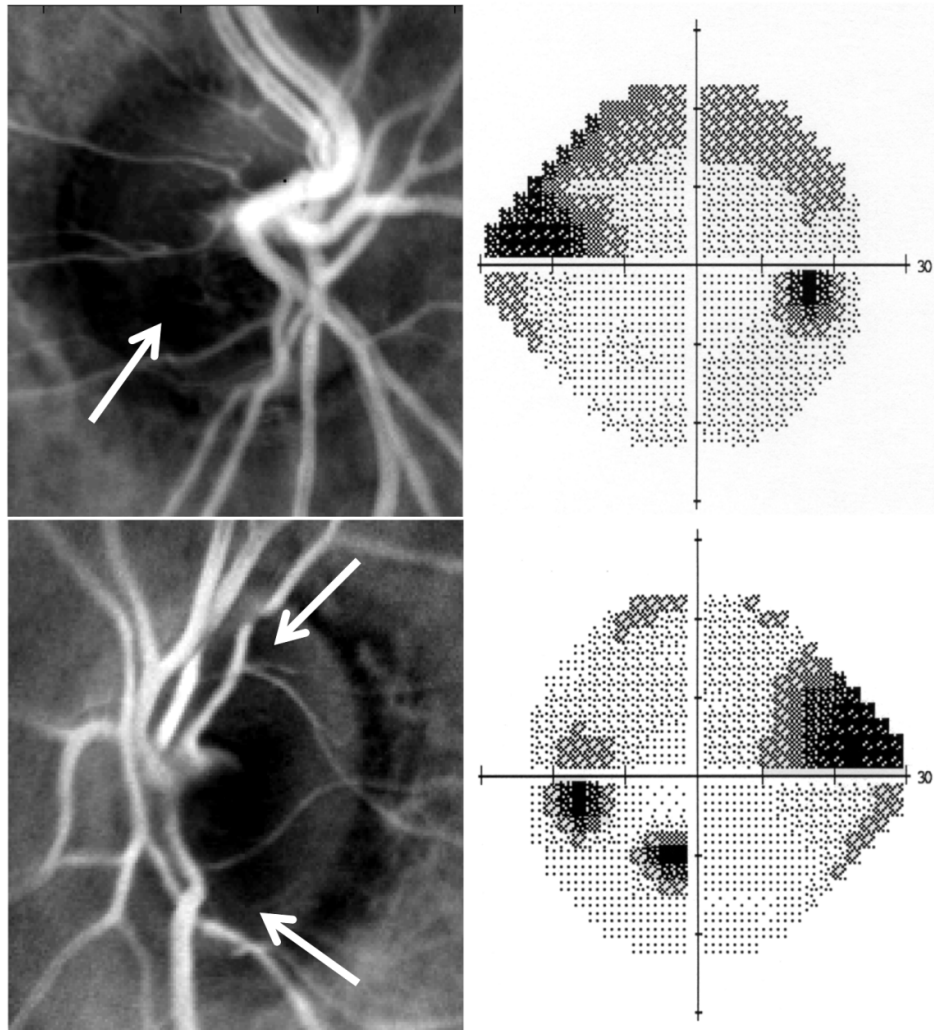


Figure 9.3: Spatial oxygenation maps of the optic discs of 2 patients (left) with corresponding visual field greyscale plots (right). In the oxygenation maps brighter areas represent areas of greater oxygenation and darker areas represent areas of less oxygenation. The arrows in the oxygenation maps point to darker areas (areas of lower oxygenation) which correspond to the visual field defects shown.

9.4.1 Altitudinal relationships

Differences in optic disc oxygenation and neuroretinal rim area above and below the horizontal midline were compared with differences in visual field sensitivity above and below the horizontal midline. First, the difference between the mean sensitivity of the entire superior and inferior hemifields (excluding blind spot points) was compared to the difference in mean oxygenation and total neuroretinal rim area between the superior and inferior portions of the optic disc. Results are shown in figure 9.4.

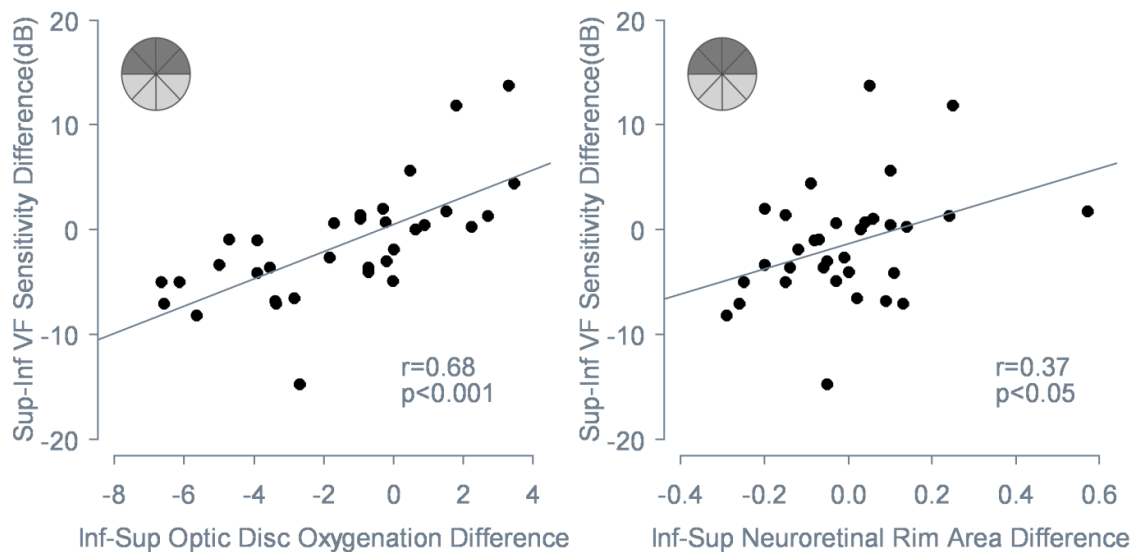


Figure 9.4: Inferior-superior differences in optic disc oxygenation (arbitrary units, left) and neuroretinal rim area (mm^2 , right) vs. superior-inferior difference in visual field sensitivity. The plots include Pearson correlation coefficients and associated p-values for the relationships shown as well as a diagrammatic representation of the optic disc sectors considered.

Differences between individual vertically opposing optic disc sectors were then considered, comparing them to the difference in mean sensitivity between corresponding visual field areas (as described in figure 9.2). Significant relationships were found between difference in oxygenation and visual field sensitivity in sectors A/E and B/D and also between difference in neuroretinal rim area and visual field sensitivity in sectors A/E. The relationships for sectors A/E and B/D are shown in figure 9.5.

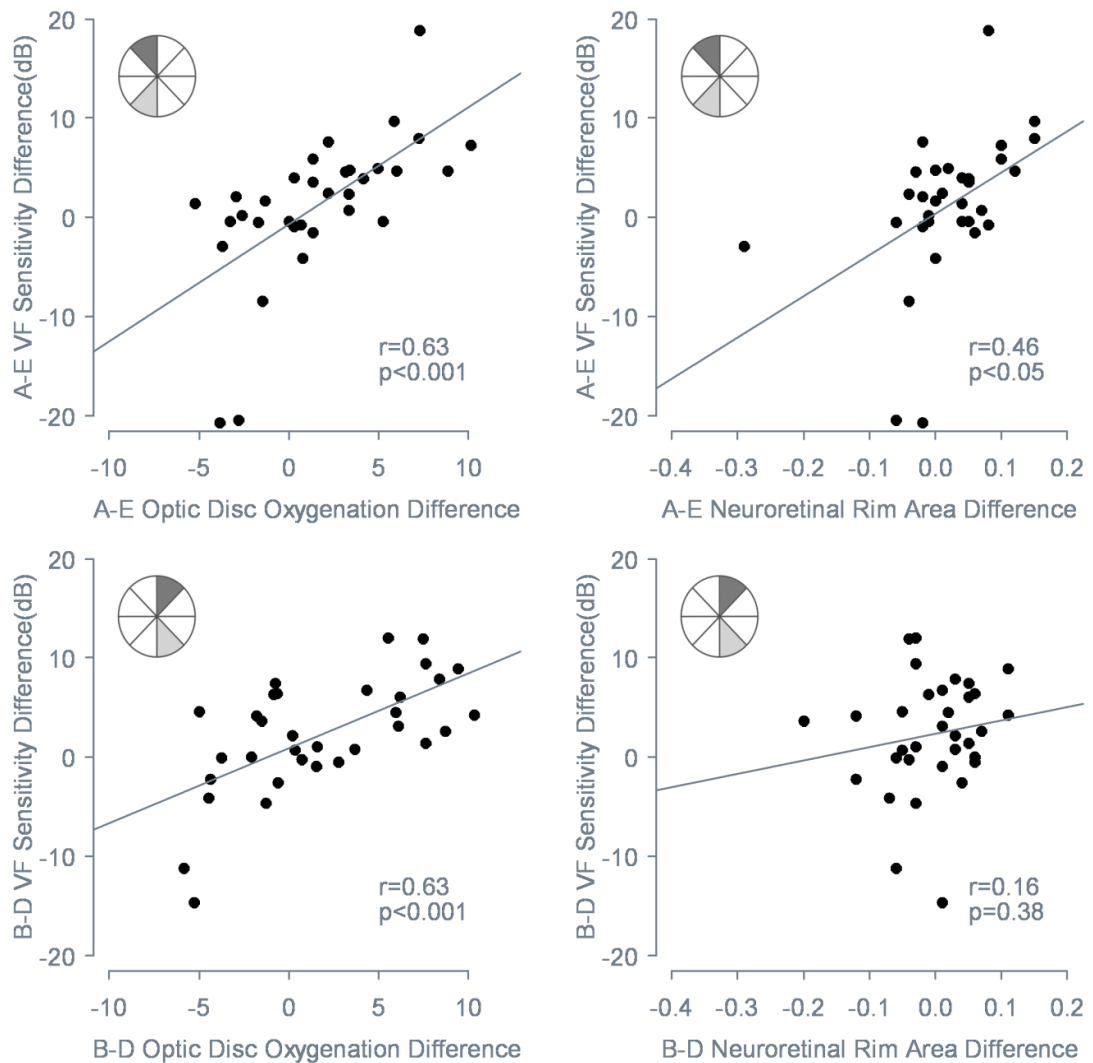







Figure 9.5: Differences in oxygenation (arbitrary units, left) and neuroretinal rim area (mm^2 right) between vertically opposing optic disc sectors vs differences between sensitivity of corresponding visual field areas. The plots include Pearson correlation coefficients and associated p-values for the relationships shown as well as a diagrammatic representation of the optic disc sectors considered (for a right eye) and sectors are labelled as in figure 9.2.

Considering the nasal (sector C) and temporal (sector F) segments of the optic disc which we split into superior and inferior portions, only one significant association was found; that between the difference in neuroretinal rim area above and below the midline in the temporal optic disc (sector F) and the sensitivity difference in corresponding areas of the visual field ($r=-0.39, p<0.05$). However, the relationship was negative, not particularly strong, and based on relatively small areas of the visual field.

For ease of comparison, the Pearson correlation coefficients and associated p-values for each tested relationship are shown in table 9.1. This table shows that in every case there is a stronger positive correlation found when differences in optic disc oxygenation rather than neuroretinal rim area are compared to differences in visual field sensitivity above and below the horizontal midline.

Table 9.1: Pearson correlation coefficients and associated p-values for differences in optic disc oxygenation and neuroretinal rim area compared to differences in visual field sensitivity in corresponding areas. Relationships significant at the 5% level are shown in italics. Sectors (shaded grey for a right eye) relate to those shown in figure 9.2, and describe the vertically opposing sectors between which the difference was calculated in the visual field and optic disc.

Sectors	Oxygenation <i>r</i> (<i>p</i>)	Neuroretinal rim area <i>r</i> (<i>p</i>)
 Superior-inferior	<i>0.68 (<0.001)</i>	<i>0.37 (<0.05)</i>
 A-E	<i>0.63 (<0.001)</i>	<i>0.46 (<0.05)</i>
 B-D	<i>0.63 (<0.001)</i>	0.16 (=0.38)
 Csup-Cinf	0.31 (=0.07)	-0.04 (=0.81)
 Fsup-Finf	0.36 (=0.06)	<i>-0.39 (<0.05)</i>

9.4.2 Global relationships

Total neuroretinal rim area was moderately associated with visual field MD ($r=0.40$, $p<0.05$). Mean optic disc oxygenation was not significantly associated with MD ($r=-0.18$, $p=0.31$), and neither measure was significantly associated with PSD (oxygenation $r=-0.01$, $p=0.96$, neuroretinal rim area $r=-0.21$, $p=0.24$).

9.5 Discussion

Multispectral imaging of the optic disc was performed successfully on a group of patients with a wide spectrum of functional loss from primary open-angle glaucoma. The technique used was non-invasive, comfortable for the patient and allowed us to produce good quality spatial oxygenation maps of the optic disc which allowed for discrimination of differences in tissue oxygenation.

To our knowledge, this is the first detailed report relating a measure of optic disc tissue oxygenation to functional changes in glaucoma. Previous studies have investigated oxygenation in small regions of peripapillary retina (Ito et al., 2008) or blood flow in retinal and optic disc blood vessels (Michelson et al., 1998a). There are two major advantages of imaging the optic disc tissue directly as in the present study, rather than using measurements from blood vessels as a surrogate. First, we do not have the problem of identifying with certainty which vessels supply the tissue (Hayreh, 2001). Second, we bypass the effects of between-patient differences in oxygen transfer from retinal or optic disc arterioles to tissue capillaries.

Mean optic disc oxygenation was not found to be related to the visual field global measures MD or PSD. This finding is consistent with previous studies of optic nerve blood flow (Michelson et al., 1998a) which found that the blood supply to the optic nerve head varies widely in both the healthy and glaucomatous populations such that what constitutes a severely reduced blood supply for one patient may be perfectly normal for another. It follows logically that oxygenation of supplied tissues may follow a similar pattern, as found by Ito *et al* (2008), although further study is required to verify this. Also, between-patient differences in reflectance properties such as due to concentration of pigments in the imaged tissue may account for some of this variability (Delori and Pflibsen, 1989).

Significant associations were found between superior-inferior differences in visual field sensitivity and inferior-superior differences in optic disc oxygenation and neuroretinal rim area (measured by HRT3). These associations were found both when the entire hemifield was

considered along with the entire inferior/superior portions of the optic disc, as well as when only the superior- and inferior-temporal optic disc sectors were considered along with their corresponding visual field areas (sectors A and E in figure 9.2). Interestingly, a similar significant association was found between differences in the oxygenation of the superior- and inferior-nasal sectors and differences in the sensitivity of their corresponding visual field areas (B and D in figure 9.2), but no such association was found between differences in neuroretinal rim area and visual field sensitivity in these sectors. A possible explanation for this lack of association is that this is the area where major blood vessels tend to exit the optic disc, affecting the surface topography measurements made by the HRT3. Indeed, based on our finding that the relationship between superior-inferior differences in neuroretinal rim area and visual field sensitivity is actually stronger when only the superior- and inferior-temporal optic disc sectors are considered, rather than the whole superior/inferior portion of the optic disc, we hypothesise that blood vessel placement may be a major source of variability for investigations of the topographic structure-function relationship in glaucoma using the HRT.

It is not surprising that strong associations were not found between oxygenation or neuroretinal rim area differences in the nasal (Csup and Cinf) and temporal (Fsup and Finf) optic disc sectors and sensitivity differences in their corresponding visual field areas since there are very low numbers of visual field test locations in these sectors (4 and 5 respectively). One might expect that stronger associations might be found if the visual field were better sampled in these areas (e.g. with a 10-2 test pattern for the temporal sectors).

In all sectors considered in this study a stronger positive relationship was found between superior-inferior differences in visual field sensitivity and optic disc oxygenation than neuroretinal rim area. A hypothesis test to directly compare the correlation coefficients between these measures was not performed as the effects of the relatively small sample size and use of both eyes of some patients would have made the results very difficult to interpret. When comparing the correlation coefficients between the visual field measures and oxygenation/neuroretinal rim area differences one should also consider the different units and measured ranges of the two instruments in this sample. Use of Spearman rank correlation

coefficients (not reported here) in future studies may reduce this effect making comparison easier. Nevertheless, the finding of stronger positive relationships between superior-inferior differences in visual field sensitivity and optic disc oxygenation than neuroretinal rim area suggests that oxygenation measurements by multispectral imaging may provide clinically valuable complementary information to the structural information provided by the HRT3 in predicting glaucomatous functional loss. This may be in the form of identifying neuroretinal rim tissue which is present but lacking oxygenation and therefore functioning poorly, or conversely where neuroretinal rim area is low but well-perfused and therefore functioning adequately for normal visual function.

The main limitation of our method comes from the simple Beer-Lambert law model we use to calculate oxygenation, and the various assumptions associated to it. One such assumption is that incident light of different wavelengths travels the same distance in the absorbing medium, however the longer wavelengths penetrate deeper into the tissue before being back-scattered (Delori et al., 1977, Berendschot et al., 2003). With refinements to this model such as path length scaling (Malonek and Grinvald, 1996) and wavelength-dependent correction (Mayhew et al., 1999) we expect to be able to make more precise estimates of oxygenation, and also to assign units ($\text{mmol}\cdot\text{mm}^{-2}$) to the oxygenation values. Another limitation of this particular study is the elapsed time between visual field testing and optic disc imaging, during which time either parameter may have changed, weakening the relationships found.

Sequential image capture holds the advantage over simultaneous capture that exposure time may be varied for different incident wavelengths. This allows each individual image to be correctly exposed, thereby yielding maximal information. Although this technique necessitates alignment of the monochromatic images, this is not a problem as it can be done accurately using established techniques (Nourrit et al., 2008).

Further work with a larger cohort of patients and an improved model for calculation of oxygenation may lead to improvements in the relationship between optic disc oxygenation and visual field losses in glaucoma. Longitudinal studies may also be indicated to establish the

power of temporal changes in optic disc oxygenation measured by multispectral imaging in predicting subsequent glaucomatous functional losses, and to evaluate the effects of therapeutic interventions (Traustason et al., 2009, Siesky et al., 2008) on optic disc perfusion.

In conclusion, significant associations were found between superior-inferior differences in optic disc oxygenation and superior-inferior differences in visual field sensitivity in glaucoma. Multispectral imaging shows considerable promise as a clinical tool to provide important information on optic disc perfusion. This information may complement current structural imaging techniques in predicting glaucomatous functional loss.

10. The relationship between neuroretinal rim oxygenation and visual field sensitivity in glaucoma

Contribution

This project was carried out by our multispectral imaging group comprising of myself, David Henson (DBH), Ingo Schiessl (IS), Vincent Nourrit (VN) and Cecilia Fenerty (CHF). The idea to remove the optic cup from the oxygenation maps and repeat the previous analysis came from myself and DBH. The use of overlaid HRT topographies to define the cup was my idea, and was carried out using an MATLAB alignment routine adapted by myself and VN from the one previously produced by VN for alignment of monochromatic images. I also wrote the MATLAB script to remove the cups from the optic disc oxygenation maps and carried out this process myself. The statistical analysis was performed by myself and I also wrote the chapter featured here with helpful comments from the group.

Publications (in preparation)

Denniss J, Schiessl I, Nourrit V, Fenerty CH, Henson DB (2010) Neuroretinal rim oxygenation and visual field sensitivity in patients with glaucoma (manuscript in preparation)

10.1 Abstract

10.1.1 Purpose

To investigate the relationship between neuroretinal rim (NRR) oxygenation and visual field (VF) sensitivity in patients with glaucoma and to assess whether combining information on NRR area and oxygenation strengthens this relationship.

10.1.2 Methods

Multispectral optic disc images, HRT3 optic disc topographies and visual fields of 18 patients acquired for a previous study (“The relationship between optic disc oxygenation and visual field sensitivity in glaucoma”) were used for this study. The oxygenation maps produced from the multispectral images were re-analysed for this study to isolate only the NRR tissue from each one, as defined by the HRT3 topography. Differences in NRR oxygenation between both superior/inferior portions and vertically opposing 45° sectors were compared with differences in sensitivity between corresponding VF sectors. Multiple regression analysis was used to evaluate whether stronger relationships with the VF can be found when NRR area and oxygenation data are combined.

10.1.3 Results

Significant relationships were found between superior-inferior hemifield difference in VF sensitivity and superior-inferior difference in NRR oxygenation ($r=0.61$, $p<0.001$). Significant relationships were also found between difference in sensitivity between corresponding VF sectors and: (1) superior-/inferior-temporal NRR oxygenation difference ($r=0.61$, $p<0.001$) and (2) superior-/inferior-nasal NRR oxygenation difference ($r=0.63$, $p<0.001$). Combining NRR area and oxygenation data in a multiple regression analysis did not improve these relationships since NRR area did not contribute significantly.

10.1.4 Conclusions

Superior-inferior differences in NRR oxygenation are related to superior-inferior differences in VF sensitivity in patients with glaucoma. This relationship cannot be improved by taking NRR area into account. Multispectral imaging shows considerable promise as a clinical tool to provide important information on optic disc perfusion.

10.2 Introduction

In a previous study (“The relationship between optic disc oxygenation and visual field sensitivity in glaucoma”) we demonstrated a relationship between differences in oxygenation between the superior and inferior portions of the optic disc and altitudinal differences in visual field sensitivity in patients with glaucoma.

The study used multispectral imaging to measure relative oxygenation of the optic disc in a cohort of glaucoma patients. This technique relies on the wavelength-dependency of light absorption properties of blood components; by imaging tissue at a range of wavelengths tailored to produce maximally different images relating to oxygen levels, relative oxygenation maps of the imaged tissue can be produced.

The optic disc oxygenation maps produced were masked to segment the optic disc from its surrounding retina and to remove blood vessels from the image. We then divided the optic disc into eight 45° sectors and the visual field into corresponding sectors according to a published map (Garway-Heath et al., 2002). Oxygenation of the whole area falling into an optic disc sector was considered, such that the calculation encompassed areas of both neuroretinal rim (NRR) and optic cup.

As discussed in the previous study, a common feature of both structural and functional damage in glaucoma is vertical within-eye asymmetry (Jonas et al., 1999, Jonas and Budde, 2000, Asman and Heijl, 1992, Mikelberg and Drance, 1984, Hart and Becker, 1982), for example visual field defects tend to affect the superior and inferior hemifields unequally. Because of the large between-subject variability in blood flow/oxygenation it was deemed beneficial to look at within-eye differences in oxygenation and visual field sensitivity. In this way the eye acts as its own reference, negating the need for normative population data. For this reason we calculated superior-inferior differences in relative optic disc oxygenation and found a strong relationship with superior-inferior differences in visual field sensitivity.

A potential limitation of the previous analysis is that the mean oxygenation calculated within an optic disc sector was affected by the cup area which generally exhibits very low oxygenation. This means that the relationships found may have also taken partial account of the proportion of cup vs. NRR in the sectors.

Since the NRR is the area through which the retinal ganglion cell fibres pass on their way from the retina to the optic nerve, it is likely to be this area of the optic disc where oxygenation is critical. Hypothetically, oxygen deficits here could lead to loss of ganglion cell function, and ultimately to ganglion cell death. These would manifest in visual field loss for the patient. For this reason it is the oxygenation of the NRR which is potentially of most interest in glaucoma. Furthermore, by looking for oxygenation deficits within the NRR, we look for areas of dysfunction where future structural damage may occur, rather than looking at areas where damage has already occurred.

In this study we re-analyse the spatial optic disc oxygenation maps produced in the previous study to now consider relative oxygenation of the NRR in isolation from the rest of the optic disc. We evaluate the relationship between superior-inferior differences in NRR oxygenation and superior-inferior differences in visual field sensitivity and compare these to the previous results. We also evaluate the effect of combining information on NRR oxygenation and area on this relationship.

10.3 Methods

10.3.1 Patients

This study used the images collected from the patients in the previous study (“The relationship between optic disc oxygenation and visual field sensitivity in glaucoma”). The dataset included 33 eyes of 18 patients (17 left, 15 right eyes, mean patient age 73 ± 7 years). The study adhered to the tenets of the Declaration of Helsinki and was approved by the NHS Central Manchester Research Ethics Committee. The recruitment of patients and how they were examined is described in the previous chapter (section 9.3.1)

10.3.2 Multispectral Imaging

Details of how the monochromatic image series were captured and how the spatial oxygenation maps were produced from these can be found in the previous chapter (section 9.3.2).

10.3.3 Data analysis

10.3.3.1 Isolation of neuroretinal rim tissue from spatial oxygenation maps

Image processing was carried out in MATLAB (R2008a, The Mathworks Inc, Natick, MA, USA). HRT3 optic nerve head topography images were re-sampled and aligned with the optic disc oxygenation maps using the same alignment method as described above for alignment of the monochromatic images. A mask was then created based on the NRR area defined in the aligned HRT3 topography (the area within the optic disc whose surface height is above a reference plane located parallel to the peripapillary retinal surface and 50 μ m below the retinal surface at the point where the papillo-macular bundle and optic disc margin coincide). This mask was then applied to the oxygenation maps to isolate only the NRR tissue (i.e. the peripapillary retina and optic cup was removed). A second mask was then applied to remove visible blood vessels from the maps, leaving only optic disc tissue. Masking was performed manually by one author (JD) with reference to the relevant HRT3 topographies and original monochromatic images at each wavelength. Oxygenation levels were then calculated in eight 45° sectors from the masked maps, as shown in figure 10.1 and identically to the previous study.

10.3.3.2 HRT3 optic nerve head topography

Neuroretinal rim area was calculated in each of the eight 45° sectors shown in figure 10.1 (corresponding to those described above) using the custom sectors feature of the instrument's in-built software (version 3.1.2.0).

10.3.3.3 Comparison with visual field data

In order to facilitate comparison of altitudinal differences in visual field sensitivity with differences in oxygenation of NRR tissue above and below the horizontal midline of the optic disc, visual field sensitivities were grouped according to a published map (Garway-Heath et al.,

2002) (figure 10.1). The map describes the anatomical relationship between optic disc sectors and 24-2 visual field test locations as found by using fundus photographs to trace visible retinal nerve fibre layer bundles or defects from their insertion at the optic disc to the points of an overlaid 24-2 test grid. For this study, measured sensitivities at points within each group were averaged for comparison to corresponding NRR sectors. In the cases of sectors Csup, Cinf, Fsup and Finf which are combined into two sectors in the published map, we split the visual field sectors relating to these two sectors at the horizontal midline (corresponding to the optic disc sectors which are also split at the horizontal midline). For some comparisons we combine sectors ourselves, for example to compare the entire superior and inferior hemifields.

We also use multiple regression analysis to evaluate the combined ability of superior-inferior differences in NRR oxygenation and area (from the HRT3) to predict superior-inferior differences in visual field sensitivity in the same sectors.

All left eyes were converted to right for analysis and statistical analysis was carried out in the open-source environment *R* (version 2.11.1).

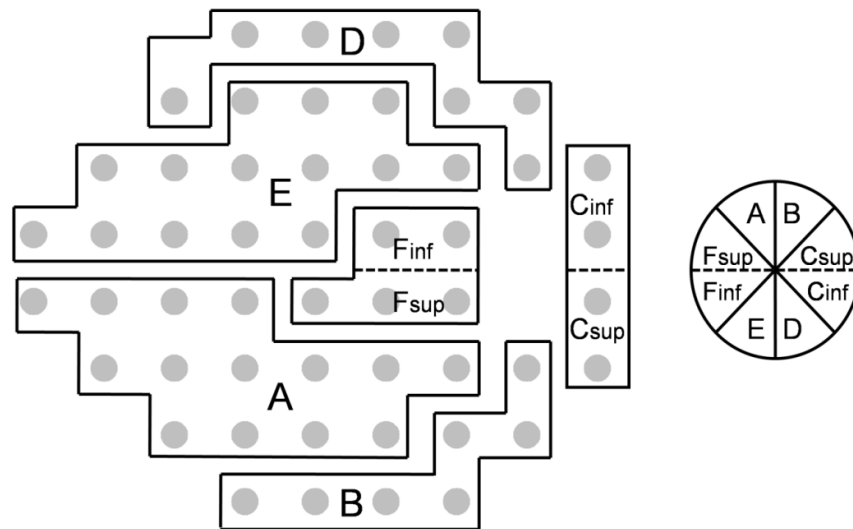


Figure 10.1: Diagram of optic disc (right) and visual field (left) sectors for a right eye, adapted from Garway-Heath *et al* (2002). The dashed lines show where we split the original sectors described by Garway-Heath *et al* at the horizontal midline. Sectors are labelled as they are referred to in the text. In this study the optic disc sectors are the sectors within which the neuroretinal rim tissue oxygenation was calculated.

10.4 Results

Visual field mean MD was -6.2dB (range +0.6 to -19.8dB) and mean PSD was 5.0dB (range 1.8 to 10.7dB). Mean neuroretinal rim oxygenation (in arbitrary units) was 22.2 ± 7.4 units (range 13.5 to 39.7 units).

Figure 10.2 shows an example of an oxygenation map, aligned HRT3 topography image and the resultant masked oxygenation map leaving only NRR tissue. In the oxygenation maps brighter areas represent areas of greater oxygenation and darker areas represent areas of less oxygenation. In the HRT3 topography image the central mid-grey area represents the optic cup, and the outer light-grey area represents the NRR tissue. The black area between the two is a transitional area which for this study was regarded as part of the NRR, so the mask was based around the outer edge of the central mid-grey area to define the inner limit of the NRR and the outer edge of the light grey area to define the optic disc margin.

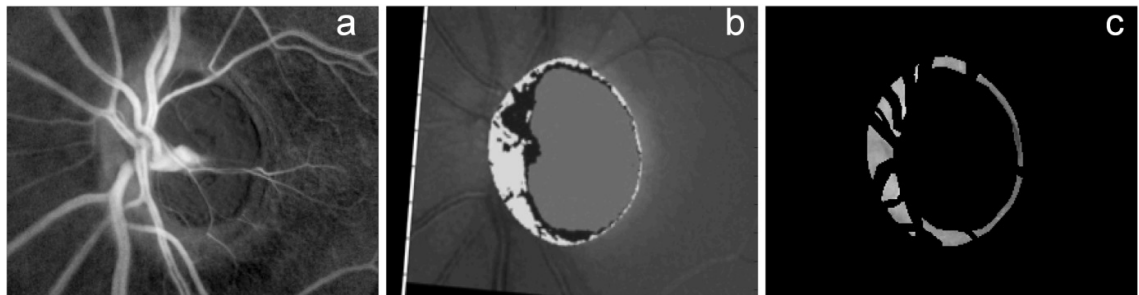


Figure 10.2: Example of a spatial oxygenation map (a), re-sampled and aligned HRT3 topography image (b), and masked oxygenation map leaving only neuroretinal rim tissue (c). In the oxygenation maps brighter areas represent areas of greater oxygenation and darker areas represent areas of less oxygenation. In the HRT3 topography image the neuroretinal rim is represented by the light grey and black areas combined and it was on this area that the mask used to create (c) was based.

10.4.1 Altitudinal relationships

Differences in NRR oxygenation above and below the horizontal midline were compared with differences in visual field sensitivity above and below the horizontal midline. First, the difference between the mean sensitivity of the entire superior and inferior hemifields (excluding

blind spot points) was compared to the difference in mean NRR oxygenation between the superior and inferior portions of the optic disc. Results are shown in figure 10.3.

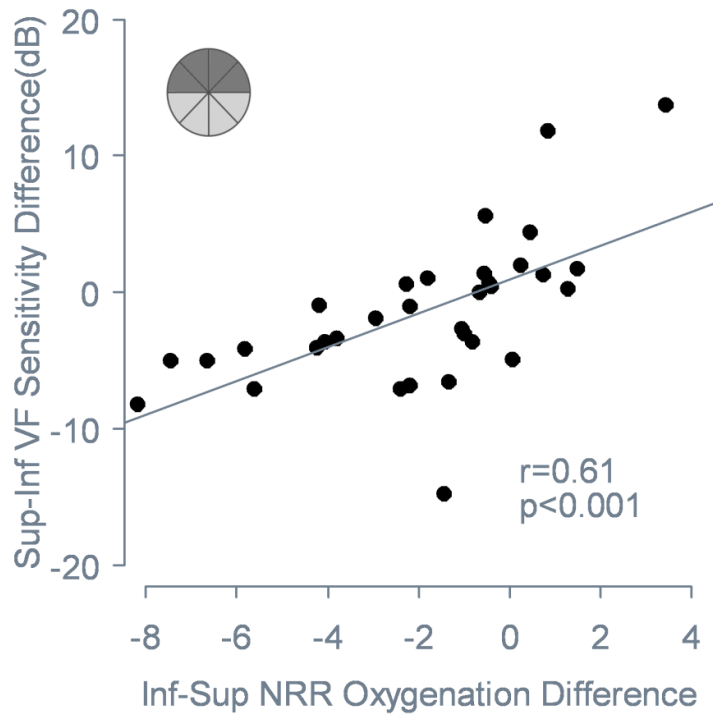


Figure 10.3: Inferior-superior differences in neuroretinal rim oxygenation (arbitrary units) vs. superior-inferior difference in visual field sensitivity. The plot includes the Pearson correlation coefficient and associated p-value as well as a diagrammatic representation of the optic disc sectors within which the neuroretinal rim oxygenation was considered.

Differences in NRR oxygenation between individual vertically opposing optic disc sectors were then considered, comparing them to the difference in mean sensitivity between corresponding visual field areas (as described in figure 10.1). Significant relationships were found between difference in NRR oxygenation and visual field sensitivity in sectors A/E, B/D and Csup/Cinf. The relationships for all vertically-opposing sector pairs are shown in figure 10.4.

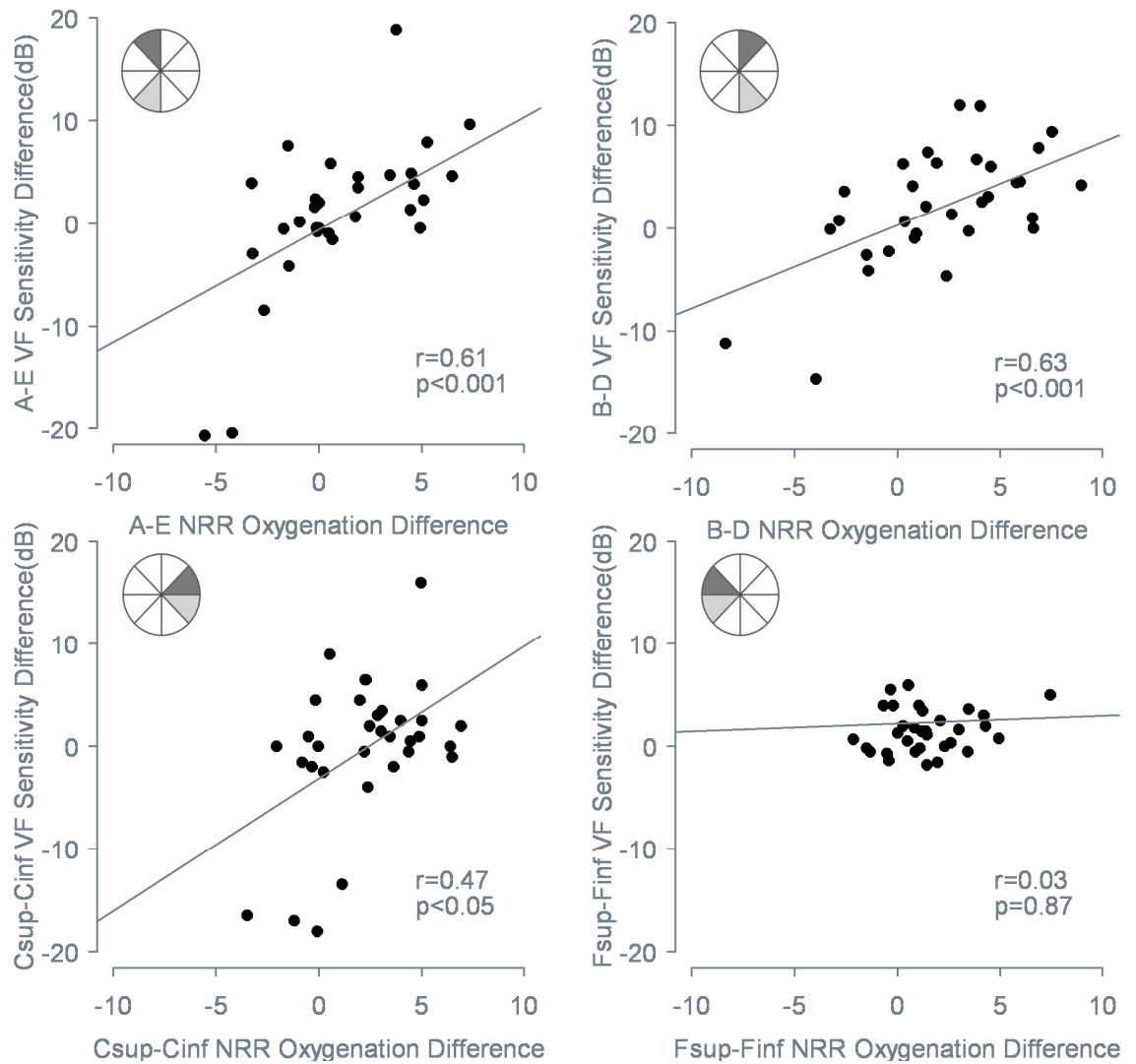







Figure 10.4: Differences in neuroretinal rim (NRR) oxygenation (arbitrary units) between vertically opposing optic disc sectors vs. differences between sensitivity of corresponding visual field areas. The plots include Pearson correlation coefficients and associated p-values as well as a diagrammatic representation of the optic disc sectors considered (for a right eye) and sectors are labelled as in figure 10.1.

The correlation coefficient and associated p-value for sectors Csup/Cinf should be viewed with caution since, as can be seen in the plot (bottom-left in figure 10.4), the regression line appears to be 'pulled' by a group of outliers and in fact when these outliers are excluded the relationship is no longer statistically significant ($r=0.15$, $p=0.44$).

To facilitate comparison with the results from the previous study, the Pearson correlation coefficients and associated p-values for each tested relationship when considering oxygenation differences between either whole optic disc sectors (previous study) or the NRR within sectors only (the present study) are shown in table 10.1. This table shows that where highly significant relationships were found in the previous study, they remain when only the oxygenation of the NRR is considered.






Table 10.1: Pearson correlation coefficients and associated p-values for differences in oxygenation between whole optic disc sectors (previous study) and the NRR within optic disc sectors (present study) compared to differences in visual field sensitivity in corresponding areas. Relationships significant at the 5% level are shown in italics. Sectors (shaded grey for a right eye) relate to those shown in figure 10.1, and describe the vertically opposing sectors between which the difference was calculated in the visual field and optic disc.

Sectors	Whole sector oxygenation r (p)	Neuroretinal rim oxygenation r (p)
 Superior-inferior	<i>0.68 (<0.001)</i>	<i>0.61 (<0.001)</i>
 A-E	<i>0.63 (<0.001)</i>	<i>0.61 (<0.001)</i>
 B-D	<i>0.63 (<0.001)</i>	<i>0.63 (<0.001)</i>
 Csup-Cinf	0.31 (=0.07)	<i>0.47 (<0.05)*</i>
 Fsup-Finf	0.36 (=0.06)	0.03 (=0.87)

*in the presence of outliers, with outliers removed r=0.15, p=0.44

In order to assess whether combining the information on superior-inferior differences in oxygenation of the NRR from the multispectral system and NRR area from the HRT3 could better predict altitudinal differences in visual field sensitivity we carried out multiple regression analysis. The results are shown in table 10.2.

Table 10.2: Pearson correlation coefficient, adjusted r^2 and contribution of individual variables to multiple regression of superior-inferior differences in NRR area and oxygenation vs. superior-inferior differences in visual field sensitivity in corresponding areas. Relationships significant at the 5% level are shown in italics. Sectors (shaded grey for a right eye) relate to those shown in figure 10.1, and describe the vertically opposing sectors between which the difference was calculated in the visual field and optic disc.

Sectors	<i>r (p)</i>	Adjusted r^2	NRR oxygenation contribution (sig)	NRR area contribution (sig)
 Superior-inferior	<i>0.61 (<0.001)</i>	<i>0.34</i>	<i>p<0.005</i>	p=0.85
 A-E	<i>0.62 (<0.001)</i>	<i>0.35</i>	<i>p<0.01</i>	p=0.47
 B-D	<i>0.65 (<0.001)</i>	<i>0.38</i>	<i>p<0.001</i>	p=0.24
 Csup-Cinf	<i>0.47 (<0.05)</i>	<i>0.17</i>	<i>p<0.01*</i>	p=0.66
 Fsup-Finf	<i>0.44 (<0.05)</i>	<i>0.14</i>	p=0.21	<i>p<0.05**</i>

*in the presence of outliers, relationship not significant when outliers excluded

**negative regression coefficient, probably chance relationship as discussed in previous study

From table 10.2 we can see that adding NRR area as a variable makes no significant difference to the relationships found, and that in fact the strongest relationships are generally found when superior-inferior differences between oxygenation of whole optic disc sectors are considered. The exceptions to this are in the Csup/Cinf and Fsup/Finf sectors where the results should be viewed with caution for reasons explained above in the case of the Csup/Cinf sectors, and as discussed in the previous study for the Fsup/Finf sectors.

10.4.2 Global relationships

Mean NRR oxygenation was not significantly associated with MD ($r=0.23$, $p=0.19$) or PSD ($r=0.04$, $p=0.83$).

10.5 Discussion

This study represents a re-analysis of the images captured in a previous study, “The relationship between optic disc oxygenation and visual field sensitivity in glaucoma”. In the previous study superior-inferior differences in optic disc oxygenation between vertically-opposing pairs of 45° sectors were compared with differences in sensitivity of corresponding visual field sectors and significant relationships were found between certain sectors. In the present study, the NRR within these sectors was isolated according to HRT3 topography images (figure 10.2) and superior-inferior differences in NRR oxygenation were then compared with superior-inferior differences in sensitivity of corresponding visual field sectors as in the previous study.

The present study found significant relationships between superior-inferior differences in NRR oxygenation and visual field sensitivity in all the cases where significant relationships were found in the previous study when considering the entire optic disc sector (table 10.1). In general the relationships in the present study were only very slightly weaker than in the previous study. This finding strongly suggests that the major contributor to the relationships found in the previous study was the oxygenation of the NRR. This finding is not surprising since the NRR is the area where neural tissue is lost in glaucoma so one would expect that any oxygen deficit which may precede this loss would also be apparent in this area. The findings of this study confirm that multispectral imaging can identify NRR tissue which is present but lacking oxygenation and therefore functioning poorly, or conversely where NRR area is low but well-perfused and therefore functioning adequately for normal visual function. This information may be clinically important in predicting glaucomatous functional loss.

Similar to the previous study it is not surprising that strong associations were not found between NRR oxygenation differences in the nasal (Csup and Cinf) and temporal (Fsup and Finf) optic disc sectors and sensitivity differences in their corresponding visual field areas since there are very low numbers of visual field test locations in these sectors (4 and 5 respectively, see figure 10.1). One might expect that stronger associations might be found if the visual field were better sampled in these areas (e.g. with a 10-2 test pattern for the temporal sectors).

Combining the information on superior-inferior differences in NRR oxygenation from the multispectral system and NRR area from the HRT3 did not generally strengthen the relationship with superior-inferior differences in visual field sensitivity (table 10.2). This was because the NRR area from the HRT3 did not contribute significantly to the multiple regression. In fact, the relationships found were not quite as strong as those found in the previous study when oxygenation of entire optic disc sectors was considered. This may be because this measure does in fact contain some indirect information on NRR area since the cup is an area of much lower oxygenation than the NRR, so the proportion of cup within a sector affects the calculation of mean oxygenation within a sector. One potential way to increase the effect of NRR area information on the relationship and thereby potentially strengthen the relationship might be to look at the amount of NRR area lost in the course of the disease. This would obviously require longitudinal data however, and the calculation of differences between vertically opposing sectors goes some way to approximate this by looking for areas of asymmetry where focal losses may have occurred. A limitation of this method is that it doesn't take into account pre-disease asymmetry in NRR thickness (Jonas et al., 1988), which could be added as an improvement to the analysis if data from a healthy population became available.

Consistent with the previous study, no relationship was found between mean NRR oxygenation and the visual field global measures MD or PSD. This finding is again consistent with previous studies of optic nerve blood flow (Michelson et al., 1998a) which found that the blood supply to the optic nerve head varies widely in both the healthy and glaucomatous populations such that what constitutes a severely reduced blood supply for one patient may be perfectly normal for another. It follows logically that oxygenation of supplied tissues may follow a similar pattern, as found by Ito *et al* (2008), although further study is required to verify this. Also, between-patient differences in reflectance properties such as due to concentration of pigments in the imaged tissue may account for some of this variability (Delori and Pflibsen, 1989).

Since this study used the same images and method of producing spatial oxygenation maps as the previous study, the main limitations of the previous study remain for this one.

Consequently, as is discussed in the previous study further work with a larger cohort of patients and an improved model for calculation of oxygenation may lead to improvements in the relationship between NRR oxygenation and visual field losses in glaucoma. Longitudinal studies may also be indicated to establish the power of temporal changes in NRR oxygenation measured by multispectral imaging in predicting subsequent glaucomatous functional losses, and to evaluate the effects of therapeutic interventions (Traustason et al., 2009, Siesky et al., 2008) on NRR perfusion.

In conclusion, similar significant associations were found between superior-inferior differences in NRR oxygenation and superior-inferior differences in visual field sensitivity in glaucoma as were found in the previous study where whole optic disc sectors were considered. Multispectral imaging therefore can identify poorly oxygenated areas of NRR which are related to visual field loss in patients with glaucoma. Altitudinal differences in visual field sensitivity cannot be better predicted by combining information on NRR oxygenation and area, and in fact the strongest relationships are found when oxygenation differences between whole optic disc sectors are considered. Multispectral imaging shows considerable promise as a clinical tool to provide important information on optic disc perfusion.

11. Conclusions

There are many considerable challenges in the search for a better understanding of primary open-angle glaucoma (POAG), a leading cause of blindness throughout the world. Progressive structural damage to the optic nerve head and retinal nerve fibre layer (RNFL) with concurrent visual field loss are now well-established hallmarks of the disease, whilst raised intraocular pressure (IOP), once thought to be the defining feature of POAG, is now considered a risk factor for development and progression of POAG only.

The separation of those with true POAG from those with risk factors but without actual disease is the crux of glaucoma diagnosis. There are many cases where diagnosis of POAG is relatively simple, but there are also large numbers of 'glaucoma suspects' for whom long-term follow-up at great cost and inconvenience is the only way to establish whether or not they are at risk of functional loss. Diagnosis of POAG is hampered by the wide normal ranges and considerable overlap between health and disease of many of the very parameters affected by POAG. For example, thin neuroretinal rim (NRR), low RNFL thickness, high IOP and low ocular blood flow are all useful signs of POAG, but there are many healthy eyes which exhibit these same features and many glaucomatous eyes which do not. Functional measures such as visual field measurement meanwhile are time consuming and difficult for some patients, and can require many repeat examinations over a long period of time to elicit a conclusive result. Concurrent ocular or neural pathology affecting the visual field can further confuse diagnosis.

In Chapter 6, "Discus –Investigating subjective judgement of glaucomatous damage in optic disc photographs" the study investigated the ability of a group of experts to distinguish between cases of POAG (defined by visual field loss) and healthy eyes based on optic disc appearance. Even when the judgements of the experts were combined as if they were working together, discrimination of health and disease was far from perfect, demonstrating the difficulty of separating true POAG from 'suspect' or 'at risk' cases. The software used in the study is freely available, and it has since been used by several training institutions as a teaching and assessment tool. The expert data collected in the study serves as a reference standard against which others may compare their performance, and may be considered a 'best case' assessment

of subjective optic disc assessment. The study clearly demonstrates a need for different methods of examination to be combined and/or better diagnostic methods to be developed in order to improve POAG diagnosis.

Combining methods of examination is a logical way to increase 'hit rates' and reduce 'false alarms' in glaucoma diagnosis. Particularly if structural and functional measurements could be combined, confusion arising from visual field defects of alternative etiology would be reduced and those patients with a slightly 'suspicious' optic disc and mild, potentially but not conclusively glaucomatous visual field loss might finally receive a firm diagnosis of POAG or otherwise. However the weak relationship between structure and function in glaucoma makes combining such test results a hit and miss affair at best. Clinicians are often happy to make a diagnosis of POAG when, for example, a slightly thin inferior NRR presents alongside a small superior arcuate scotoma, but the diagnosis is less certain when the scotoma presents in the opposite hemifield. The results of the study presented in chapter 7, "Evaluating the strength of the topographic structure-function relationship in glaucoma", suggest that perhaps this shouldn't be the case, and that particularly in early glaucoma the location of visual field defects arising from a certain perceived structural damage may not be an exact science within current understanding. The strongest topographic relationships between the optic disc and visual field bore little resemblance to those that would be expected based on the anatomy of the RNFL, and suggested that the variability in this relationship may come partly from variations in the disease process itself. More complex structural analysis of the optic disc in the study may have yielded slightly stronger relationships but would have limited the applicability of the study to clinical scenarios. The study highlights the limitations of current 'snapshot' assessments of the optic disc in POAG, since a potentially more fruitful method would have been to look at optic disc sector change from baseline. Further investigation into the exact mechanism which relates optic disc damage and loss of visual function in POAG may be needed before we can fully understand this relationship.

A major goal of glaucoma research should now be to develop methods of separating patients likely to lose visual function from those unlikely to change. Perhaps then it is better to concentrate our efforts on longitudinal studies and detection of disease progression rather than

presence? After all, if a patient's disease is not progressive then there is no risk of blindness, and if progression is detectable a diagnosis of POAG becomes much simpler. Unfortunately, since POAG is a relatively slowly progressing disease it is extremely time consuming to collect longitudinal data on the efficacy of a certain treatment, or the ability of a certain instrument or measurement to predict or detect change. This provides a barrier to the development of new technologies which may assist in predicting future functional loss and/or the efficacy of treatment.

Ideally one would measure the parameter which causes disease progression for both diagnosis and monitoring. In this way, patients with true POAG could be separated from those currently considered 'suspects' without having to undergo irreversible loss of vision. Of course in POAG this is difficult as the exact mechanisms behind the disease are the subject of continued controversy. It seems likely however, that at least in some patients changes in oxygenation of the optic nerve head play a significant role in the death of retinal ganglion cells and resultant functional loss.

Chapters 9 ("The relationship between optic disc oxygenation and visual field sensitivity in glaucoma") and 10 ("The relationship between neuroretinal rim oxygenation and visual field sensitivity in glaucoma") present promising results from the multispectral imaging system, described and tested in chapter 8, "Testing of a high-resolution multispectral fundus imaging system for measurement of optic disc tissue oxygenation". By looking for within-eye asymmetries in optic disc oxygenation we take a step away from the burdens of wide normal limits and parameters overlapping in health and disease from which optic disc oxygenation is not excepted. Asymmetries in optic disc oxygenation were found to be related to altitudinal differences in visual field sensitivity—a common feature of functional loss due to POAG. The relationships were much stronger than those found for NRR area, and were very nearly as strong when NRR oxygenation was considered in isolation from the rest of the optic disc. Multispectral imaging may therefore be of use in identifying areas of NRR which are functioning poorly due to lack of oxygen, or conversely areas of NRR which appear narrow but are well-oxygenated and therefore functioning adequately in the absence of other disease processes. Measurements of NRR oxygenation by multispectral imaging therefore show considerable

promise for both research and clinical use, even when using 'snapshot' cross-sectional data as in these studies, where the limitations of current structural imaging technologies are readily apparent.

A weakness of current structural imaging techniques is that they largely provide increased resolution and greater quantification of existing measures such as optic disc topography, RNFL thickness etc. Whilst this might be useful in terms of detecting disease progression, it adds little to our diagnostic ability. The measurement of optic disc oxygenation by multispectral imaging is different in that the imaging technology is used to yield new information which cannot be readily observed by clinicians. This oxygenation information can then be used to complement existing structural and functional data.

Refinements to the Beer-Lambert law model used to calculate oxygenation from the monochromatic images may further improve the accuracy of the measurements made, and larger studies with more patients will more precisely define the relationship between within-eye optic disc oxygenation asymmetry and altitudinal differences in visual field sensitivity. Further work is then indicated with multispectral imaging to address the important questions of whether oxygenation measurements can predict future functional loss, and whether the effects of treatment can be measured. The former requires a longitudinal trial with large patient numbers and sufficient time to allow for a significant number of patients to exhibit progression. This may therefore have to wait until the next major clinical trial in glaucoma is underway, but if successful it would be a big step forward in the accurate diagnosis of POAG. A more practical study is to investigate the effect of IOP-lowering medication on optic disc oxygenation. It may be that multispectral imaging is useful in quickly assessing whether a certain treatment is likely to be successful in preventing disease progression (i.e. optic disc oxygenation is improved), or whether an alternative treatment should be considered. This is impossible with current methods of examination, where the only method of evaluating the success of a treatment is to monitor the patient over long periods of time, and it would represent a major breakthrough in POAG care.

In summary, multispectral imaging shows considerable promise to aid clinicians where some of the pitfalls of current methods of examination exist. Whilst detection of those at risk of POAG is important, it is critical that those with true POAG and likely future disease progression are correctly diagnosed. These studies have highlighted the potential of multispectral imaging to complement current methods of examination in these areas, and provide a basis for further work with the technology.

Appendix I: Beer-Lambert Law determination of chromophore concentrations

Our multispectral image analysis aimed to determine the contributions to light absorbance of three components of the imaged tissue. Two of the components are the chromophores oxygenated haemoglobin and deoxygenated haemoglobin whose light absorption is related to their concentration and the third is the physical effect of tissue scattering of incident light. For this we used a Beer-Lambert law model (Berwick et al., 2005, Malonek and Grinvald, 1996, Mayhew et al., 1999) which can be represented as follows:

$$-\log[I_{\lambda}/I_{iso}] = \Delta C_{oxy} \epsilon_{oxy}(\lambda) + \Delta C_{deoxy} \epsilon_{deoxy}(\lambda) + \Delta C_{scattering} \epsilon_{scattering}(\lambda)$$

In the model I_{λ} is the pixel intensity at wavelength λ , I_{iso} is the pixel intensity at the isobestic wavelength 570nm, ΔC_{oxy} and ΔC_{deoxy} are the changes of chromophores (oxygenated and deoxygenated haemoglobin) and ϵ_{oxy} and ϵ_{deoxy} are extinction coefficients for the same. $\Delta C_{scattering}$ and $\epsilon_{scattering}$ are the components for tissue scattering.

The model was applied to each pixel in the aligned monochromatic images. A detailed description of how this is done in MATLAB follows:

- 1) Monochromatic images are captured at 496, 550, 570, 575, 580, 586, 610 and 700nm.

These wavelengths were chosen for the following reasons:

- a. 496nm allows good visualisation of RNFL pathways –this wavelength is not required for this analysis and is included for another project not reported here.
- b. 550nm and 570nm are both isobestic wavelengths where light absorption by oxygenated and deoxygenated haemoglobin is equal.
- c. 575nm, 580nm, and 586nm and 610nm are all wavelengths where the ratio between light absorption by oxygenated and deoxygenated haemoglobin is maximal.

- d. At 700nm tissue scattering of light contributed maximally to the image.
- 2) The monochromatic images are aligned, such that a given pixel represents the same area of tissue in every image.
 - 3) The monochromatic image taken at 496nm is discarded as it is not required for this analysis.
 - 4) Each pixel intensity value in each monochromatic image is scaled to compensate for the inhomogeneous sensitivity of the system across different wavelengths. The values are scaled according to a correction factor derived from images taken of a white surface with a flat absorption spectrum at the same wavelengths.
 - 5) Each pixel intensity value in each monochromatic image is then divided by the common logarithm of the corresponding pixel intensity value from the 570nm isobestic image. The logarithm is because the relationship between attenuation of light and chromophore concentration is logarithmic and the division by the isobestic image is to de-emphasize the effect of overall blood volume on the final oxygenation map.
 - 6) The isobestic images are then discarded as they are no longer required.
 - 7) For each pixel, the concentration of each chromophore (oxygenated haemoglobin, deoxygenated haemoglobin and tissue scattering of light) is determined in arbitrary units by finding the 'least squares' solution to the over-determined system of linear equations represented by:

$$C = \epsilon(\lambda) \cdot I(\lambda)$$

Where C is the concentration of the chromophore in arbitrary units, $\epsilon(\lambda)$ is the extinction coefficient of the chromophore at each wavelength (λ) from OMLC (1998) and $I(\lambda)$ is the pixel intensity value at each wavelength (λ).

Once this calculation has been performed for each pixel the results are displayed as oxygenation maps. To do this the calculated concentration of oxygenated haemoglobin at each pixel is used as the 'grey value' for display. The values are scaled for display, but the original calculated values are retained for further analysis such as calculating mean oxygenation within an optic disc sector. These values multiplied by 10000 for simplicity represent the 'arbitrary units'

referred to in the main text. In the oxygenation maps produced, brighter areas (higher 'grey values') represent areas of greater oxygenation whilst darker areas (lower 'grey values') represent areas of lower oxygenation.

Of course, spatial maps of deoxygenated haemoglobin concentration and tissue scattering of light can also be produced by the same method.

Appendix II: Complete List of Publications

Peer-reviewed publications

Denniss J, Echendu D, Henson DB, Artes PH (2010) Discus –Investigating subjective judgement of glaucomatous damage in optic disc photographs. *Optometry Vision Sci. (glaucoma special edition, in press)*

Muqit MMK, **Denniss J**, Nourrit V, Marcellino GR, Henson DB, Schiessl I, Stanga PE (2010) Spatial and Spectral Imaging of Retinal Laser Photocoagulation Burns. *Invest. Ophth. Vis. Sci. (in press)*

Denniss J & Henson DB (2009) The Structure-Function Relationship in Glaucoma: Implications for Disease Detection *Optom. Pract.*10: 95-104

Manuscripts currently under peer-review

Denniss J, Henson DB, Schiessl I (2010) Evaluating the strength of the topographic structure-function relationship in glaucoma

Denniss J, Schiessl I, Nourrit V, Fenerty CH, Henson DB (2010) The relationship between optic disc oxygenation and visual field sensitivity in glaucoma

Nourrit V, **Denniss J**, Muqit MMK, Schiessl I, Fenerty C, Stanga PE, Henson DB (2010) High resolution hyperspectral imaging of the retina with a modified fundus camera

Manuscripts in preparation

Denniss J, Schiessl I, Nourrit V, Fenerty CH, Henson DB (2010) Neuroretinal rim oxygenation and visual field sensitivity in patients with glaucoma

Appendix III: Complete List of Conference Presentations

Nourrit V, **Denniss J**, Schiessl I, Henson DB (2010) Hyperspectral image processing for automatic feature extraction and white light image synthesis. EMVPO 2010, Stockholm, Sweden.

Denniss J, Schiessl I, Nourrit V, Fenerty C, Henson DB (2010) Spatial Oxygenation Mapping of the Optic Disc in Glaucoma by Multispectral Imaging. *Invest Ophthalmol Vis Sci* 2010; 51: E-Abstract 2730 (ARVO 2010 Annual Meeting poster presentation, Fort Lauderdale, Florida, USA).

Denniss J, Schiessl I, Nourrit V, Fenerty C, Henson DB (2010) Preliminary results from multispectral imaging of the optic nerve head in glaucoma. College of Optometrists Research Symposium 2010, York, UK (paper presentation).

Denniss J, Henson DB, Schiessl I (2010) Evaluating the strength of the topographic structure-function relationship in glaucoma. Imaging & Perimetry Society (IPS) Congress 2010, Puerto de la Cruz, Tenerife, Spain (paper presentation).

Denniss J, Echendu D, Henson DB, Harper RA, Harding AK, Artes PH (2008) Interpretation of optic disc images for glaucomatous damage: Reference data from specialists. International Perimetric Society (IPS) Congress 2008, Nara, Japan (paper presentation).

Denniss J, Echendu D, Henson DB, Artes PH (2008) The Interpretation of Optic Disc Images for Glaucomatous Damage by Specialist Clinicians. *Invest Ophthalmol Vis Sci* 2008;49: E-Abstract 3625 (ARVO 2008 Annual Meeting poster presentation, Fort Lauderdale, Florida, USA)

Henson DB, **Denniss J**, Echendu D, Artes PH (2007) *Discus* –a software package for analysing the clinical grading of glaucomatous optic discs. UK & Eire Glaucoma Society Annual Meeting 2007, Cardiff, UK.

References

- ABRAMS, L. S., SCOTT, I. U., SPAETH, G. L., QUIGLEY, H. A. & VARMA, R. (1994) Agreement among optometrists, ophthalmologists, and residents in evaluating the optic disc for glaucoma. *Ophthalmology*, 101, 1662-1667.
- AMERICAN NATIONAL STANDARDS INSTITUTE (2001) Safe use of lasers. Z-136, 1-2000.
- ANDERSON, R. S. (2006) The psychophysics of glaucoma: Improving the structure/function relationship. *Prog Retin Eye Res*, 25, 79-97.
- ANTON, A., YAMAGISHI, N., ZANGWILL, L., SAMPLE, P. A. & WEINREB, R. N. (1998) Mapping structural to functional damage in glaucoma with standard automated perimetry and confocal scanning laser ophthalmoscopy. *Am J Ophthalmol*, 125, 436-446.
- ARTES, P. H. (2008) Progression: Things we need to remember but often forget to think about. *Optometry Vision Sci*, 85, E380-E385.
- ARTES, P. H. & CHAUHAN, B. C. (2005) Longitudinal changes in the visual field and optic disc in glaucoma. *Prog Retin Eye Res*, 24, 333-354.
- ARTES, P. H. & CRABB, D. P. (2010) Estimating normative limits of Heidelberg Retina Tomograph optic disc rim area with quantile regression. *Invest Ophthalm Vis Sci*, 51, 355-361.
- ASMAN, P. & HEIJL, A. (1992) Glaucoma Hemifield Test: Automated visual field evaluation. *Arch Ophthalmol*, 110, 812-819.
- AZUARA-BLANCO, A., KATZ, L. J., SPAETH, G. L., VERNON, S. A., SPENCER, F. & LANZL, I. M. (2003) Clinical agreement among glaucoma experts in the detection of glaucomatous changes of the optic disk using simultaneous stereoscopic photographs. *Am J Ophthalmol*, 136, 949-950.
- BEACH, J., NING, J. & KHOUBEHI, B. (2007) Oxygen saturation in optic nerve head structures by hyperspectral image analysis. *Curr Eye Res*, 32, 161-170.
- BEACH, J. M., SCHWENZER, K. J., SRINIVAS, S., KIM, D. & TIEDEMAN, J. S. (1999) Oximetry of retinal vessels by dual-wavelength imaging: Calibration and influence of pigmentation. *J Appl Physiol*, 86, 748-758.
- BENESCH, R.E., BENESCH, R., YUNG, S. (1973) Equations for the spectrophotometric analysis of haemoglobin mixtures. *Anal Biochem*, 55, 245-248.
- BENGTSSON, B. (2000) Reliability of computerized perimetric threshold tests as assessed by reliability indices and threshold reproducibility in patients with suspect and manifest glaucoma. *Acta Ophthalmol Scan*, 78, 519-522.
- BENGTSSON, B. & HEIJL, A. (2008) A Visual Field Index for calculation of glaucoma rate of progression. *Am J Ophthalmol*, 145, 343-353.
- BERENDSCHOT, T. T. J. M., DELINT, P. J. & VAN NORREN, D. (2003) Fundus reflectance -historical and present ideas. *Prog Retin Eye Res*, 22, 171-200.

- BERWICK, J., JOHNSTON, D., JONES, M., MARTINDALE, J., REDGRAVE, P., MCLOUGHLIN, N., SCHIESSL, I. & MAYHEW, J. E. W. (2005) Neurovascular coupling investigated with two-dimensional optical imaging spectroscopy in rat whisker barrel cortex. *Eur J Neurosci*, 22, 1655-1666.
- BJERRUM, J. (1889) Om en tilføjelse til den sædvanlige synsfelt – undersøgelse samt om synsfeltet ved glaukom. *Nordisk ophthalmol.*
- BLAND, J. M. & ALTMAN, D. G. (1986) Statistical methods for assessing agreement between two methods of clinical measurement. *Lancet*, i, 307-310.
- BLAND, J. M. & ALTMAN, D. G. (1996) Measurement error. *Brit Med J*, 312, 1654.
- BODEN, C., SAMPLE, P. A., BOEHM, A. G., VASILE, C., AKINEPALLI, R. & WEINREB, R. N. (2002) The structure-function relationship in eyes with glaucomatous visual field loss that crosses the horizontal meridian. *Arch Ophthalmol*, 120, 907-912.
- BOLAND, M. & QUIGLEY, H. (2007) Risk factors and open-angle glaucoma: Classification and application. *J. Glaucoma*, 16, 406-18.
- BONOMI, L., MARCHINI, G., MARRAFFA, M., BERNARDI, P., MORBIO, R. & VAROTTO, A. (2000) Vascular risk factors for primary open angle glaucoma : The Egna-Neumarkt Study. *Ophthalmology*, 107, 1287-1293.
- BROADWAY, D. C. & DRANCE, S. M. (1998) Glaucoma and vasospasm. *Brit J Ophthalmol*, 82, 862-870.
- BROADWAY, D. C., NICOLELA, M. T. & DRANCE, S. M. (1999) Optic disk appearances in primary open-angle glaucoma. *Surv Ophthalmol*, 43, S223-43.
- BRUSINI, P. & JOHNSON, C. A. (2007) Staging functional damage in glaucoma: Review of different classification methods. *Surv Ophthalmol*, 52, 156-179.
- CAPRIOLI, J. (1989) Correlation of visual function with optic nerve and nerve fiber layer structure in glaucoma. *Surv Ophthalmol*, 33, 319-330.
- CAPRIOLI, J. (1994) Clinical evaluation of the optic nerve in glaucoma. *T Am Ophthal Soc*, 92, 589.
- CAPRIOLI, J. & MILLER, J. M. (1988) Correlation of structure and function in glaucoma. Quantitative measurements of disc and field. *Ophthalmology*, 95, 723-727.
- CHAUHAN, B. C., BLANCHARD, J. W., HAMILTON, D. C. & LEBLANC, R. P. (2000) Technique for detecting serial topographic changes in the optic disc and peripapillary retina using scanning laser tomography. *Invest Ophth Vis Sci*, 41, 775-782.
- CHAUHAN, B. C., MCCORMICK, T. A., NICOLELA, M. T. & LEBLANC, R. P. (2001) Optic disc and visual field changes in a prospective longitudinal study of patients with glaucoma comparison of scanning laser tomography with conventional perimetry and optic disc photography. *Arch Ophthalmol*, 119, 1492-1499.
- COLEMAN, A. L. (1999) Glaucoma. *Lancet*, 354, 1803-1810.

- COLLABORATIVE NORMAL-TENSION GLAUCOMA STUDY GROUP (1998) The effectiveness of intraocular pressure reduction in the treatment of normal-tension glaucoma. *Am J Ophthalmol*, 126, 498-505.
- COOPS, A., HENSON, D. B., KWARTZ, A. J. & ARTES, P. H. (2006) Automated analysis of Heidelberg Retina Tomograph optic disc images by Glaucoma Probability Score. *Invest Ophthalm Vis Sci*, 47, 5348-5355.
- CUBBIDGE, R. (2005) *Visual Fields*, UK, Butterworth-Heinemann Elsevier.
- DANESH-MEYER, H. V., KU, J. Y. F., PAPCHENKO, T. L., JAYASUNDERA, T., HSIANG, J. C. & GAMBLE, G. D. (2006) Regional correlation of structure and function in glaucoma, using the disc damage likelihood scale, Heidelberg Retina Tomograph, and visual fields. *Ophthalmology*, 113, 603-611.
- DELEON-ORTEGA, J. E., ARTHUR, S. N., MCGWIN JR, G., XIE, A., MONHEIT, B. E. & GIRKIN, C. A. (2006) Discrimination between glaucomatous and nonglaucomatous eyes using quantitative imaging devices and subjective optic nerve head assessment. *Invest Ophthalm Vis Sci*, 47, 3374-80.
- DELORI, F. C., GRAGOUDAS, E. S., FRANCISCO, R. & PRUETT, R. C. (1977) Monochromatic ophthalmoscopy and fundus photography. *Arch Ophthalmol*, 95, 861-868.
- DELORI, F. C. & PFLIBSEN, K. P. (1989) Spectral reflectance of the human ocular fundus. *Appl Optics*, 28, 1061-1077.
- DRANCE, S., ANDERSON, D. R. & SCHULZER, M. (2001) Risk factors for progression of visual field abnormalities in normal-tension glaucoma. *Am J Ophthalmol*, 131, 699-708.
- EGPS GROUP (2007) Predictive factors for open-angle glaucoma among patients with ocular hypertension in the European Glaucoma Prevention Study. *Ophthalmology*, 114, 3-9.
- FECHTNER, R. D. & WEINREB, R. N. (1994) Mechanisms of optic nerve damage in primary open angle glaucoma. *Surv Ophthalmol*, 39, 23-42.
- FEINSTEIN, A. R. & CICCHETTI, D. V. (1990) High agreement but low kappa: I. The problems of two paradoxes. *J Clin Epidemiol*, 43, 543-549.
- FINGERET, M., MEDEIROS, F. A., SUSANNA JR, R. & WEINREB, R. N. (2005) Five rules to evaluate the optic disc and retinal nerve fiber layer for glaucoma. *Optometry*, 76, 661-668.
- FITZGIBBON, T. & TAYLOR, S. F. (1996) Retinotopy of the human retinal nerve fibre layer and optic nerve head. *J Comp Neurol*, 375, 238-251.
- FLAMMER, J., DRANCE, S. M. & ZULAUF, M. (1984) Differential light threshold. Short-and long-term fluctuation in patients with glaucoma, normal controls, and patients with suspected glaucoma. *Arch Ophthalmol*, 102, 704-706.
- FLAMMER, J., HAEFLIGER, I. O., ORGUL, S. & RESINK, T. (1999) Vascular dysregulation: A principal risk factor for glaucomatous damage? *J Glaucoma*, 8, 212-219.

- FLAMMER, J. & ORGUL, S. (1998) Optic nerve blood-flow abnormalities in glaucoma. *Prog Retin Eye Res*, 17, 267-289.
- FLAMMER, J., ORGUL, S., COSTA, V. P., ORZALESI, N., KRIEGLSTEIN, G. K., SERRA, L. M., RENARD, J. & STEFANSSON, E. (2002) The impact of ocular blood flow in glaucoma. *Prog Retin Eye Res*, 21, 359-393.
- FLAMMER, J., PACHE, M. & RESINK, T. (2001) Vasospasm, its role in the pathogenesis of diseases with particular reference to the eye. *Prog Retin Eye Res*, 20, 319-349.
- FLEISS, J. L. (1971) Measuring nominal scale agreement among many raters. *Psychol Bull*, 76, 378-382.
- FOSTER, P. J., BUHRMANN, R., QUIGLEY, H. A. & JOHNSON, G. J. (2002) The definition and classification of glaucoma in prevalence surveys. *Brit J Ophthalmol*, 86, 238-242.
- GARDINER, S. K., JOHNSON, C. A. & CIOFFI, G. A. (2005) Evaluation of the structure-function relationship in glaucoma. *Invest Ophth Vis Sci*, 46, 3712-3717.
- GARWAY-HEATH, D. F. (2008) Early diagnosis in glaucoma. IN NUCCI, C., CERULLI, L., OSBORNE, N. N. & BAGETTA, G. (Eds.) *Prog Brain Research*.
- GARWAY-HEATH, D. F. & HITCHINGS, R. A. (1998) Quantitative evaluation of the optic nerve head in early glaucoma. *Brit J Ophthalmol*, 82, 352-361.
- GARWAY-HEATH, D. F., HOLDER, G. E., FITZKE, F. W. & HITCHINGS, R. A. (2002) Relationship between electrophysiological, psychophysical, and anatomical measurements in glaucoma. *Invest Ophth Vis Sci*, 43, 2213-2220.
- GARWAY-HEATH, D. F., POINOOSAWMY, D., FITZKE, F. W. & HITCHINGS, R. A. (2000) Mapping the visual field to the optic disc in normal tension glaucoma eyes. *Ophthalmology*, 107, 1809-1815.
- GARWAY-HEATH, D. F., RUBEN, S. T., VISWANATHAN, A. & HITCHINGS, R. A. (1998) Vertical cup/disc ratio in relation to optic disc size: its value in the assessment of the glaucoma suspect. *Brit J Ophthalmol*, 82, 1118-1124.
- GASSER, P. & FLAMMER, J. (1991) Blood-cell velocity in the nailfold capillaries of patients with normal-tension and high-tension glaucoma. *Am J Ophthalmol*, 111, 585-588.
- GHERGEL, D., ORGUL, S., GUGLETA, K., GEKKIEVA, M. & FLAMMER, J. (2000) Relationship between ocular perfusion pressure and retrobulbar blood flow in patients with glaucoma with progressive damage. *Am J Ophthalmol*, 130, 597-605.
- GORDON, M. O., BEISER, J. A., BRANDT, J. D., HEUER, D. K., HIGGINBOTHAM, E. J., JOHNSON, C. A., KELTNER, J. L., MILLER, J. P., PARRISH, II & RICHARD, K. (2002) The Ocular Hypertension Treatment Study: Baseline factors that predict the onset of primary open-angle glaucoma. *Arch Ophthalmol*, 120, 714-720.

- GOTTFREDSOTTIR, M. S., SVERRISSON, T., MUSCH, D. C. & STEFANSSON, E. (1999) Chronic open-angle glaucoma and associated ophthalmic findings in monozygotic twins and their spouses in Iceland. *J Glaucoma*, 8, 134-139.
- GREANEY, M. J., HOFFMAN, D. C., GARWAY-HEATH, D. F., NAKLA, M., COLEMAN, A. L. & CAPRIOLI, J. (2002) Comparison of optic nerve imaging methods to distinguish normal eyes from those with glaucoma. *Invest Ophth Vis Sci*, 43, 140-145.
- HAAS, A., FLAMMER, J. & SCHNEIDER, U. (1986) Influence of age on the visual fields of normal subjects. *Am J Ophthalmol*, 101, 199-203.
- HAMARD, P., HAMARD, H., DUFAUX, J. & QUESNOT, S. (1994) Optic nerve head blood flow using a laser Doppler velocimeter and haemorheology in primary open angle glaucoma and normal pressure glaucoma. *Brit Med J*, 78, 449-453.
- HANLEY, J. A. (1989) Receiver operating characteristic (ROC) methodology: The state of the art. *Crit Rev Diagn Imag*, 29, 307-335.
- HANLEY, J. A. & MCNEIL, B. J. (1982) The meaning and use of the area under a receiver operating characteristic (ROC) curve. *Radiology*, 143, 29-36.
- HARASYMOWYCZ, P., DAVIS, B., XU, G., MYERS, J., BAYER, A. & SPAETH, G. L. (2004) The use of RADAAR (ratio of rim area to disc area asymmetry) in detecting glaucoma and its severity. *Can J Ophthalmol*, 39, 240-244.
- HARDARSON, S. H., HARRIS, A., KARLSSON, R. A., HALLDORSSON, G. H., KAGEMANN, L., RECHTMAN, E., ZOEGA, G. M., EYSTEINSSON, T., BENEDIKTSSON, J. A., THORSTEINSSON, A., JENSEN, P. K., BEACH, J. & STEFANSSON, E. (2006) Automatic retinal oximetry. *Invest Ophth Vis Sci*, 47, 5011-5016.
- HARIZMAN, N., OLIVEIRA, C., CHIANG, A., TELLO, C., MARMOR, M., RITCH, R. & LIEBMANN, J. M. (2006) The ISNT Rule and differentiation of normal from glaucomatous eyes. *Arch Ophthalmol*, 124, 1579-1583.
- HARPER, R., HENSON, D. & REEVES, B. C. (2000a) Appraising evaluations of screening/diagnostic tests: the importance of the study populations. *Brit J Ophthalmol*, 84, 1198-1202.
- HARPER, R., RADI, N., REEVES, B. C., FENERTY, C., SPENCER, A. F. & BATTERBURY, M. (2001) Agreement between ophthalmologists and optometrists in optic disc assessment: training implications for glaucoma co-management. *Graef Arch Clin Exp*, 239, 342-50.
- HARPER, R. & REEVES, B. (2000) The sensitivity and specificity of direct ophthalmoscopic optic disc assessment in screening for glaucoma: a multivariate analysis. *Graef Arch Clin Exp*, 238, 949-955.
- HARPER, R., REEVES, B. & SMITH, G. (2000b) Observer variability in optic disc assessment: implications for glaucoma shared care. *Ophthal Physl Opt*, 20, 265-73.
- HART, W. M. & BECKER, B. (1982) The onset and evolution of glaucomatous visual field defects. *Ophthalmology*, 89, 268-279.

- HARWERTH, R. S., CARTER-DAWSON, L., SHEN, F., SMITH, E. L. & CRAWFORD, M. L. J. (1999) Ganglion cell losses underlying visual field defects from experimental glaucoma. *Invest Ophthalm Vis Sci*, 40, 2242-2250.
- HARWERTH, R. S., CARTER-DAWSON, L., SMITH, E. L., BARNES, G., HOLT, W. F. & CRAWFORD, M. L. J. (2004) Neural losses correlated with visual losses in clinical perimetry. *Invest Ophthalm Vis Sci*, 45, 3152-3160.
- HARWERTH, R. S., CARTER-DAWSON, L., SMITH III, E. L. & CRAWFORD, M. L. J. (2005) Scaling the structure-function relationship for clinical perimetry. *Acta Ophthalmol Scan*, 83, 448-455.
- HARWERTH, R. S., CRAWFORD, M. L. J., FRISHMAN, L. J., VISWANATHAN, S., SMITH III, E. L. & CARTER-DAWSON, L. (2002) Visual field defects and neural losses from experimental glaucoma. *Prog Retin Eye Res*, 21, 91-125.
- HARWERTH, R. S. & QUIGLEY, H. A. (2006) Visual field defects and retinal ganglion cell losses in patients with glaucoma. *Arch Ophthalmology*, 124, 853-859.
- HARWERTH, R. S., SMITH, E. L. & DESANTIS, L. (1993) Behavioural perimetry in monkeys. *Invest Ophthalm Vis Sci*, 34, 31-40.
- HARWERTH, R. S., SMITH, E. L., III & DESANTIS, L. (1997) Experimental glaucoma: Perimetric field defects and intraocular pressure. *J Glaucoma*, 6, 390-401.
- HARWERTH, R. S., VILUPURU, A. S., RANGASWAMY, N. V. & SMITH 3RD, E. L. (2007) The relationship between nerve fibre layer and perimetry measurements. *Invest. Ophthalm. Vis. Sci.*, 48, 763-773.
- HAYREH, S. S. (1974) Anatomy and physiology of the optic nerve head. *Transactions - American Academy of Ophthalmology and Otolaryngology*, 78, OP240-254.
- HAYREH, S. S. (1978) Fluids in the anterior part of the optic nerve in health and disease. *Surv Ophthalmol*, 23, 1-25.
- HAYREH, S. S. (2001) The blood supply of the optic nerve head and the evaluation of it-myth and reality. *Prog Retin Eye Res*, 20, 563-93.
- HEIJL, A., LESKE, M. C., BENGTSSON, B., HYMAN, L., BENGTSSON, B. & HUSSEIN, M. (2002) Reduction of intraocular pressure and glaucoma progression results from the Early Manifest Glaucoma Trial. *Arch Ophthalmology*, 120, 1268-1279.
- HENSON, D. B. (2000) *Visual Fields, Second Edition*, Oxford, Butterworth-Heinemann, UK.
- HENSON, D. B., ARTES, P. H. & CHAUHAN, B. C. (1999) Diffuse loss of sensitivity in early glaucoma. *Invest Ophthalm Vis Sci*, 40, 3147-3151.
- HENSON, D. B., CHAUDRY, S., ARTES, P. H., FARAGHER, E. B. & ANSONS, A. (2000) Response variability in the visual field: Comparison of optic neuritis, glaucoma, ocular hypertension, and normal eyes. *Invest Ophthalm Vis Sci*, 41, 417-421.

- HENSON, D. B. & HARPER, R. (2007) Diagnosis of the glaucomas 1: Visual field changes. IN EDGAR, D.F. & RUDNICKA, A.R. (Eds.) *Glaucoma Identification & Co-management*. USA, Butterworth-Heinemann Elsevier.
- HERNDON, L. W., WEIZER, J. S. & STINNETT, S. S. (2004) Central corneal thickness as a risk factor for advanced glaucoma damage. *Arch Ophthalmol*, 122, 17-21.
- HILLMAN, E. (2007) Optical brain imaging in vivo: Techniques and applications from animal to man. *J Biomed Opt*, 12, 051402.
- HODAPP, E., PARRISH, R. K. & ANDERSON, D. R. (1993) Classification of defects. *Hodapp E, Parish RK Jr, Anderson DR. Clinical decisions in glaucoma. St. Louis: Mosby, USA* 52-61.
- HOLLOWS, F. C. & GRAHAM, P. A. (1966) Intra-ocular pressure, glaucoma, and glaucoma suspects in a defined population. *Brit J Ophthalmol*, 50, 570-586.
- HOOD, D. C., ANDERSON, S. C., WALL, M. & KARDON, R. H. (2007) Structure versus function in glaucoma: An application of a linear model. *Invest Ophth Vis Sci*, 48, 3662-3668.
- HOOD, D. C. & KARDON, R. H. (2007) A framework for comparing structural and functional measures of glaucomatous damage. *Prog Retin Eye Res*, 26, 688-710.
- HOUGAARD, J. L., HEIJL, A. & KROGH, E. (2004) The nerve fibre layer symmetry test: computerized evaluation of human retinal nerve fibre layer thickness as measured by optical coherence tomography. *Acta Ophthalmol Scan*, 82, 410-418.
- HRYNCHAK, P., HUTCHINGS, N., JONES, D. & SIMPSON, T. (2004) A comparison of cup-to-disc ratio measurement in normal subjects using optical coherence tomography image analysis of the optic nerve head and stereo fundus biomicroscopy. *Ophthal Physl Opt*, 24, 543-550.
- IHAKA, R. & GENTLEMAN, R. (1996) R: A language for data analysis and graphics. *J Comput Graph Stat*, 5, 299-314.
- ITO, M., MURAYAMA, K., DEGUCHI, T., TAKASU, M., GIL, T., ARAIE, M., PEYMAN, G. & YONEYA, S. (2008) Oxygen saturation levels in the juxta-papillary retina in eyes with glaucoma. *Exp Eye Res*, 86, 512-518.
- JOHNSON, C. A., ADAMS, A. J. & LEWIS, R. A. (1989) Evidence for a neural basis of age-related visual field loss in normal observers. *Invest Ophth Vis Sci*, 30, 2056-2064.
- JOHNSON, C. A., CIOFFI, G. A., LIEBMANN, J. R., SAMPLE, P. A., ZANGWILL, L. M. & WEINREB, R. N. (2000) The relationship between structural and functional alterations in glaucoma: A review. *Semin Ophthalmol*, 15, 221-233.
- JONAS, J. B. & BUDDE, W. M. (2000) Diagnosis and pathogenesis of glaucomatous optic neuropathy: Morphological aspects 1. *Prog Retin Eye Res*, 19, 1-40.
- JONAS, J. B., BUDDE, W. M. & PANDA-JONAS, S. (1999) Ophthalmoscopic evaluation of the optic nerve head. *Surv Ophthalmol*, 43, 293-320.
- JONAS, J. B., GUSEK, G. C. & NAUMANN, G. O. (1988) Optic disc, cup and neuroretinal rim size, configuration and correlations in normal eyes [published

- errata appear in *Invest Ophthalmol Vis Sci* 1991 May; 32 (6): 1893 and 1992 Feb; 32 (2): 474-5]. *Invest Ophthalmol Vis Sci*, 29, 1151-1158.
- JONAS, J. B., NGUYEN, X. N., GUSEK, G. C. & NAUMANN, G. O. (1989) Parapapillary chorioretinal atrophy in normal and glaucoma eyes. I. Morphometric data. *Invest Ophthalmol Vis Sci*, 30, 908-918.
- JONAS, J. B., SCHMIDT, A. M., MULLER-BERGH, J. A., SCHLOTZER-SCHREHARDT, U. M. & NAUMANN, G. O. (1992) Human optic nerve fiber count and optic disc size. *Invest Ophthalmol Vis Sci*, 33, 2012-2018.
- KAHNEMAN, D., SLOVIC, P. & TVERSKY, A. (1982) *Judgement under uncertainty: Heuristics and biases*, Cambridge, Cambridge University Press, UK.
- KANSKI, J. J. (2003) *Clinical ophthalmology -a systematic approach*, USA, Butterworth-Heinemann.
- KASS, M. A., HEUER, D. K., HIGGINBOTHAM, E. J., JOHNSON, C. A., KELTNER, J. L., MILLER, J. P., PARRISH, II, RICHARD, K., WILSON, M. R. & GORDON, M. O. (2002) The Ocular Hypertension Treatment Study: A randomized trial determines that topical ocular hypotensive medication delays or prevents the onset of primary open-angle glaucoma. *Arch Ophthalmol*, 120, 701-713.
- KELTNER, J. L., JOHNSON, C. A., ANDERSON, D. R., LEVINE, R. A., FAN, J., CELLO, K. E., QUIGLEY, H. A., BUDENZ, D. L., PARRISH, R. K., KASS, M. A. & GORDON, M. O. (2006) The association between glaucomatous visual fields and optic nerve head features in the Ocular Hypertension Treatment Study. *Ophthalmology*, 113, 1603-12.
- KELTNER, J. L., JOHNSON, C. A., CELLO, K. E., EDWARDS, M. A., BANDERMANN, S. E., KASS, M. A. & GORDON, M. O. (2003) Classification of visual field abnormalities in the Ocular Hypertension Treatment Study. *Arch Ophthalmol*, 121, 643-650.
- KERRIGAN-BAUMRIND, L. A., QUIGLEY, H. A., PEASE, M. E., KERRIGAN, D. F. & MITCHELL, R. S. (2000) Number of ganglion cells in glaucoma eyes compared with threshold visual field tests in the same persons. *Invest Ophthalmol Vis Sci*, 41, 741-748.
- KHOUBEHI, B., BEACH, J. M. & KAWANO, H. (2004) Hyperspectral imaging for measurement of oxygen saturation in the optic nerve head. *Invest Ophthalmol Vis Sci*, 45, 1464-1472.
- KLEIN, B. E. K., KLEIN, R., MEUER, S. M. & GOETZ, L. A. (1993) Migraine headache and its association with open-angle glaucoma: the Beaver Dam Eye Study. *Invest Ophthalmol Vis Sci*, 34, 3024-3027.
- KROESE, M. & BURTON, H. (2003) Primary open angle glaucoma. The need for a consensus case definition. *J Epidemiol Commun H*, 57, 752-754.
- LIDLAW, D. A. H., BLOOM, P. A., HUGHES, A. O., SPARROW, J. M. & MARMION, V. J. (1994) The sight test fee: effect on ophthalmology referrals and rate of glaucoma detection. *Brit J Ophthalmol*, 309, 634-636.

- LE, A., MUKESH, B. N., MCCARTY, C. A. & TAYLOR, H. R. (2003) Risk factors associated with the incidence of open-angle glaucoma: The Visual Impairment Project. *Invest Ophth Vis Sci*, 44, 3783-3789.
- LESKE, M. C. (2007) Open-angle glaucoma - an epidemiologic overview. *Ophthalmic Epidemiol*, 14, 166-172.
- LESKE, M. C. (2009) Ocular perfusion pressure and glaucoma: Clinical trial and epidemiologic findings. *Curr Opin Ophthalmol*, 20, 73-78.
- LESKE, M. C., CONNELL, A. M. S., WU, S.-Y., NEMESURE, B., LI, X., SCHACHAT, A., HENNIS, A. & FOR THE BARBADOS EYE STUDIES, G. (2001) Incidence of open-angle glaucoma: The Barbados Eye Studies. *Arch Ophthalmol*, 119, 89-95.
- LESKE, M. C., EDERER, F. & PODGOR, M. (1981) Estimating incidence from age-specific prevalence in glaucoma. *Am J Epidemiol*, 113, 606-613.
- LESKE, M. C., HEIJL, A., HUSSEIN, M., BENGTSSON, B., HYMAN, L. & KOMAROFF, E. (2003) Factors for glaucoma progression and the effect of treatment. The Early Manifest Glaucoma Trial. *Arch Ophthalmol*, 121, 48-56.
- LESKE, M. C., WU, S.-Y., HENNIS, A., HONKANEN, R. & NEMESURE, B. (2008) Risk factors for incident open-angle glaucoma: The Barbados Eye Studies. *Ophthalmology*, 115, 85-93.
- LICHTER, P. R. (1976) Variability of expert observers in evaluating the optic disc. *T Am Ophthal Soc*, 74, 532.
- LICHTER, P. R., MUSCH, D. C., GILLESPIE, B. W., GUIRE, K. E., JANZ, N. K., WREN, P. A. & MILLS, M. (2001) Interim clinical outcomes in the collaborative initial glaucoma treatment study comparing initial treatment randomized to medications or surgery. *Ophthalmology*, 108, 1943-1953.
- LIN, S., SINGH, K., JAMPEL, H., HODAPP, E., SMITH, S., BA, F., DUEKER, D., FECHTNER, R., SAMPLES, J., SCHUMAN, J. & MINCKLER, D. (2007) Optic nerve head and retinal nerve fibre layer analysis -a report by the American Academy of Ophthalmology. *Ophthalmology*, 114, 1937-1949.
- LORD, F. M. (1980) *Applications of item response theory to practical testing problems*, Hillsdale, NJ, USA, Lawrence Erlbaum Associates.
- MALONEK, D. & GRINVALD, A. (1996) Interactions between electrical activity and cortical microcirculation revealed by imaging spectroscopy: Implications for functional brain mapping. *Science*, 272, 551-554.
- MARDIN, C. Y. & JÜNEMANN, A. G. M. (2001) The diagnostic value of optic nerve imaging in early glaucoma. *Curr Opin Ophthalmol*, 12, 100-104.
- MAYHEW, J., ZHENG, Y., HOU, Y., VUKSANOVIC, B., BERWICK, J., ASKEW, S. & COFFEY, P. (1999) Spectroscopic analysis of changes in remitted illumination: The response to increased neural activity in brain. *Neuroimage*, 10, 304-326.
- MEDEIROS, F. A., NG, D., ZANGWILL, L. M., SAMPLE, P. A., BOWD, C. & WEINREB, R. N. (2007) The effects of study design and spectrum bias on the

evaluation of diagnostic accuracy of confocal scanning laser ophthalmoscopy in glaucoma. *Invest Ophth Vis Sci*, 48, 214-222.

- MEDEIROS, F. A., ZANGWILL, L. M., BOWD, C. & WEINREB, R. N. (2004) Comparison of the GDx VCC scanning laser polarimeter, HRT II confocal scanning laser ophthalmoscope, and Stratus OCT optical coherence tomograph for the detection of glaucoma. *Arch Ophthalmol*, 122, 827-837.
- MENDEL, M. J., TOI, V. V., RIVA, C. E. & PETRIG, B. L. (1993) Eye-tracking laser Doppler velocimeter stabilized in two dimensions: Principle, design and construction. *J Opt Soc Am*, 10, 1663-1669.
- MICHELSON, G., LANGHANS, M. J., HARAZNY, J. & DICHTL, A. (1998a) Visual field defect and perfusion of the juxtapapillary retina and the neuroretinal rim area in primary open-angle glaucoma. *Graefes Archive Clin Exp Ophthalmol*, 236, 80-85.
- MICHELSON, G., WELZENBACH, J., PAL, I. & HARAZNY, J. (1998b) Automatic full field analysis of perfusion images gained by scanning laser Doppler flowmetry. *Brit J Ophthalmol*, 82, 1294-1300.
- MIKELBERG, F. S. & DRANCE, S. M. (1984) The mode of progression of visual field defects in glaucoma. *Am J Ophthalmol*, 98, 443-445.
- MINCKLER, D. S. (1980) The organization of nerve fiber bundles in the primate optic nerve head. *Arch Ophthalmol*, 98, 1630-1636.
- MITCHELL, P., HOURIHAN, F., SANDBACH, J. & JIN WANG, J. (1999) The relationship between glaucoma and myopia: The Blue Mountains Eye Study. *Ophthalmology*, 106, 2010-2015.
- MITCHELL, P., SMITH, W., ATTEBO, K. & HEALEY, P. R. (1996) Prevalence of open-angle glaucoma in Australia. The Blue Mountains Eye Study. *Ophthalmology*, 103, 1661-1669.
- MORGAN, J. E., SHEEN, N. J. L., NORTH, R. V., CHOONG, Y. & ANSARI, E. (2005) Digital imaging of the optic nerve head: Monoscopic and stereoscopic analysis. *Brit J Ophthalmol*, 89, 879-884.
- MORGAN, W. H., HAZELTON, M. L., AZAR, S. L., HOUSE, P. H., YU, D. Y., CRINGLE, S. J. & BALARATNASINGAM, C. (2004) Retinal venous pulsation in glaucoma and glaucoma suspects. *Ophthalmology*, 111, 1489-1494.
- MUKESH, B., MCCARTY, C., RAIT, J. & TAYLOR, H. (2002) Five-year incidence of open-angle glaucoma: The Visual Impairment Project. *Ophthalmology*, 109, 1047-1051.
- NEMESURE, B., HONKANEN, R., HENNIS, A., WU, S. Y. & LESKE, M. C. (2007) Incident open-angle glaucoma and intraocular pressure. *Ophthalmology*, 114, 1810-1815.
- NEMESURE, B., LESKE, M. C., HE, Q. & MENDELL, N. (1996) Analyses of reported family history of glaucoma: A preliminary investigation. *Ophthalmic Epidemiol*, 3, 135-141.

- NICE (2009) Glaucoma: Diagnosis and management of chronic open angle glaucoma and ocular hypertension [internet] Available at: <http://www.nice.org.uk/nicemedia/pdf/CG85FullGuideline.pdf> (accessed 14th July 2010).
- NICOLELA, M. T. (2007) Retinal vein pulsation predicts increasing optic disc excavation. *Brit J Ophthalmol*, 91, 405-406.
- NICOLELA, M. T., DRANCE, S. M., BROADWAY, D. C., CHAUHAN, B. C., MCCORMICK, T. A. & LE BLANC, R. P. (2001) Agreement among clinicians in the recognition of patterns of optic disk damage in glaucoma. *Am J Ophthalmol*, 132, 836-44.
- NOURRIT, V., BUENO, J., VOHNSEN, B. & ARTAL, P. (2008) Non linear registration for scanned retinal images. Application to ocular polarimetry. *Appl Optics*, 47, 5341-47.
- OGDEN, T. E. (1974) The nerve-fiber layer of the primate retina: An autoradiographic study. *Invest Ophth Vis Sci*, 13, 95-100.
- OGDEN, T. E. (1983) Nerve fiber layer of the macaque retina: Retinotopic organization. *Invest Ophth Vis Sci*, 24, 85-98.
- OMLC (1998) Tabulated molar extinction coefficient for haemoglobin in water [internet]. Available at: <http://omlc.ogi.edu/spectra/hemoglobin/summary.html> (accessed 9th September 2009).
- PARKIN, B., SHUTTLEWORTH, G., COSTEN, M. & DAVISON, C. (2001) A comparison of stereoscopic and monoscopic evaluation of optic disc topography using a digital optic disc stereo camera. *Brit Med J*, 323, 1347-1351
- PHELPS, C. D. & CORBETT, J. J. (1985) Migraine and low-tension glaucoma: a case-control study. *Invest Ophth Vis Sci*, 26, 1105-1108.
- QUIGLEY, H. A. (1996) Number of people with glaucoma worldwide. *Brit J Ophthalmol*, 80, 389-393.
- QUIGLEY, H. A., ADDICKS, E. M. & GREEN, W. R. (1982) Optic nerve damage in human glaucoma. III. Quantitative correlation of nerve fibre loss and visual field defect in glaucoma, ischemic neuropathy, papilledema, and toxic neuropathy. *Arch Ophthalmol*, 100, 135-146.
- QUIGLEY, H. A., DUNKELBERGER, G. R. & GREEN, W. R. (1989) Retinal ganglion cell atrophy correlated with automated perimetry in human eyes with glaucoma. *Am J Ophthalmol*, 107, 453-464.
- QUIGLEY, H. A., VARMA, R., TIELSCH, J. M., KATZ, J., SOMMER, A. & GILBERT, D. L. (1999) The relationship between optic disc area and open-angle glaucoma: The Baltimore Eye Survey. *J Glaucoma*, 8, 347-352.
- RADIUS, R. L. & ANDERSON, D. R. (1979) The course of axons through the retina and optic nerve head. *Arch Ophthalmol*, 97, 1154-1158.
- REUS, N. J., DE GRAAF, M. & LEMIJ, H. G. (2007) Accuracy of GDx VCC, HRT I, and clinical assessment of stereoscopic optic nerve head photographs for diagnosing glaucoma. *Brit J Ophthalmol*, 91, 313-318.

- RIVA, C. E., HARINO, S., PETRIG, B. L. & SHONAT, R. D. (1992) Laser Doppler flowmetry in the optic nerve. *Exp Eye Res*, 55, 499-506.
- RIVA, C. E., ROSS, B. & BENEDEK, G. B. (1972) Laser Doppler measurements of blood flow in capillary tubes and retinal arteries. *Invest Ophthalmol*, 11, 936-944.
- RUDNICKA, A.R. & OWEN, C. (2007) Epidemiology of primary open angle glaucoma. IN EDGAR, D.F. & RUDNICKA, A.R. (Eds.) *Glaucoma Identification & Co-management*. USA, Butterworth-Heinemann Elsevier.
- RUDNICKA, A. R. & EDGAR, D. F. (2007) Interpretation of visual field measures from automated and semi-automated perimeters. IN EDGAR, D.F. & RUDNICKA, A.R. (Eds.) *Glaucoma Identification & Co-management*. USA, Butterworth-Heinemann Elsevier.
- RUDNICKA, A. R., MT-ISA, S., OWEN, C. G., COOK, D. G. & ASHBY, D. (2006) Variations in primary open-angle glaucoma prevalence by age, gender, and race: A Bayesian meta-analysis. *Invest Ophth Vis Sci*, 47, 4254-4261.
- RUMSEY, K. E., RUMSEY, J. M. & LEACH, N. E. (1990) Monocular vs. stereospecific measurement of cup-to-disc ratios. *Optometry Vision Sci*, 67, 546-550.
- SCHOFF, E., HATTENHAUER, M., ING, H., HODGE, D., KENNEDY, R., HERMAN, D. & JOHNSON, D. (2001) Estimated incidence of open-angle glaucoma in Olmsted County, Minnesota. *Ophthalmology*, 108, 882-886.
- SCHULZER, M., ALWARD, W. L., FELDMAN, F., CASHWELL, L. F., WILENSKY, J. & GEIJSEN, H. C. (1998) Comparison of glaucomatous progression between untreated patients with normal-tension glaucoma and patients with therapeutically reduced intraocular pressures. *Am J Ophthalmol*, 126, 487-497.
- SHARMA, P., SAMPLE, P. A., ZANGWILL, L. M. & SCHUMAN, J. S. (2008) Diagnostic tools for glaucoma detection and management. *Surv Ophthalmol*, 53, S17-S32.
- SIESKY, B., HARRIS, A., CANTOR, L. B., KAGEMANN, L., WEITZMAN, Y., MCCRANOR, L., MARQUES, C., WERNE, A. & STEFANSSON, E. (2008) A comparative study of the effects of Brinzolamide and Dorzolamide on retinal oxygen saturation and ocular microcirculation in patients with primary open-angle glaucoma. *Brit J Ophthalmol*, 92, 500-504.
- SING, T., SANDER, O., BEERENWINKEL, N. & LENGAUER, T. (2005) ROCR: visualizing classifier performance in R. *Bioinformatics*, 21, 3940-3941.
- SINGH, S. & DASS, R. (1960) The central artery of the retina II. Distribution and anastomoses. *Brit J Ophthalmol*, 44, 280-299.
- SOMMER, A., KATZ, J., QUIGLEY, H. A., MILLER, N. R., ROBIN, A. L., RICHTER, R. C. & WITT, K. A. (1991a) Clinically detectable nerve fiber atrophy precedes the onset of glaucomatous field loss. *Arch Ophthalmol*, 109, 77-83.
- SOMMER, A., TIELSCH, J. M., KATZ, J., QUIGLEY, H. A., GOTTSCH, J. D., JAVITT, J. & SINGH, K. (1991b) Relationship between intraocular pressure and primary open angle glaucoma among white and black Americans. The Baltimore Eye Survey. *Arch Ophthalmol*, 109, 1090-1095.

- SPALDING, J. M., LITWAK, A. B. & SHUFELT, C. L. (2000) Optic nerve evaluation among optometrists. *Optometry Vision Sci*, 77, 446-52.
- SPRY, P. G., SPENCER, I. C., SPARROW, J. M., PETERS, T. J., BROOKES, S. T., GRAY, S., BAKER, I., FURBER, J. E. & EASTY, D. L. (1999) The Bristol Shared Care Glaucoma Study: Reliability of community optometric and hospital eye service test measures. *Brit J Ophthalmol*, 83, 707-12.
- STROMAN, G. A., STEWART, W. C., GOLNIK, K. C., CURE, J. K. & OLINGER, R. E. (1995) Magnetic resonance imaging in patients with low-tension glaucoma. *Arch Ophthalmol*, 113, 168-172.
- SUNG, V. C. T., BHAN, A. & VERNON, S. A. (2002) Agreement in assessing optic discs with a digital stereoscopic optic disc camera (Discam) and Heidelberg Retina Tomograph. *Brit Med J*, 86, 196-202
- SUSANNA, R. Jr. & VESSANI, R. M. (2007) New findings in the evaluation of the optic disc in glaucoma diagnosis. *Curr Opin Ophthalmol*, 18, 122-128.
- SUSANNA, R. Jr. & MEDEIROS, F. A. (2006) Changes in the lamina cribrosa. *The Optic Nerve in Glaucoma*. Rio de Janeiro, Brazil, Cultura Medica.
- SVENSSON, E. (1997) A coefficient of agreement adjusted for bias in paired ordered categorical data. *Biometrical J*, 39, 643-657.
- TAVARES, I. M., MEDEIROS, F. A. & WEINREB, R. N. (2006) Inconsistency of the published definition of ocular hypertension. *J Glaucoma*, 15, 529-533.
- TIELSCH, J. M., KATZ, J., QUIGLEY, H. A., JAVITT, J. C. & SOMMER, A. (1995a) Diabetes, intraocular pressure, and primary open-angle glaucoma in the Baltimore Eye Survey. *Ophthalmology*, 102, 48-53.
- TIELSCH, J. M., KATZ, J., QUIGLEY, H. A., MILLER, N. R. & SOMMER, A. (1988) Intraobserver and interobserver agreement in measurement of optic disc characteristics. *Ophthalmology*, 95, 350-6.
- TIELSCH, J. M., KATZ, J., SOMMER, A., QUIGLEY, H. A. & JAVITT, J. C. (1995b) Hypertension, perfusion pressure, and primary open-angle glaucoma: A population-based assessment. *Arch Ophthalmol*, 113, 216-221.
- TIELSCH, J. M., SOMMER, A., KATZ, J., ROYALL, R. M., QUIGLEY, H. A. & JAVITT, J. (1991) Racial variations in the prevalence of primary open-angle glaucoma. The Baltimore Eye Survey. *J Amer Med Assoc*, 266, 369-374.
- TOMIC, L., MAEPEA, O., SPERBER, G. O. & ALM, A. (2001) Comparison of retinal transit times and retinal blood flow: A study in monkeys. *Invest Ophth Vis Sci*, 42, 752-755.
- TRAUSTASON, S., HARDARSON, S. H., GOTTFREDSOTTIR, M. S., EYSTEINSSON, T., KARLSSON, R. A., STEFANSSON, E. & HARRIS, A. (2009) Dorzolamide-Timolol combination and retinal vessel oxygen saturation in patients with glaucoma or ocular hypertension. *Brit J Ophthalmol*, 93, 1064-1067.
- TRAVERSO, C. E., GREHN, F., HOLLO, G., LACHKAR, Y., MIGDAL, C. & THYGESEN, J. (2003) *Terminology and Guidelines for Glaucoma*, Savona, Italy, Dogma.

- TUCK, M. W. & CRICK, R. P. (2003) The projected increase in glaucoma due to an ageing population. *Ophthal Physl Opt*, 23, 175-179.
- TURPIN, A., SAMPSON, G. P. & MCKENDRICK, A. M. (2009) Combining ganglion cell topology and data of patients with glaucoma to determine a structure-function map. *Invest Ophth Vis Sci*, 50, 3249-3256.
- TWA, M. D., JOHNSON, C. A. & KELTNER, J. L. (2008) Non-linear dimensionality reduction of visual field data in chronic open angle glaucoma. *Invest Ophth Vis Sci*, 49, E-abstract 1070.
- VAN ASSENDELFT, O.W. & ZIJLSTRA, W.G. (1975) Extinction coefficients for use in equations for the spectrophotometric analysis of haemoglobin mixtures. *Anal Biochem*, 69, 43-48.
- VAN VELDHUISEN, P. C., EDERER, F., GAASTERLAND, D. E., SULLIVAN, E. K., BECK, A., PRUM, B. E., CYRLIN, M. N. & WEISS, H. (2000) The Advanced Glaucoma Intervention study (AGIS) 7: The relationship between control of intraocular pressure and visual field deterioration. *Am J Ophthalmol*, 130, 429-40.
- VARMA, R., STEINMANN, W. C. & SCOTT, I. U. (1992) Expert agreement in evaluating the optic disc for glaucoma. *Ophthalmology*, 99, 215-21.
- VARMA, R., TIELSCH, J. M., QUIGLEY, H. A., HILTON, S. C., KATZ, J., SPAETH, G. L. & SOMMER, A. (1994) Race-, age-, gender-, and refractive error--related differences in the normal optic disc. *Arch Ophthalmol*, 112, 1068-1076.
- VINGRYS, A. J., HELFRICH, K. A. & SMITH, G. (1994) The role that binocular vision and stereopsis have in evaluating fundus features. *Optometry Vision Sci*, 71, 508-15.
- WANG, J. J., MITCHELL, P. & SMITH, W. (1997) Is there an association between migraine headache and open-angle glaucoma? Findings from the Blue Mountains Eye Study. *Ophthalmology*, 104, 1714-9.
- WEBER, A. J. & HARMAN, C. D. (2005) Structure-function relations of parasol cells in the normal and glaucomatous primate retina. *Invest Ophth Vis Sci*, 46, 3197-3207.
- WEINREB, R. N. & KHAW, P. T. (2004) Primary open-angle glaucoma. *Lancet*, 363, 1711-1720.
- WHITING, P., RUTJES, A. W. S., REITSMA, J. B., GLAS, A. S., BOSSUYT, P. M. M. & KLEIJNEN, J. (2004) Sources of variation and bias in studies of diagnostic accuracy: A systematic review. *Ann Intern Med*, 140, 189-202.
- WILKINS, M. R., SHAH, P. & KHAW, P. T. (2007) Laser and surgical treatment of glaucoma. IN EDGAR, D.F. & RUDNICKA, A.R. (Eds.) *Glaucoma Identification & Co-management*. USA, Butterworth-Heinemann Elsevier.
- WOLFS, R. C. W., KLAVER, C. C. W., RAMRATTAN, R. S., VAN DUIJN, C. M., HOFMAN, A. & DE JONG, P. T. V. M. (1998) Genetic risk of primary open-angle glaucoma: Population-based familial aggregation study. *Arch Ophthalmol*, 116, 1640-1645.

- YAMAGISHI, N., ANTON, A., SAMPLE, P. A., ZANGWILL, L., LOPEZ, A. & WEINREB, R. N. (1997) Mapping structural damage of the optic disk to visual field defect in glaucoma. *Am J Ophthalmol*, 123, 667.
- YAMAZAKI, Y. & DRANCE, S. M. (1997) The relationship between progression of visual field defects and retrobulbar circulation in patients with glaucoma. *Am J Ophthalmol*, 124, 287-295.
- YAN, S., ABIDI, S. S. R. & ARTES, P. H. (2005) Analyzing sub-classifications of glaucoma via SOM based clustering of optic nerve images. *St Heal T*, 116, 483-488.